Automatic Parcellation of Longitudinal Cortical Surfaces

By Manal H. Alassaf

B.Sc. in Computer Science, May 2004, Taif University, Saudi Arabia
M.Sc. in Computer Science, May 2010, The George Washington University, USA

A Dissertation submitted to

The Faculty of
The School of Engineering and Applied Science
of The George Washington University
in partial fulfillment of the requirements
for the degree of Doctor of Philosophy

May 17, 2015

Dissertation directed by

James K. Hahn
Professor of Engineering and Applied Science

ProQuest LLC.
789 East Eisenhower Parkway
P.O. Box 1346
Ann Arbor, MI 48106 - 1346

The School of Engineering and Applied Science of The George Washington University certifies that Manal H. Alassaf has passed the Final Examination for the degree of Doctor of Philosophy as of March 2nd, 2015. This is the final and approved form of the dissertation.

Automatic Parcellation of Longitudinal Cortical Surfaces

Manal H. Alassaf

Dissertation Research Committee:

James K. Hahn, Professor of Engineering and Applied Science, Dissertation Director

Abdou S. Youssef, Professor of Engineering and Applied Science, Committee Member

Claire Monteleoni, Assistant Professor of Computer Science, Committee Member

Mohamad Z. Koubeissi, Associate Professor of Neurology, Committee Member

Dedication

بسم الله الرحمن الرحيم

إلى والديّ الكريمين:

والدتي: فائزة بنت عساف العواجي، حفظها الله

والدي: حسين بن منصور العساف، رحمه الله

To My Parents:
Faizah Assaf Alawaji
Hussein Mansour Alassaf, 1945-2008

هذا من فضل الله

Abstract of Dissertation

Automatic Parcellation of Longitudinal Cortical Surfaces

Preterm birth incidence is a main cause of developing cognitive and neurologic disorders in childhood especially with children who are born extremely preterm. The human brain experiences significant functional and morphological changes at early development before and around birth. Understanding and modeling brain normal growth and cortical changes in early development are the keys to understanding and tracking neurologic disorders. The objective of this dissertation is to develop methods for longitudinally modeling brain development in order to provide researchers with tools for understanding normal growth patterns and for designing interventions that minimize potential preterm brain injury. We present a novel algorithm for longitudinally parcellating the developing brain at different stages of development. The algorithm assigns each cortical location to a neuroanatomical brain structure during early development. A labeled newborn brain atlas at 41 weeks gestational age (GA) is used to propagate labels of anatomical regions of interest to a spatio-temporal atlas, which provides a dynamic model of brain development at each week between 28-44 GA weeks. First, cortical labels from the volume of the newborn brain are propagated to an age-matched cortical surface from the spatio-temporal atlas. Then, labels are propagated across the cortical surfaces of each week of the spatio-temporal atlas by registering successive cortical surfaces using a new approach and using an energy optimization function. This procedure incorporates local and global, spatial and temporal information when assigning the labels. The result is a complete parcellation of 17 neonatal brain surfaces with similar points per labels distributions across weeks.

Table of Contents

List of Figures

List of Tables

List of Acronyms

2D	Two-Dimensional
3D	Three-Dimensional
4D	Four-Dimensional
AAL	Automated Anatomical Labeling
ALBERT	A Label-Based Encephalic ROI Template
B-spline	Basis spline
CC	Cross Correlation
CSF	Cerebrospinal Fluid
CT	Computed Tomography
DOF	Degrees Of Freedom
DW	Diffusion-Weighted
EM	Expectation Maximization
FFD	Free-Form Deformation
fMRI	functional MRI
GA	Gestational Age
GB	Gigabyte
GE	Ganglionic Eminence
GHz	Gigahertz
GM	Gray Matter
HAMMER	Hierarchical Attribute Matching Mechanism for Elastic Registration
HCP	Human Connectome Project
ICP	Iterative Closest Point

IDE	Integrated Development Environment
JE	Joint Entropy
JHU	John Hopkins University
LDDMM	Large Deformation Diffeomorphic Metric Mapping
MAP	Maximum-a-Posteriori
MI	Mutual Information
MNI	Montreal Neurology Institute
MoG	Mixture of Gaussian
MRF	Markov Random Field
MRI	Magnetic Resonance Imaging
NIH	National Institutes of Health
NMI	Normalized Mutual Information
NN	Nearest Neighbor
PDF	Probability Density Function
PET	Positron Emission Tomography
PTB	Preterm Birth
RAM	Random Access Memory
ROIs	Regions Of Interest
S	Source
SSD	Sum of Square Differences
SVM	Support Vector Machines
SVZ	Subventricular Zone
T	Target

UNC	University of North Carolina
U.S.	United States
VZ	Ventricular Zone
WM	White Matter
X	Transformation

Chapter 1-Introduction

In the United States, one in every eight infants is born prematurely [1]. Premature birth is ranked second among causes of infant death in the U.S. [2]. Preterm birth (PTB) refers to the birth of an infant of 37 weeks gestational age (GA) or less. Although improvements in neonatal intensive care can increase the survival rate of prematurely born infants, the development of cognitive and neurologic disorders is still common especially with those who are extremely preterm [3,4]. Special therapies are needed for the neurodevelopmental care of PTB neonates. But most importantly, understanding normal growth and development processes of the brain are the keys to understanding and tracking neurologic disorders [5,6]. The objective of this dissertation is to develop methods for longitudinal modeling and quantitative measuring of brain structures development, in order to provide researchers with tools for understanding normal growth patterns and for designing interventions that minimize potential preterm brain injury.

Invisible to human sensory perception, the brain remains a hidden world filled with mysteries awaiting scientific discovery. But what is inside the brain that scientists are interested in knowing about? How can the brain be non-invasively visualized? How can we track its development and why is it important to understand brain normal growth? Motivated by these questions, this dissertation contributes to the investigation of the developing brain. In this chapter, a general description of brain anatomy, its development, and the terminology used throughout the dissertation are presented. This includes a brief description of developing brain imaging techniques, and the challenges associated with these techniques. Finally, motivation, aim, and dissertation contribution conclude this chapter.

1.1. Brain Anatomy

The cerebrum, cerebellum, and brainstem are the main components of human brain as shown in Figure 1.1(a). Similarly, there are three main tissue classes in the brain: gray matter (GM) or cerebral cortex, white matter (WM) or subcortex, and cerebrospinal fluid (CSF). The GM contains cells and the WM contains neuronal axons myelinated sheaths. The outer layer that covers the cerebrum, or the two cerebral hemispheres, is called the cerebral cortex and forms the largest part of the human brain. Cerebral cortex has highly convoluted topography. The grooves, which encompass two-thirds of the cerebral cortex, are called sulci (s. sulcus) and the folds are called gyri (s. gyrus). Four main lobes in each hemisphere of the cerebral cortex can be recognized by obvious sulci or gyri landmarks on the cortex as shown in Figure 1.1(b). Studying the cerebral cortex is important because it plays a significant role in high-level human functions and activities such as language, memory, planning, etc., and it is important to understand the relationship between functions and structures of the human brain (discussed in details in section 2.2.1).

A number of neuroanatomical regions or structures exist in the brain and vary between neuroanatomical atlases where each atlas divides the brain into a number of regions based on relative knowledge. To identify brain structures, anatomical expertise about the geometry and the boundaries between structures is required. In addition, special radiology expertise related to classes' intensity distribution and imaging artifacts is necessary. Sometimes tissue identification is needed prior to identifying brain structures or regions [7]. The process of identifying brain structures is usually called brain tissue segmentation, while the process of labeling brain regions is referred to as anatomical segmentation, or brain parcellation which is described in depth in Chapter 2 (see Figure 1.1(c)).

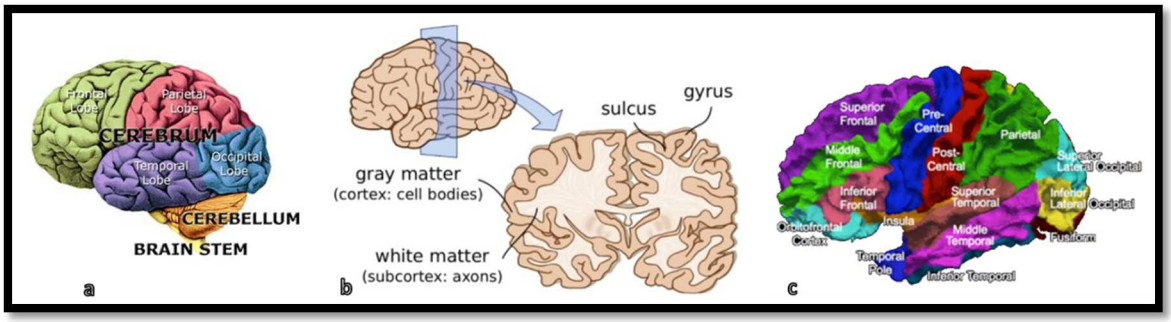

Figure 1.1. Brain Anatomy. a) Lateral view of the main three components of the brain and principal fissures and lobes of the cerebrum (Source: [8]). b) Illustration of brain tissue anatomy (Source: [9]). c) Brain parcellation of 24 regions (Source [10]).

1.2. Developing Brain Imaging

Today, advancements in technical and scientific research provide great opportunities to combine disciplines in science and technology, producing innovative ways to conduct research and to solve real world problems. The most useful technologies where engineering science and medical science intermingle are medical imaging modalities. One example that is widely used to examine the pregnant women and to image the fetus is Obstetric Ultrasonography. This technique uses an ultrasound probe to transmit ultrasound waves through the body. These waves, which are not naturally heard by humans, reflect and echo off the body tissues and are recorded as images. Even though the ultrasound images are very helpful in visualizing fetus growth and development [11], they do not provide comprehensive information about brain anatomy.

Magnetic Resonance Imaging (MRI) is a powerful, painless, non-invasive and non-ionized technique for capturing detailed images that underlay tissue characteristics within the brain. For the developing brain, it captures the entire brain including the brain soft tissues, vasculature, and microstructure [12]. MRI uses a magnetic field and radio frequency to capture these pictures. The magnetic field aligns the nuclear magnetization of

hydrogen atoms within body water, while the radio wave pulses alter these alignments causing nuclear magnetization to produce rotating magnetic fields that are detectable by the scanner and produced in gray scale images. Interpreting a brain MRI scan means finding a correspondence between gray scale intensity in each MR image and labeled anatomical tissues or regions.

MRI is not only used to investigate the anatomy and physiology of the body, but can also be fused within ultrasound or x-ray computed tomography (CT) images to reveal additional information about any organ [13]. Moreover, functional MRI (fMRI) captures activity in any region of the brain by detecting the blood flow to that region [14]. In addition, Diffusion-Weighted (DW) MRI allows visualization of the brain tissue structure and organization due to its sensitivity to the diffusion patterns of free water [15-17].

By taking serial scans during and after the gestational time, we can assess the longitudinal maturity of the brain both in utero and ex utero. However, taking MRI scans of fetal brain in utero is challenging due to fetus motion artifacts caused by limited acquisition time [18]. Recent studies have developed approaches to successfully overcome this problem [19,20]. Another challenge of scanning fetal brain using MR imaging is the variation of the magnetic field strength that is used to acquire the MR images from one scanner to another; usually between one and three Tesla. This produces intensity inhomogeneity such that the brain intensity images produced by different scanners are dissimilar. This can be problematic for image-based techniques such as registration and segmentation since these techniques depend heavily on intensity. Another challenge presented when dealing with these techniques is the partial volume effect where the resolution (sampling grid of MR signal) of scans differ from one scanner device to another

[7]. However, techniques have been developed to correct for the intensity inhomogeneity and the partial volume effect [21,22]. Despite these challenges, MRI is the most viable imaging modality to longitudinally capture and track the developing brain in utero as demonstrated in the parcellation algorithm of this dissertation.

1.3. Brain Development

Brain development starts at the embryonic period; more specifically, at the fifth week of pregnancy. Figure 1.2 illustrates the timeline of pregnancy by weeks and months of GA [23]. In the first months of pregnancy and before birth, the brain experiences the most development and changes in shape, size and structure [24,25]. Most significantly, changes occur in the size and in the cortical folding of the brain. Growth continues rapidly until the brain is two to three years old, when the process slows and stabilizes and the developing brain becomes mature. Using MR images allows for quantitative and qualitative assessment and measurement of human brain myelination (maturation) processes and growth patterns [26-30].

Myelination is the process of covering the WM by myelin, lipid bilayer. The fast myelination starts before birth and is completed within the first two or three years of life, while the long myelination continues until adulthood [31,32]. Myelin promotes efficient neural signal transmission along the nerve cells. The appearance of the developing brain in structural MRI differs significantly from the appearance of the mature adult brain. The myelinated WM in T1-weighted MRI increases in intensity from hypo intense to hyper intense relative to GM. In T2-weighted MRI WM decreases from hyper intense to hypo intense relative to GM [24,33,34]. Thus, the developing brain MR images are characterized by an inverted contrast of WM and GM as opposed to the developed brain as seen in Figure

1.3. The inverted contrast is due to WM axonal growth where myelin sheath forms around the axon tracts [35,36] (see Figure 1.4) and change occurs in the cell water content as a result of decreasing both T1 and T2 times in order to avoid fetus motion [36,37]. By the completion of the myelination process, the brain tissue contrast appears in MR images similar to the adult brain tissue contrast, while the brain structure, shape, and size are different [38].

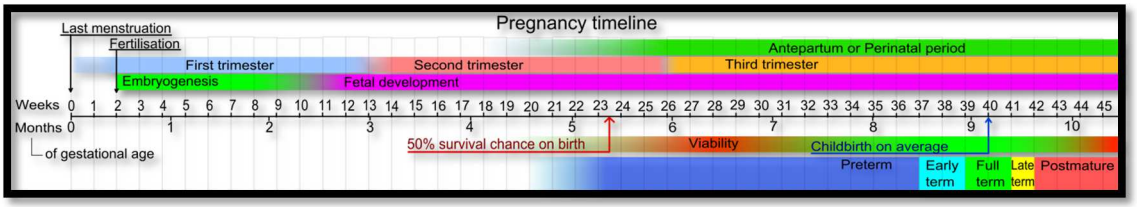

Figure 1.2. Timeline of pregnancy by weeks and months of gestational age (Source: [39]).

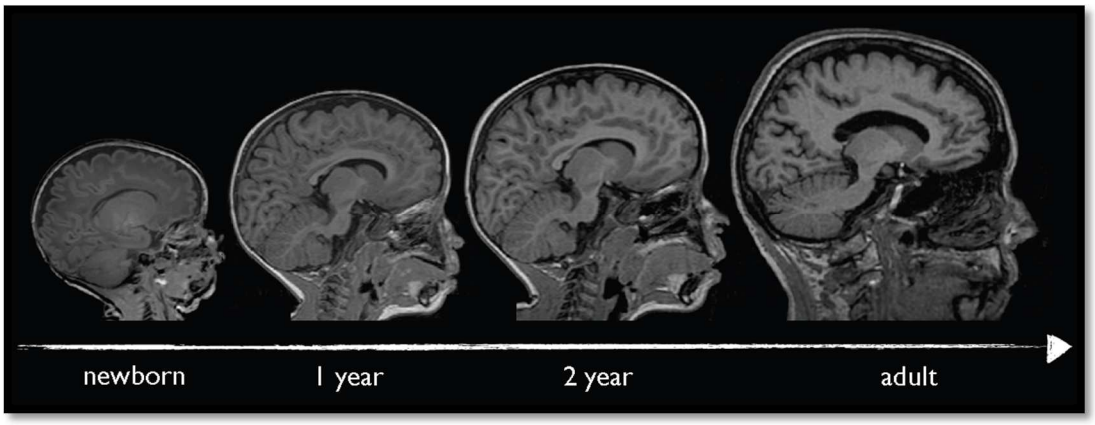

Figure 1.3. GM and WM intensities of developing brain in contrast to developed brain (Source: [40]).

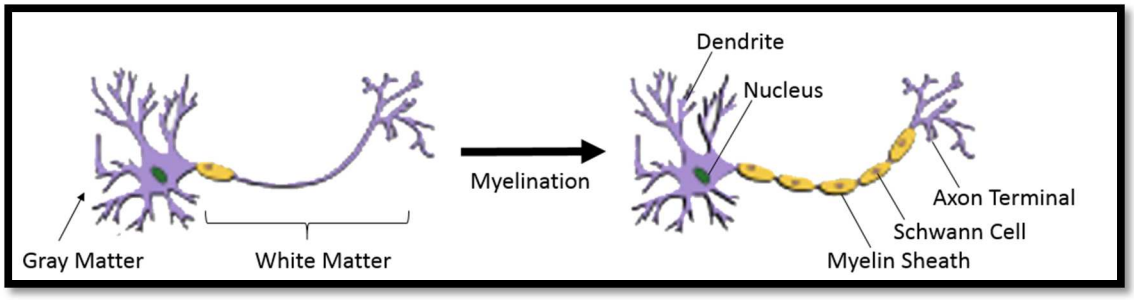

Figure 1.4. Axonal growth.

Human corticogenesis and brain growth patterns can be predicted using structural MRI, DW MRI, and histology. Corticogenesis is the process responsible for creating the cerebral cortex (GM). The cerebral cortex development starts in the embryogenesis period and continues after birth [36]. Cerebral cortex is a highly convoluted structure composed of six layers and located on the outer layer of the brain [41], which constitutes the cognitive and intellectual ability center in humans. The six layers' neurons are generated in the ventricular/subventricular zones and subpallial ganglionic eminence [42-45] and then migrate along glial cell scaffold structures to their final destination structure in the cortical plate [46-49]. During fetal development, this highly orchestrated cellular migration towards the cortical plate is characterized by having radial and tangential migrational trajectories [46,50-52]. Recently, Kolasinski et al. described the migration paths in detail using structural and DW MRI, and emphasized that the radial patterns originated from the ventricular/subventricular zone, while the tangentio-radial patterns originated in ganglionic eminence [52] (see Figure 1.5). As a result, an increase in the cerebral cortex surface area occurs [53]. At the same time, the total brain tissue volume increases at the ratio of 22ml/week [26]. The radial growth of cerebral cortex in early development is postulated by lateral spreading of the neuron cells and the increase of the cortical surface area [51,53,54]. However, local cortical growth and folding which form the sulci and gyri

during early developments [24] are more complicated. Several methods are proposed to mathematically simulate local cortical growth using elasticity and plasticity [55], tension forces [56], and a reaction-diffusion system [57]. Recently, Budday et al. proposed a differential growth mechanical model for the developing brain to simulate cortical folding. In their model, the cortex (GM) grows morphogenetically at a constant rate and the subcortex (WM) grows in response to overstretch [9]. To date, no defined model that precisely underlay the mechanism of local brain folding and convoluting in detail during gestational time has been produced [6,9]. In this dissertation, we rely on the global, concentric, and radial growth hypothesis to track the local regions of interest (ROIs) development when parcellating the developing brain longitudinal MRI scans' surfaces.

1.4. Motivation

Automatic analysis of the developing brain is challenging and needs special dedicated image analysis algorithms that account for the intensity change over time. Cerebral cortex poses a special challenge due to its convolution nature that varies from one person to another. Surface based analysis of such a structure is necessary to account for the convolution and to capture the buried regions [58]. Establishing a benchmark to assess the developing brain anatomical ROIs growth of PTB children requires surface-based studies [59]. Limited studies have attempted to identify typical patterns of growth using surfaces such as growth trajectories [60] and structural development biomarkers [61]. Other studies have aimed to identify cortical folding or cortical thickness in the developing brain [62,63] while others focused on analyzing the intellectual and functional abilities and abnormalities on the PTB brain [64]. Also, studies have focused on tracking the developmental changes

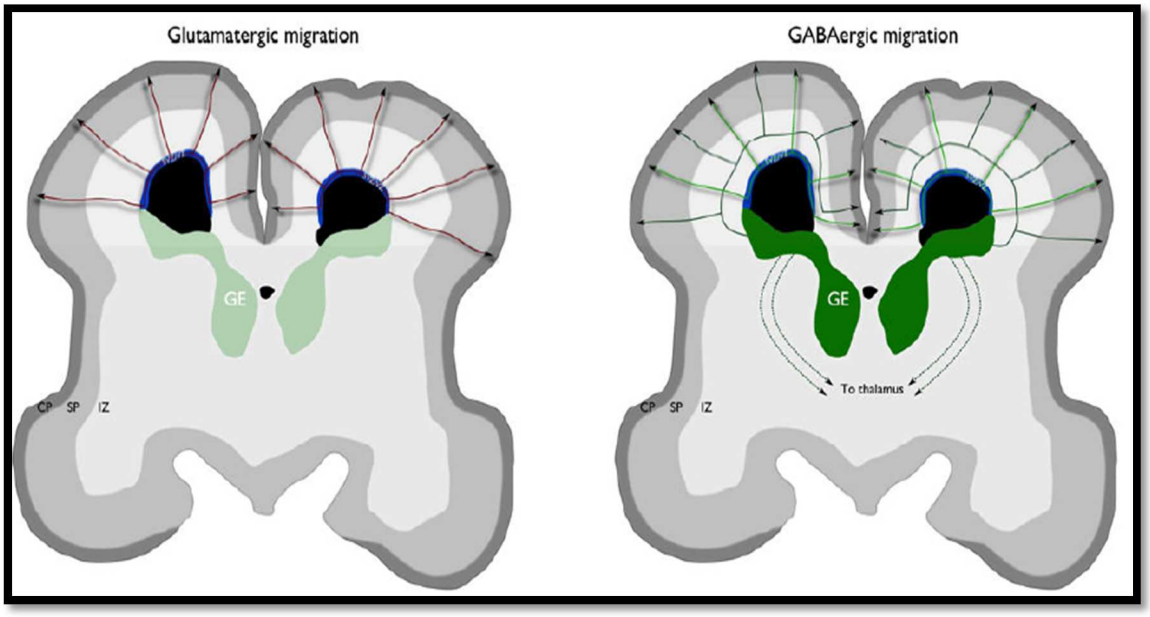

Figure 1.5. Two-dimensional representation of the pallial and subpallial origins and the GABAergic and glutamatergic radial and tangential migratory paths in human fetus brain at 19 post-conceptual weeks. Tangential migration can occur within the subventricular/ventricular zone (SVZ/VZ, blue area) in the pallial SVZ/VZ where glutant neurons originate. However, as the blue arrows show, radial migration occurs along radial glial fascicles, forming a dominate pattern that is perpendicular to cortical plate (CP) orientation. In the pallial SVZ/VZ and subpallial ganglionic eminence (green), human brain GABAergic neurons develop. The green arrows identify the tangential corridors of radial trajectory of GABAergic neurons in intermediate zone as it moves towards the CP after presenting its original migration pattern as tangentially oriented to the CP. Revealing a radial trajectory to the CP, the light green arrows show GABAergic neuronal migration that develops in the SVZ/VZ as it has been found to present in human and non-human primates. As indicated, ganglionic eminence (GE), where ganglionic neurons originate, also transfers to thalamus by way of subcortical paths (Source: [52]).

related to the intensity color change between GM and WM in MR images [65,66]. Until recently only a few quantitative studies have analyzed the longitudinal regional growth trajectories [60]. However, there is a lack of surface-based studies compared to volumetric image-based ones especially at early age of brain development.

Viewed from another perspective, several studies have shifted focus to creating developing brain probabilistic atlases, which provide a reference of knowledge for physiological functional disorders and abnormalities research [67-69]. As discussed in

Chapter 2, some of the existing neonatal developing brain atlases are constructed with tissue segmentation without parcellation. If they account for parcellation, it is performed manually [70-73]. In addition, the parcellation is provided for a single GA week as a single-subject atlas [71,72] or population-average atlas [70,71,73]. UNC Infant 0-1-2 Atlas is the first publically available neonate automatically parcellated developing brain atlas [74]. Nevertheless, this neonate parcellated atlas is also single aged, at 41 GA week. Conclusively, no longitudinal parcellation maps exist for neonatal developing brain at early GA.

1.5. Aim

Most neuroimaging studies of the developing brain have developed algorithms for intensities in MR images. Therefore, these studies were performed on the image space. Few studies have focused on the cortical surfaces of the developing brain within the age range of birth until adulthood. Neither have these studies included early GA brain development. This dissertation presents work on surface-based longitudinal (spatio-temporal) atlas analysis of early brain development starting from 28 week GA to 44 week GA. The purpose is to provide automated methods for spatio-temporal parcellation with quantitative measures of brain development. These methods can assist researchers in understanding normal growth patterns and in designing interventions to reduce preterm brain injury.

1.6. Dissertation Contributions

The dissertation describes methods for modeling the normal growth in prematurely born infants. More specifically, it identifies methods for tracking the growth of different cortical anatomical structures' ROIs at early GA. In addition, it offers an automated longitudinal parcellation method for the developing brain. The proposed parcellation algorithm uses preterm brain spatio-temporal brain atlas with tissue-segmentations and infant brain parcellated atlas to longitudinally parcellate the developing brain at different stages of development. Chapter 2 sheds light on previous related work and provides background on techniques employed throughout the dissertation. Chapter 3 proposes a novel framework for solving the problem of registering and propagating the labels of a parcellated atlas across longitudinal surfaces with large curvature variation. In Chapter 4, quantitative results of modeling the regional growth of the developing brain will be presented, which can offer a useful marker of neurodevelopmental changes. Finally, Chapter 5 contains conclusions and recommendations for future work directions.

1.7. Summary

In this chapter, knowledge about brain development, its anatomy, and developing brain imaging modalities are presented. Also, the chapter delineated the motivation for solving the problem of how to longitudinally parcellate the developing brain. Justifications of the need for providing a solution is emphasized.

"The brain, the masterpiece of creation, is almost unknown to us."

Nicolaus Steno, 1669

Is it known now?

Chapter 2: Background and Related Work

Based on:

***MH Alassaf**, Y Yim, JK Hahn. "Non-rigid Surface Registration using Cover Tree based Clustering and Nearest Neighbor Search", Proceedings of the 9th International Conference on Computer Vision Theory and Applications. (2014) 579-587.*

***MH Alassaf,** JK Hahn. "Probabilistic Developing Brain Atlases: A Survey". 2015 (In Submission).*

2.1. Introduction

As a biological structure, there is none more complex than the human brain. For centuries, scientists have worked to discover the relationship between the brain's structures and functions. This chapter presents the literature review (section 2.2) of related work in the relationship between brain structure and functions, constructing digital brain atlases techniques, and parcellated brain atlases methods. The chapter provides a general overview of the techniques used throughout the dissertation, such as image registration and brain parcellation in section 2.3. Also, discussed are the challenges of applying these techniques to MR images of the developing brain.

2.2. Related Work

2.2.1. Brain Structures and Functions

Historically, brain drawings from the Middle Ages were primarily schematic rather than anatomical, aiming to determine which brain sections were associated with brain functions. Ibn al-Haytham (965 – 1040 AD), an Arab scholar known to the west as Alhazen, was the first to anatomically illustrate the eye and its visual function in his book "Kitab Al-manazir" [75,76] (The Book of Optics). The brain was shown

schematically as in Figure 2.1(a). Islamic scholar Ibn Sīnā (980 – 1037AD), known to the west as Avicenna, was the first medical philosopher to anatomically divide the brain into three compartments called “cellula”. In his book “Al-Canon fi Al-Tebb” (The law of Medicine), he further labeled the cerebral ventricles with five labels based on their functionality. These consisted of: "sensus communis", "fantasia", "ymaginativa", "cogitativa seu estimativa", and "memorativa" [77] which correspond with common sense, fantasy, imagination, reasoning and cognition, and memory, respectively (Figure 2.1(b)). Later, illustrations by Leonardo da Vinci (1452 – 1519AD), an Italian scholar known for his contributions to both science and art, complimented Avicenna’s illustrations by further anatomically describing the brain in cross sections [76] as seen in Figure 2.1(c). However, in the early modern age, Belgian scientist Andreas Vesalius (1514 – 1564 AD) who was also known as the founder of modern human anatomy, produced more authentic illustrations of the brain in his book “De Humani Commis Fabrica” (On the Structure of the Human Body) [78]. An example of the illustrations can be seen in Figure 2.1(d).

With the discovery of modern age technologies, more comprehensive descriptions of the whole volume of the brain began to emerge. In 1909 using a microscope, German neurologist Korbinian Brodmann (1868 – 1918AD), distinguished 52 distinct regions in the cerebral cortex from their cytoarchitectonic (histological) features such as cortical thickness, laminae thickness, number and type of cells, and other features [79] as seen in Figure 2.1(e). Brodmann’s discovery of these regions has allowed their extensive use in many brain studies to relate function with its corresponding brain structures. His work was based on German anatomist Franz Joseph

Gall's (1758 – 1828 AD) belief in localization of brain functions to several locations on the brain cerebral cortex. Using a microscope to divide the brain frontal lobe into eight zones based on nerve cells shape, volume, and arrangement, Sandies (1914 – 1984 AD) described the distinct function of each division in his cytoarchitectural and myeloarchitectural studies [68]. In 1957, neuroscientist and professor at John Hopkins University Vernon Mountcastle (1918 – 2015 AD) discovered the columnar organization of the neocortex, which form the basis for most recent studies focusing on the relationship between brain function and structure [67]. In Mountcastle's description of neocortex columnar organization, he divided the cerebral cortex into modules each of which plays the role of functional processing unit that receives input and produces output.

Today, scientists divide each brain hemisphere into four lobes: the frontal lobe, temporal lobe, parietal lobe, and occipital lobe with each lobe being associated with distinct functions [69] (see Figure 1.1(a)). In partial agreement with Avicenna, the frontal lobe is the center of cognitive activities like planning, predicting, decision making and long-term memory. The temporal lobe is involved in processing sensory input such as auditory, visual perception, and languages. The parietal lobe is involved in sensory information like perception, navigation, spatial orientation, touch and pain, while the occipital lobe is involved in appropriately transforming vision for parietal and temporal processing.

Through the evolvement of medical imaging technologies, more sophisticated studies relating brain structures with functions have emerged using MRI, fMRI, DW MRI, and PET (Positron Emission Tomography). In particular, these are highly useful

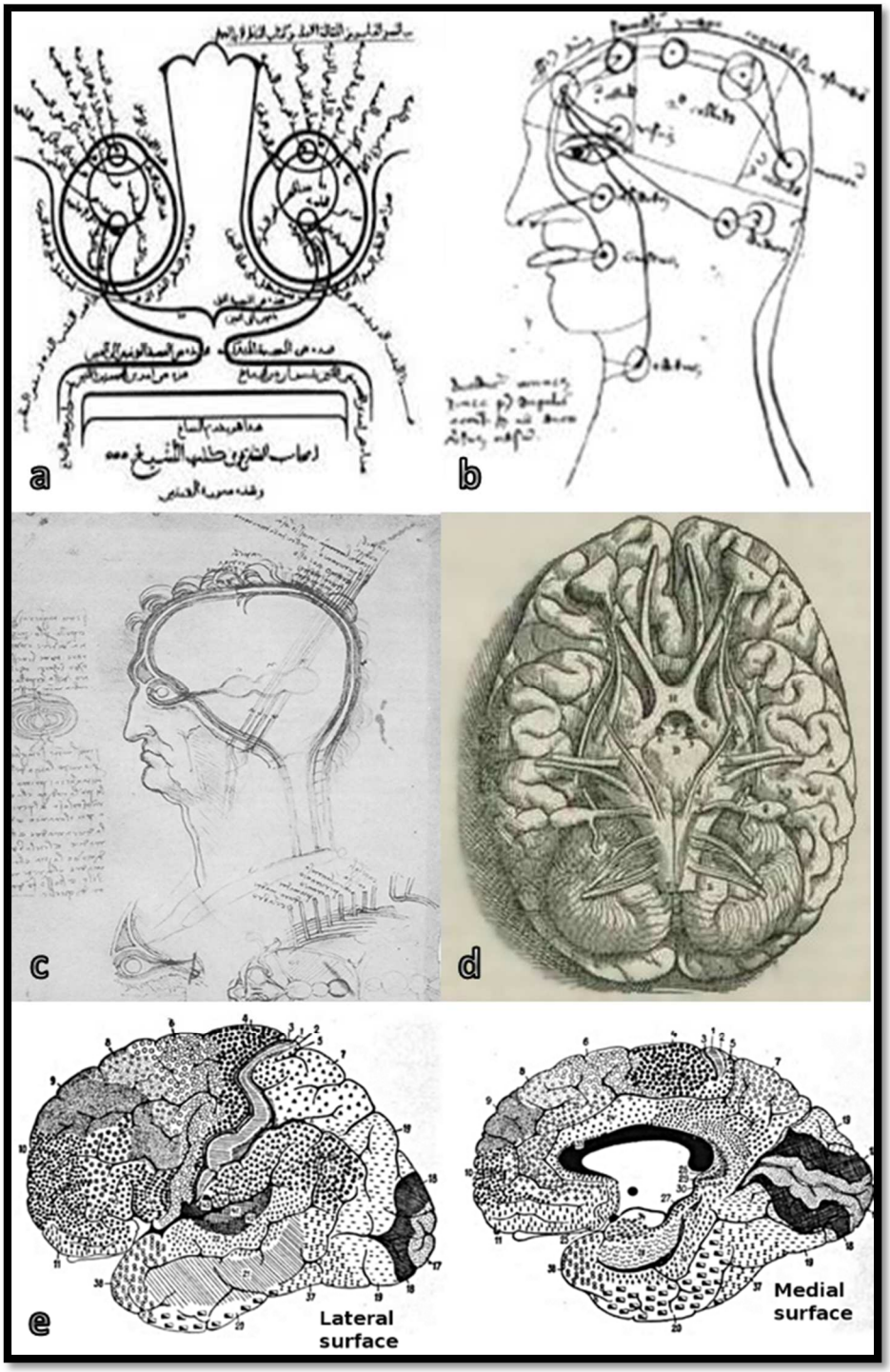

Figure 2.1. Old Brain Illustrations. a) The eye and the visual system schematic by Alhazen which forms the basis of vision and light radiated in straight light theories, dated 1038 AD (Sources: [75,76]). b) Avicenna's brain illustration of the three brain parts and five cerebral areas, dated 1347 AD (Source: [77]). c) Leonardo da Vinci's illustration of the brain and introduction of the cross sections drawing to further describe 3D anatomy, dated (1490-1500 AD) (Source: [76]). d) Vesalius's detailed illustration of the physical brain, dated 1543 AD (Source: [78]). e) The Brodmann brain numerical map of 52 discrete regions based on histological differences between regions, dated 1909 AD (Source: [76]).

for cortical morphology caused by brain disease studies such as migraine [80], schizophrenia [81-83], and Alzheimer [84-87] studies to name a few. Since fMRI gives information about the functionally activated area in the brain but does not provide structure information, coupling it with structure information from MRI is important in order to determine relationships in areas of the cerebral cortex [88]. For example, the Human Connectome Project (HCP) is a currently active project funded by National Institutes of Health (NIH) and aims to provide a mapping of the structural and functional neural connections of the human brain primarily using fMRI and MRI [89,90].

Human brain cortex can be further neuroanatomically divided into a number of regions, each of which is described by a label and associated with specific functions. The process of recognizing structures formations in brain MR images is called parcellation.

2.2.2. Brain Parcellation

Parcellation is the process of labeling the cortical geometric features and can be performed on brain MR images or on surfaces constructed from those images. After parcellation, regional and sub-regional studies can be performed to more deeply understand human brain functions and activities.

As previously mentioned, the first attempt to parcellate the human brain based on cytoarchitectonic characteristics was done by Brodmann. Currently, *in vivo* parcellation is done on MR images or on surfaces constructed from these images (see

section 2.3.1 for surface construction). Hence, high-resolution structural MRI (i.e. 1.5 or 3 Tesla) is preferable because it reveals more structure information and detailed anatomical landmark. Historically, cortical parcellation was done manually by an anatomical expert who gave each pixel on each MRI slice a label, either axial, sagittal, or coronal. "Talairach- Tournoux" is an example of such an atlas [91]. Talairach and Tournoux labeled post-mortem brain slices of a 60 year old French woman with anatomical labels based on sulci and gyri and Brodmann cytoarchitectonic areas estimations. They also introduced the Talairach coordinate system with nine degree of freedom (DOF) transformation (including 3 for scaling and 6 for rigid transformation), which maps any brain to the Talairach atlas and localizes the brain regions in functional imaging studies (see Figure 2.7 for linear transformation models).

Manual parcellation involves knowledge in different disciplines such as: brain geometry and region landmark, relationship between structure and function, cytoarchitectonics and myeloarchitectonics, and radiology [92]. Roland and Zilles offer additional information in their paper which describes in detail the criteria and properties of parcellating the human brain cerebral cortex [93]. Generally, the process of manual labeling is time and labor intensive [10,92,94,95]. It consumes several hours (e.g. 12-14) to parcellate one conventional MRI scan [96]. Further, it could take up to a week to parcellate one high resolution MRI scan [92]. In addition, intra- and inter- rater differences compromise manual parcellation validity. Therefore, there is a need to automate the process, which is not a trivial task. The inter-subject cortical geometric patterns' heterogeneity has made automating the parcellation process a challenging problem especially when the brain is developing. Thus parcellation based on a

population-average atlas is preferable since it eliminates the inter-subject variability (see section 2.3.3).

Automatic parcellation of the brain cortex of MRI relies on the same criterion used in manual parcellation including cytoarchitectonic characteristics (intensity values), sulci or gyri landmarks (curvature), and global and local position in the brain. Two main approaches have been developed to automate any MRI brain parcellation; one using image/surface registration and the other using image/surface segmentation [10]. Image/surface registration is based on registering a labeled brain atlas image/surface to the unlabeled brain and then warping the labels from the atlas into the unlabeled brain using the deformation field generated from the registration. The segmentation approach is based on segmenting sulci or gyri on unlabeled brain image/surface and delineating the sub-regions based on this segmentation. In this dissertation we focus on developing brain surface parcellation using image and surface registration-based approaches.

Usually in the registration-based approach, automatic cortical parcellation is done by registering an unlabeled brain with either a manually labeled single-subject atlas or a population-average brain atlas, to propagate the labels [10]. For the registration, landmarks between neuroanatomical regions drive the surface registration while intensity values drive the image registration of the two brains. This approach has been used by researchers to parcellate the human brain cortex. Some researchers have used semi-automatic interactive affine [97,98], or non-rigid [99,100] image registration to propagate the labels using either single-subject atlas [101] or population-average

atlas [102,103]. Still, others have used fully automatic non-rigid surface registration to propagate the labels with automatic topology correction [88,92].

Image/surface registration plays an important role in driving correct label propagation. Another more important registration role appears when building a population-based average atlas, because it is important to align the population correctly to build the atlas. To register the cortical surfaces of two mature brains, the surface geometry (i.e. sulci and gyri) defines landmarks between neuroanatomical regions. Spherical inflation is the most well-known solution for automatically registering the cortical surfaces of mature brains by minimizing the mean square difference between surface folding patterns [104]. This technique is implemented in FreeSurfer tool which provides a successful parcellation of any registered brain into a built-in parcellated mature brain template [92]. While a marker-less surface parcellation called Spherical Demons has been proposed, the process still involves spherical inflation [105,106].

In spherical inflation, forces are applied to flatten one hemisphere cortical surface, unfolding the buried regions such that the whole cortical surface becomes visible [107] (see Figure 2.2 (a) and (d)). This flattening is followed by mapping to a specific coordinate system; in this case spherical as shown in Figure 2.2(c). With this coordinate system, corresponding landmarks between surfaces are located and used to minimize the mean-squared difference employed by the registration algorithm. Spherical inflation is used to register cortical surfaces and is also used to construct an atlas from a population after aligning the surfaces (see Figure 2.2(d)). Even though spherical inflation succeeds in registering mature cortical surface, it has several drawbacks. First, the original surface metric properties are not preserved due to the

applied force, which introduces an average of 15% distortion onto the surface [107]. Secondly, the process restricts the points on the flattened plane borders and treats them differently from the internal points, which in the case of spherical the border points are the ones closest to the polar regions [107]. Lastly, the process as a whole is time consuming and computationally expensive, especially with high-resolution surfaces [94].

The parcellation that follows spherical inflation in FreeSurfer is based on an estimation of probabilistic information with reference to parcellated brain atlases at any location of the brain [92] (see Figure 2.2(e)). By registering a new cortical surface into labeled atlases, labels can be propagated based on Markov Random Field (MRF) model prediction. The used parcellated atlases are for mature brains, which will introduce a bias if used to parcellate the developing brain. Goualher et al. used another approach to propagate the labels [108]. They built a graph where the sulci are the nodes and the neighboring relationships between them form the edges. Labels are learned for each sulcus using likelihood estimation based on the manually labeled training set [108].

MRI surface based parcellation is better than image based parcellation for the following reasons:

1. The nature of the cerebral cortex, which consists of convolutions, makes it more appealing to study as a 3D surface instead of a 3D volume.
2. Sulci and gyri, which are intensively used in defining the landmark between structures, are best represented in a surface form rather than in intensity domain.

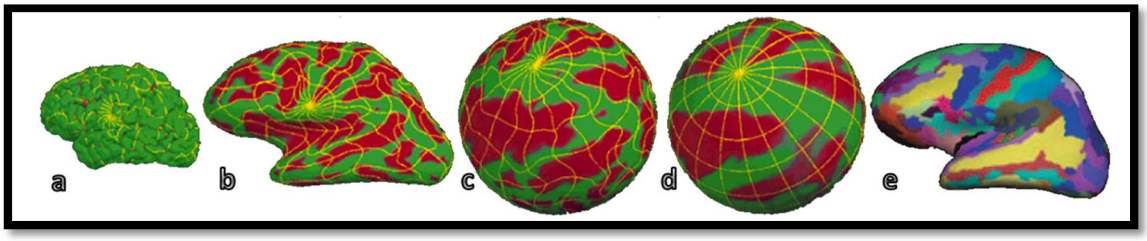

Figure 2.2. FreeSurfer generated surfaces where green represents gyri and red represents sulci: a) Pial surface constructed from one subject brain MRI at the GM-CSF border. b) Inflated cortical surface. c) Spherical surface. d) Average atlas of a population in the spherical coordinate. e) Single subject cortical surface after automatic parcellation with 36 ROIs. (Sources: [92,104]).

3. Using cortical 3D surface form, more accurate measurements including curvature, deepness of sulci, and structure area can be used.

2.2.3. Brain Atlases

A brain atlas is a repository of knowledge that provides a representation of anatomical structure as reference information in a spatial framework. In addition to maps of the subject of study, terminology associated with that particular domain along with coordinate system that describes the study focus are inclusive in that repository. By having an atlas with properties that provide a reference guide, allied disciplines have effective and authoritative communication within the field targeting a specific issue. There are many advantages of digital brain atlases when compared to their counterpart conventional printed atlases [58]. Primarily, the advantages are that digital atlas is searchable, extendable, provide precise delineation of anatomy, and can be used in many population studies for automatic analysis with less human intervention [30,58,74]. In addition, they can be used as references in brain tissue-segmentation and parcellation [30,74,109].

The early brain atlases were constructed from a single-subject such as the Brodmann atlas in 1909 [79], Talairach and Tournoux atlas in 1988 [91], and Montreal Neurology Institute (MNI) digital atlas in 2002 [110]. Recent studies focus on constructing a digital brain atlas using many subjects in order to best represent the anatomical variability of the population. Therefore, building a digital brain atlas usually involves collecting a large number of MRI brain scans. If the brain is developing, the same number of scans is needed for each time point/age of development. For example, to construct a developing brain atlas for fetus in utero, we need to scan the brain of *n* fetuses at each week of gestation. However, these population-based atlases are harder to construct than single-subject atlases keeping in mind the inherited differences in the brain structure and function from one subject to another. If constructed unbiased and using suitable techniques, the resultant repository provide tremendous amount of neurobiological information which is the common language of neuroscientific communication.

A fundamental question in this topic is: what is the best way to construct a digital brain atlas? Brain atlas has to model an infinite number of brain physical representations to accurately and probabilistically provide a reference that best describes the population. The digital brain atlas construction process itself involves three main steps (see Figure 2.3). The first step involves brain image preprocessing and cleaning. The second step consists of normalizing all brains images of each age to a common space using image registration techniques [109]. Finally, it is necessary to fuse the grouped normalized brain images per age to create a common reference atlas for that age [109]. If multiple channels or scanning modalities are used in the atlas

construction, additional information can be provided such as tissue segmentation maps or neuroanatomical ROIs maps. The result is one brain atlas per age or group, with tissue probability maps, and sometimes with label (parcellation) map identifying a number of neuroanatomical ROIs (see Figure 2.4).

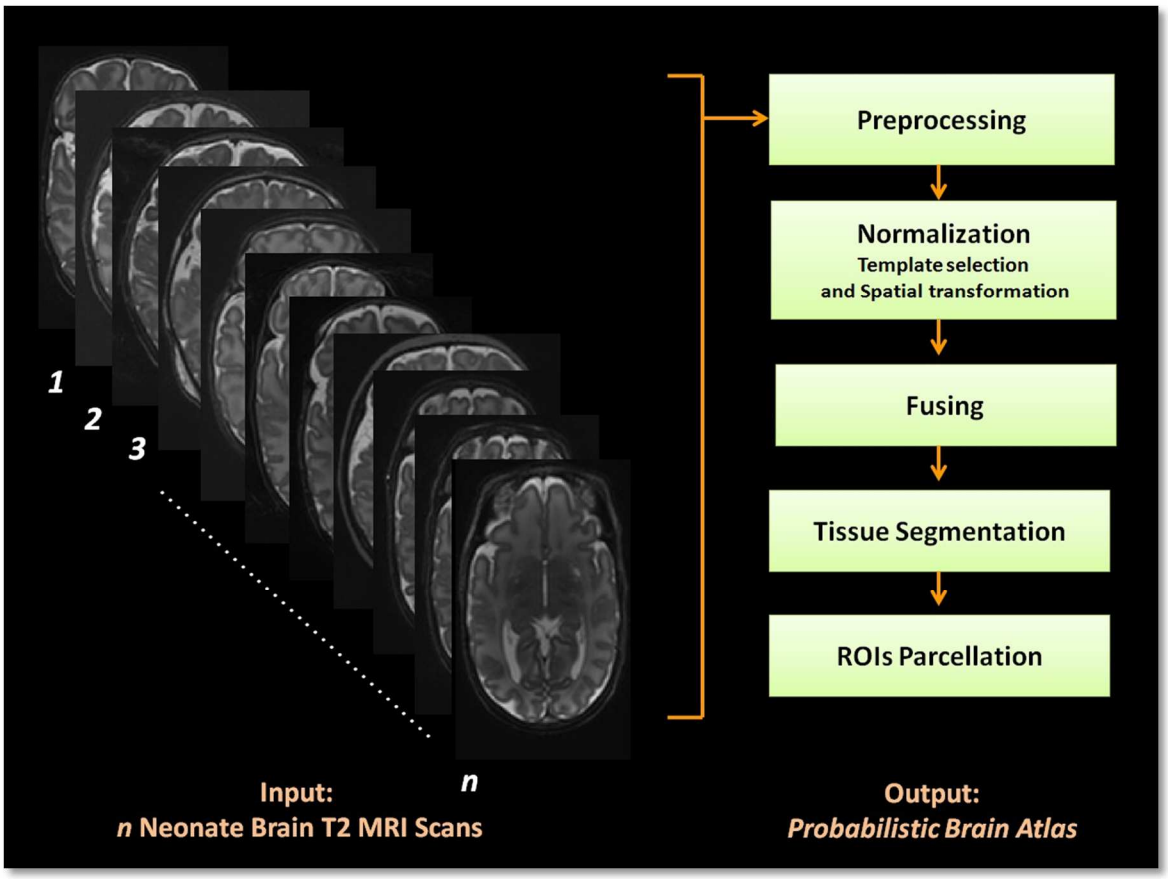

Figure 2.3. Pipeline of probabilistic developing brain atlas construction stages.

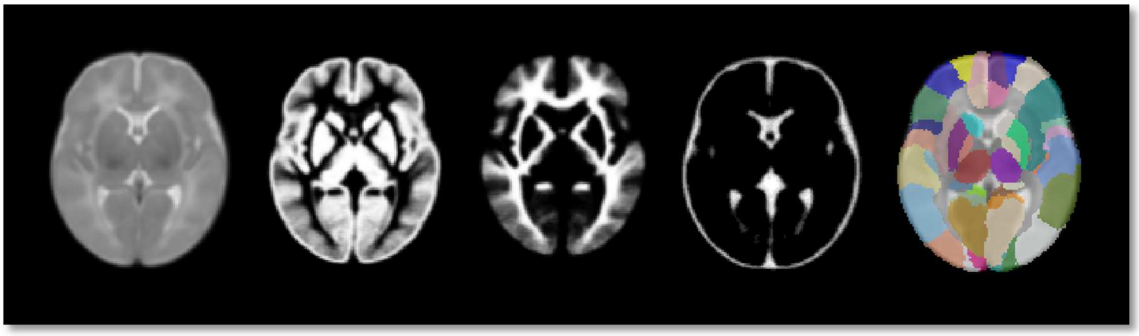

Figure 2.4. Two-year-old brain of UNC infant atlas [74], from left to right: T1-weighted image, CSF, GM, WM, and anatomical parcellation map.

Step 1: Preprocessing

MRI is the most useful modality for constructing brain atlases since it offers a non-invasive window to look into the human brain. Because early age developing brain T2-weighted MRI image has better tissue contrast than T1-weighted MRI image, most of the developing brain studies use T2- weighted MRI in contrast to developed brain studies, which use T1-weighted MRI [111,112]. To construct a brain probabilistic atlas from *n* MRI scans, all the non-brain tissues and organs, e.g. skull and eyes, need to be removed from each scan. Usually, either the Brain Extraction Tool (BET) [113], Brain Surface Extractor (BSE) [114], or BrainVoyager QX [115] is used for this process. In addition, the resulting brain images are corrected for field inhomogeneity or intensity nonuniformity, where N3 or N4 algorithms are generally used for this correction [21,22]. Sometimes intensity rescaling is necessary to compensate for intensity differences between scans [116]. To construct probability maps in addition to the atlas, special kinds of brain segmentations algorithms are needed. Different probability maps require different segmentations, either tissue segmentation or ROIs segmentation. Depending on the age of the studied group, this segmentation is done manually, as for example, the case of fetal brain ROIs segmentation, or by utilizing some developed

algorithms and available tools or priors such as FSL [117], SPM [118], or FreeSurfer [119] like in the case of adult tissue and ROIs segmentations.

After preprocessing the images, the probabilistic brain atlas estimation problem statement can be clearly defined as follows: given n images taken by a single imaging modality I_i, $i \in [1,n]$, and represented as intensity values $I_i(x)$ we need to achieve a representative image for the n scans, $\hat{I}$, having two goals in mind: 1) $\hat{I}$ requiring the least energy to deform into each image of the population I_i and 2) $\hat{I}$ retaining sufficient information from each image I_i that authorize it to represent the population. The first goal is met through normalization step, and the second goal is met through the fusing step.

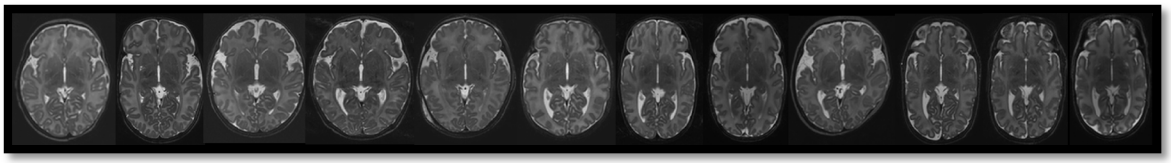

Figure 2.5: T2 mid-axial slices are presented to demonstrate the variation of natural brain shape within a population of 12 healthy neonates [72] aging 37–43 GA weeks.

Step 2: Normalization

The aim of the normalization step is to map all the scans into a common space. Each scan represents one subject at a specific time, and each subject has unique brain structure as shown in Figure 2.5. In order to build a reference brain atlas from many scans, these scans need to be aligned in a unified space. Normalizing brain scans of single imaging modality, e.g. MRI, utilizes registration techniques. For registration, two important factors need to be specified: 1) the choice of the *common space*, which is also referred to as *template*, *target* or *reference*; and 2) the type of *spatial transformation* needed, or in other words the *DOF* level for the required alignment.

1) Common Space Selection

Since we have many scans from which an atlas is built, mapping them into a common space, or template, in the normalization step is important to account for variability of individual morphology. The template selection is a major topic in medical imaging studies related to atlas construction. Several brain atlas studies reported different selections of templates. In the simplest case, the template is chosen as one subject of the scans as proposed by Evans et al. [120]. However, it is difficult to choose the subject scan that best represents the population as a template; therefore, choosing one could introduce a bias. By bias we mean the resulting atlas is generally optimized so as to be similar to the selected template. Many approaches have been developed to reduce or overcome this bias. For example, Park et al. [121] used Multi-Dimensional Scaling (MDS) [122] to select the most similar subject to the population geometrical mean as the template in order to reduce the bias. However, while choosing the optimal single subject reduces risk of bias in the final registration, it does not totally overcome it. Seghers et al. [116] used pairwise registration between all pairs of subjects in the population, where a single subject image is deformed by averaging all the estimated deformations between it and its pairs in the population images. However, pairwise registration is computationally expensive especially with large number n. Avants and Gee [123], Joshi et al. [124], and Bhatia et al. [125] proposed groupwise registration of all scans into a hidden mean space simultaneously, which will result in an atlas that is optimized to be similar to the population-average. Avants et al. [126] employed diffeomorphisms transformation space to iteratively generate the template by averaging the minimum shape distance between the images and the initial template.

However, a template-free registration approach is proposed by Miller et al. [127] using entropy based groupwise registration method where they use the sum of entropies along pixel stacks of the *n* images as a joint alignment criterion. Building on this registration approach, Rohlfing et al. [128] constructed a template-free brain atlas using unbiased non-rigid registration algorithm similar to the one proposed by Balci et al. [129]. Balci et al. extended Miller's approach to include B-splines-based free-form deformations in 3D and stochastic gradient descent-based multi-resolution setting optimization [129]. Lorenzen et al. [130] utilized Fréchet mean estimation and large deformations metric mapping to form an unbiased statistical framework for brain atlas constructing. While, Jia et al. [131] made use of hierarchical groupwise registration framework where iteratively each subject image is restricted to deform locally with respect to its neighbors' images within the learned global image manifold.

2) Spatial Transformation Types

The selected template will play the role of the target in the image registration process [132]. The aim of image registration is to find the spatial transformation *X* that maps points of the source image, also called the float, to the corresponding points of the target image, also called the reference. Registration is used in correlating information obtained from same or different imaging modalities, like PET or MRI scans. In addition, registration is a very valuable tool for tracking time series information about the development of an organ, or of a disease. In the context of brain atlas construction, which usually uses single imaging modality (hence MRI), we focus on intra-modality registration techniques.

Generally, MR images are obtained by sampling a 3D intensity volume of voxels into a discrete grid of points. To register two MR images the source S and the target T, a transformation X is estimated to align S points into T points; $X: (x_S, y_S, z_S) \rightarrow (x_T, y_T, z_T)$. Registration is an iterative process where individual iteration consists of many stages such as similarity computation, interpolation, regularization and optimization. A similarity metric is used to pair S and T points by measuring the intensity similarity or minimizing distance between point pairs after a single iteration. When registering images, interpolation is needed to obtain intensity where a transformed S point is located on a non-grid position on T image. The topology is assumed to be preserved when transforming similar images such as brain images. Also, transformation is constrained to be smoothed by regularization.

The registration problem can be classified into three broad categories based on the type of spatial transformation; rigid (also called linear), affine, and non-rigid (also called non-linear or deformable) registration (see Figures 2.6 and 2.7). The needed spatial transformation depends on the problem at hand and the nature of the images being registered. In case we want to register rigid structure of the same subject in two images, linear alignment is enough. But if we want to register same structure of two different subjects, affine transformation is needed. Additionally, if we want to register soft tissue of non-rigid structure that varies across subjects, non-linear transformation is necessary. These three registration categories are discussed in details in section 2.3.2.

Step 3: Fusing

Now that we have all brain scans normalized into one common space, each denoted by $\bar{I}_i$, we need to fuse their information to produce one template atlas $\hat{I}$. It

should be noted that the variations in brain position in space is taken care of as the normalization step corrects for differences in location. Furthermore, in case of using affine and non-rigid registration, a correction is made to accommodate head size or head shape differences.

Several techniques have been employed to fuse the information of all the normalized images, such as weighted [133] or uniform averaging [134], voting, patch-based voting and sparse-based learning. Usually, all normalized images are treated equally voxel-by-voxel to construct the atlas by averaging the correspondence voxels [71,132]. To achieve better atlas construction, weighted averaging based on similarity measure between voxels can be used, as demonstrated in equation (2.1) where w_i is the weight of the i^{th} normalized image $\bar{I}_i$:

$$\hat{I}(x) = \frac{\sum_{i=1}^{n} w_i \bar{I}_i(x)}{\sum_{i=1}^{n} w_i} \tag{2.1}$$

In fact, if an outlier is present in the population used to create the atlas, the level of representation of the atlas to the population will be reduced [109]. To overcome this problem, dictionary-based learning can be utilized such that a synthetic image is learned by looking-up similar patches in a dictionary. Recently, Shi et al. used batch-based dictionary in group sparsity framework to construct an atlas, where the neighbors of the voxel in 3D patch of all subjects participate to vote for that voxel value in the resultant atlas [109]. This method preserves finer anatomical details in the constructed atlas [109].

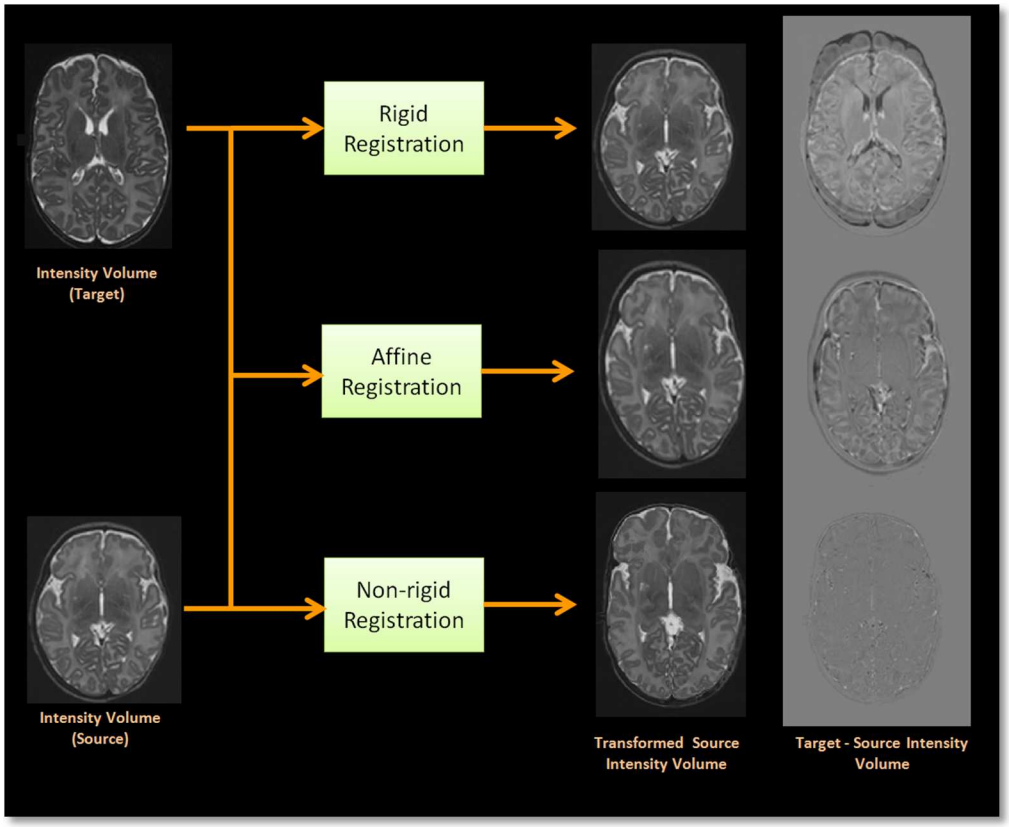

Figure 2.6: Comparison of different registration types between two neonates brain T2 MRI scans. Top row: The source brain is rigidly aligned to the target brain (6 DOF) and the difference between the two scans is extreme due to each neonate having different brain size. Middle row: The source brain is affinely aligned to the target brain (12 DOF). This alignment corrects for the brain size differences while preserving the convolution patterns inside the source brain. Bottom row: the source brain is non-rigidly aligned to the target brain and optimized to look similar to it. The difference between the target and the deformed source is minimal in the case of non-rigid registration.

In the case of constructing 4D brain atlas, usually referred to as spatio-temporal or longitudinal atlases, where time is the fourth dimension, special care of the time parameter is needed. Hence, time plays a significant role in dividing the population into groups. Each group of images are fused together to construct the targeted group atlas, which represents one time in the spatio-temporal atlas. Time dependent kernel regression [135] is used to estimate the weight of each scan in the population-average. Hence, Gaussian kernel is used to produce the weight w to the k^{th} scan at time t as given in equation (2.2):

$$w(t_k, t) = \frac{1}{\sigma\sqrt{2\pi}} e^{\frac{-(t_k - t)}{2\sigma^2}} \quad (2.2)$$

Accordingly, the average atlas at time *t* is given by equation (2.3):

$$\hat{I}^t(x) = \frac{\sum_{i=1}^{n} w(t_i,t)\bar{I}_i(x)}{\sum_{i=1}^{n} w\,(t_i,t)} \quad (2.3)$$

Davis et al. [136] and Ericsson et al. [137] used time-dependent kernel regression in order to construct spatio-temporal atlases by which they made the contribution of the subjects closer to the template time higher than far away subjects. Similarly, time-dependent kernel regression and Gaussian weighted averaging are employed to construct the spatio-temporal neonates atlas with constant kernel width σ as in [30,138,139] and with variant width σ as in [140].

2.2.3.1. Multi-channel Brain Atlases

Brain tissue segmentation is the process of assigning each pixel in the MR images, or voxel in the MRI volume, to a tissue class in the brain, either GM, WM, or cerebrospinal fluid (CSF) based on physiological properties. Parcellation, as defined previously, is the process of segmenting the brain image into different structures, referred to as ROIs, based on specified knowledge. Both processes are needed by which we delineate a structure or tissue on medical imaging data either to visualize it or to identify it in pathological reports. By adding the tissue and/or structure segmentation into the brain atlas construction, multi-channel brain atlases are produced.

2.2.4. Developing Brain Atlases

Before we report the developing brain atlases available in literature, and techniques in constructing them, it is important to describe how these developing brain MRIs are tissue segmented or ROIs labeled.

2.2.4.1. Developing Brain Atlases with Tissue Segmentation

MR images represent intensities where each intensity range falls within a specific tissue type (GM, WM, CSF), allowing us to segment the tissue. In the case of developing brain, the intensity change of WM during the myelination process imposes a challenge for its segmentation. In addition, the differences in the intensities range from one scanning protocol to another and the large overlapping between tissue intensities in MR images complicate the process and postulate the need for spatial prior information to initialize the segmentation process. This spatial prior is built by collecting manual segmentations done by experts, or automatic segmentation done by developed algorithms, and fusing them into a common space, for example, using a probabilistic brain atlas with tissue segmentation maps. Most of the neonatal brain developing image segmentation used an atlas as prior to guide the segmentation [36,141-145]. Some studies address this intensity variability using probability density function (PDF) non-parametric estimation or a mixture of Gaussian (MoG) modeling. In general, atlas based segmentation algorithms performs two steps. Step one involves registering the tissue segmented atlas into the brain in query for segmentation. Step two includes segmenting the query brain using the segmented atlas priors. Some brain segmentation studies have performed the two steps sequentially [146-148], while other studies have performed them jointly [149-152].

Weisenfeld and Warfield proposed fused classification algorithm to automatically learn the subject specific tissue class-conditional PDFs [145]. They used tissue segmented atlas as reference to obtain the prior tissue information, and employed MRF prior in a neighborhood around each pixel to account for spatial homogeneity [145]. Further, they differentiated between myelinated WM and unmyelinated WM classes [145]. Anbeek et al. made use of K-nearest neighbor (k-NN) classification to segment the neonatal MRI by employing voxel coordinate and voxel intensities as features for the classifier [153]. Habas et al. [154] constructed a probabilistic fetal spatio-temporal atlas with tissue maps by utilizing the Expectation Maximization (EM) classification [155], where the brain scans are manually tissue segmented, and the atlas tissue segmentation maps are produced by tissue class membership modeling after normalizing all the scans. Also, Kuklisova-Murgasova et al. [30] built a probabilistic neonatal spatio-temporal atlas with tissue maps by incorporating the prior information into the EM algorithm. They extended the method to refine the partial volume misclassification between tissue boundaries like CSF-GM boundary. Similar to Kuklisova-Murgasova et al., Serag et al. [112] developed a probabilistic neonatal spatio-temporal atlas while employing non-rigid registration in the normalization step instead of affine registration. Serag et al. used Free-Form Deformation (FFD) based non-rigid pairwise registration in the normalization step with variant kernel regression in the fusing step. In addition, Serag et al. [112] created a probabilistic fetal spatio-temporal atlas using the same approach of the neonatal construction albeit having the prior segmented manually. Schuh et al. [139] also used the prior tissue segmentation information to construct neonatal spatio-temporal atlas with probabilistic tissue maps

similar to Serag et al., differing by using parametric diffeomorphic deformation registration algorithm and with fixed kernel width. Shi et al. [111] used late time (2 years) tissue segmented brain atlas to segment early time (1 year and neonate) brain atlases. They segmented the late time brain atlas using fuzzy segmentation algorithm [142], after which the segmentation is carried into earlier time using a joint registration-segmentation framework that incorporates EM algorithm [149,150].

On the other hand, some studies segmented the developing brain without using an atlas as prior information. Song et al. [156] used fuzzy nonlinear Support Vector Machines (SVM) [157] to learn the intensity-based prior from training data, then incorporating this prior in the Maximum-a-Posteriori (MAP) within a graph-cut framework [158] to obtain the segmentation. Xue et al. [159] adopted EM-MRF scheme for tissue segmentation after reducing the partial volume effect by incorporating a knowledge-based prior in each iteration of the EM algorithm, resulting in correction of the boundaries of the CSF-GM and CSF-background. However, a problem arises in purely intensity-based methods such that they are prone to systematic misclassifications when the distributions of WM and GM tissue classes overlap.

2.2.4.2. Developing Brain Atlases with Parcellation

In spite of parcellation methodology, and as in the case of brain tissue segmentation, some parcellation techniques used prior information encoded in an atlas, while others depend on data-driven information without incorporating an atlas [160,161]. For developing brains, due to rapid brain development during gestational time, the use of adult or even pediatric atlases as prior information to parcellate the

developing brain is not suitable and will introduce a bias. There is a need for providing a specialized prior for developing brain parcellation. Historically, parcellating the developing brain was done manually. Manual parcellation involves knowledge in different disciplines such as: brain geometry and region landmark, relationship between structure and function, cytoarchitectonics and myeloarchitectonics, and radiology [92]. Gilmore et al. used anatomy experts to manually parcellate the brain of 74 neonates into 38 ROIs for the purpose of studying the GM growth and the asymmetry in the neonatal brain [70]. In this study, the individual parcellation maps are used to compare individual brains. Oishi et al. manually parcellated an atlas built from 25 neonate into 122 ROIs [71]. Gousias et al. designed a delineation protocol to manually parcellate the brains of 20 preterm and term neonates into 50 ROIs based on macro-anatomical landmarks [72]. In this work, all brains were segmented region by region by the same rater instead of brain by brain. The result includes 20 templates of neonate brains with their parcellation maps, called a label-based encephalic ROI template (ALBERT). Out of these 20 parcellation maps, Gousias et al. constructed different atlases based on the age at scan using pairwise registration and label fusion [73]. The result consists of 40 atlases where each atlas is the result of label fusion of the remaining 19 ALBERTs (20 atlases), 14 ALBERTs in the cases of preterms (15 atlases), or 4 ALBERTs in the cases of terms (5 atlases). However, these atlases are not internet accessible or available; only the 20 templates of the individual with manual parcellation maps are internet accessible.

Manual parcellation is time and labor intensive and can suffer from intra- and inter- rater differences and disagreements [92]. Therefore, Automated Anatomical

Labeling (AAL) is desirable. The first publically available neonate automatically parcellated atlas was constructed by Shi et al. and called UNC Infant 0-1-2 Atlas [74]. This neonate parcellated atlas is part of infant atlas ranging from neonate to one to two years old. In this atlas, the adult parcellation map of MNI called Colin27 (average of 27 subjects) with 90 ROIs was warped into each subject of the two year old images (total is 95 subjects) in order to propagate the labels by using a hierarchical nonlinear deformable registration algorithm called HAMMER [162]. Then, labels are propagated from two years to one year old, then to neonate, using the correspondences established by longitudinal deformation fields. The parcellation maps of all subjects per age are then fused together using majority voting to generate one parcellation map per age. The resulting neonate parcellated atlas represents only one age, 41 GA week. Recently, Alassaf and Hahn [163] proposed a method to carry on this neonate one age parcellation map prior of Shi et al. into other GA weeks in the spatio-temporal atlas of Serag et al. Their longitudinal method depends on modeling the shortest path of growth from one week surface to another as rays. Each ray is originating from the unlabeled surface week and intersecting the labeled surface week, where the label propagation is based on optimizing ray-triangle intersection framework, resulting in parcellating spatio-temporal neonatal atlas of 28-44 GA weeks.

Without using an atlas as prior, Shi et al. proposed a multi-region multi-reference neonate atlas construction by parcellating the brain population-average atlas into 76 different ROIs using watershed algorithm [164], then used affinity propagation [165] to cluster the ROIs. The result is used within a joint registration-segmentation

framework to parcellate new query brain, resulting in subject-specific parcellated atlas [161].

Having described brain atlas construction, segmentation, and parcellation techniques, the following section will present a literature review on existing developing brain atlases, their properties, and the employed techniques in constructing each of them.

2.2.4.3. Developing Brain Atlases Available in Literature

Brain atlases for neonate at one age exist in the literature. Gilmore et al. utilized FFD based non-rigid registration to construct one probabilistic neonate brain atlas using 74 MRI brain scans of neonate aging between 38.8 to 47.8 GA weeks with manual parcellation map of 38 ROIs [70]. Weisenfeld and Warfield used affine registration to construct one probabilistic neonate brain atlas using 15 subjects at 42 GA week with tissue segmentation maps [145]. Similarly, Oishi et al. used affine registration among 25 neonates ranging in age between 38 and 41 post-conceptional weeks to construct a probabilistic atlas with manual parcellation into 122 ROIs [71]. For Gousias et al., pairwise registration and label fusing were used to construct different atlases out of 20 manually parcellated scans of neonates, 15 subjects aged between 37 and 43 postmenstrual weeks, and 5 subjects aged between 39 and 45 postmenstrual weeks [73]. Their manual parcellation delineated 50 ROIs. Shi et al. used groupwise registration diffeomorphic non-rigid registration to construct a probabilistic brain atlas out of 73 neonates aging roughly at 41 GA week with tissue segmentation maps [109]. List of these single time neonatal atlases are presented in Table 2.1.

Table 2.1. Neonatal Developing Brain Single time Atlases

Atlas/ Year	# of Subjects	Age Range	Probability map (Tissue segmentation)	Label Map (ROI Parcellation)	Bias?	Available online	Used Registration
Gilmore et al., 2007 [70]	74	38.8–47.8 GA weeks	No	Yes manually to 38 ROIs	-	-	Nonlinear (FFD) using mutual information (MI)
Weisenfeld and Warfield, 2009 [145]	15	42 GA	Yes, GM, CSF, myelin WM, unmyelinated WM, and subcortical GM	No	-	-	Affine
Oishi et al. 2011 [71]	25	38–41 post-conceptional weeks(0–4 days)	-	Yes manually to 122 ROIs	-	http://lbam.med.jhmi.edu/ Or www.mri.kennedykrieger.org	Affine
Gousias et al. 2012 [72]	20	postmenstrual 15 in 37–43 weeks and 5 in 39–45 weeks	-	Yes, to 50 ROIs	-	http://biomedic.doc.ic.ac.uk/brain-development/index.php?n=Main.Neonatal3	Manually
Gousias et al. 2013 [73]	20	postmenstrual 15 in 37–43 weeks and 5 in 39–45 weeks	-	Yes to 50 ROIs	No	-	Pairwise registration and label fusion
Shi et al. 2014 [109]	73	postnatal 24±10 (9–55 days) (≈41 GA Week)	Yes for GM, WM, CSF	No	No	-	Groupwise Nonlinear registration (Diffeomorphic Demons)

Most recently, population based longitudinal atlases have begun to emerge for developing brain. Many studies have been conducted to construct longitudinal neonatal brain atlases. The first attempt to create 4D neonatal atlas was by Kazemi et al. [160], who used 7 neonates of 39 to 42 GA weeks to construct two templates; one from 39-40 GA weeks and the other from 41 to 42 GA weeks by performing non-rigid registration into a template and then averaging the voxels. Habas et al. constructed a spatio-temporal atlas with tissue maps for fetal brain using tissue probability maps prior and kernel regression from 20 fetuses with age range of 20.5 to 24.7 weeks GA [166].

Kuklisova-Murgasova et al. developed a 4D probabilistic atlas with tissue maps of neonates that covers the range of 29 to 44 GA weeks by using regression kernel and affinely registering the subjects into an average space [30]. Serag et al. used pairwise non-rigid registration and kernel regression to produce a 4D probabilistic multi-channel atlas out of 204 neonates and 80 fetuses that cover the range of 28 to 44 GA weeks and 23 to 37 GA weeks, respectively. Shi et al. constructed a longitudinal infant atlas at birth (neonate), one year old, and two years old from 95 infants using groupwise nonlinear registration with tissue and parcellation maps. Schuh et al. constructed a neonatal 4D atlas of 118 subjects using pairwise parametric diffeomorphic deformation and kernel regression with tissue maps. Gholipour et al. constructed a 4D atlas of 40 fetuses using symmetric diffeomorphic deformation and kernel regression [138]. Table 2.2 provides a list of available 4D fetal and neonatal probabilistic atlases.

Table 2.2. Developing Brain Spatio-temporal and Longitudinal (4D) Atlases

Atlas/ Year	# of Subjects	Age Range	Fetal (Fet.) /Neonatal (Neo.)	Probability map (Tissue segmentation)	Label Map (ROI Parcellation)	Bias?	Available online	Used Registration
Kazemi et al. 2007 [160]	7	39 – 42 GA weeks	Neo.	No	No	Yes	http://www.u-picardie.fr/labo/GRAMFC	Nonlinear (squared difference minimization)
Habas et al. 2009 & 2010 [166]	20	20-24 GA Weeks	Fet.	Yes, GM, WM, the germinal matrix and ventricles	No	No	-	Nonlinear (template-free, groupwise), kernel regression
Kuklisova-Murgasova et.al. 2011 [30]	142	29-44 GA weeks	Neo.	Yes for six Structures: cortex, white matter, subcortical grey matter, brainstem, cerebellum and cerebro-spinal fluid	No	No	www.brain-development.org	Affine, pairwise, kernel regression
Serag et al. 2012 [140]	204	28-44 GA weeks	Neo.	Yes for GM, WM, CSF	No	No	www.brain-development.org	Nonlinear (FFD), pairwise, kernel regression

Serag et al. 2012 [140]	80	23-37 GA weeks	Fet.	Yes for GM, WM, CSF	No	No	www.brain-development.org	Nonlinear (FFD), pairwise, kernel regression
Shi et al. 2011 [74]	95	Neo- 1-2- years (38.7 - 46.4 GA weeks)	Neo.	Yes for GM, WM, CSF	Yes to 90 ROIs (Using MNI Colin 27)	No	http://www.med.unc.edu/bric/ideagroup/free-softwares/unc-infant-0-1-2-atlases	Nonlinear using feature-based groupwise registration algorithm
Gholipour et al. 2014 [138]	40	26 - 35 GA weeks	Fet.	-	No	No	crl.med.harvard.edu/research/fetal brain atlas/	Nonlinear (symmetric diffeomorphic deformation), kernel regression
Schuh et al. 2015 [139]	118	28-44 GA Weeks	Neo.	Yes for GM, WM, CSF	No	No	-	Nonlinear (parametric diffeomorphic deformation), pairwise, kernel regression

2.3. Background

2.3.1. MRI Surface Construction

Segmenting the brain tissues (GM, WM, and CSF) in any MRI results in a mapping of tissue value at each voxel. This mapping allows for constructing a specific surface for each tissue. Cortical surfaces of the brain can be constructed to visualize the CSF-GM border or GM-WM border. These surfaces can be generated from the tissue classified MR images using Marching Cubes algorithm [167]. In general, Marching Cubes algorithm extracts polygonal or triangular mesh of iso-surface from three dimensional (3D) scalar volume of voxels. By specifying tissue value, cube is marching the volume voxels and determining whether or not each voxel belongs to this tissue. If all cube corners belong to this tissue, the voxel is below the iso-surface. If there is no match at any of the cube corners, the voxel is above the iso-surface. If there is partial matching, the surface is passing through the voxel. By interpolating values along the cube edges, polygons can be constructed and later fused together to generate the final

iso-surface that represents this tissue. The cortical surfaces used in this dissertation are constructed from the GM-WM border (referred to as WM surfaces).

2.3.2. Image/Surface Registration

Registration is introduced in 2.2.3. The aim of image/surface registration is to find the spatial transformation that maps points of the source image/surface, also called the float, to the corresponding points of the target image/surface, alscalled the reference. To register two MR images/surfaces the source S and the target T, a transformation X is estimated to align S points into T points; $X : (x_S, y_S, z_S) \rightarrow (x_T, y_T, z_T)$.

There are three broad categories of spatial transformation; rigid (also called linear), affine, and non-rigid (also called non-linear or deformable) registration. These three categories are explained next. More types of transformation (shown in Figure 2.7) are occasionally needed for special registrations.

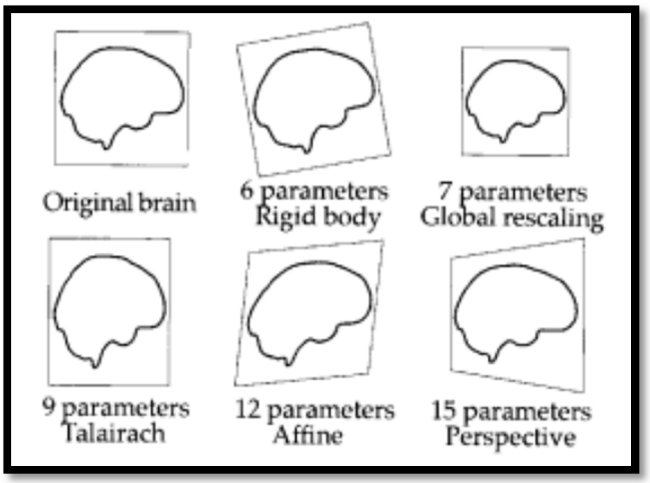

Figure 2.7. Linear Transformation Models (Source: [76]).

2.3.2.1. Rigid Transformations

Three-dimensional (3D) rigid transformation has six degree of freedom (DOF) and can be described by a translation vector $\boldsymbol{d}$ and 3x3 orthogonal rotation matrix $\boldsymbol{R}$ for any given point $x = (x, y, z)^T$ as in equation (2.4):

$$X_{rigid}(x) = \boldsymbol{R}x + \boldsymbol{d} \tag{2.4}$$

These transformations preserve the points being transformed and the distance between them.

2.3.2.2. Affine Transformations

Three-dimensional (3D) affine transformation has twelve DOF considering the sheering and the scaling beside the translation and the rotation. When the transformation and the rotation are insufficient to align the source into the target, 3D affine transformation is needed. Affine transformation is described by a translation vector $\boldsymbol{d}$ and 9 parameters matrix $\boldsymbol{M}$ encoding rotation, scaling and shearing for any given point $x = (x, y, z)^T$ as in equation (2.5):

$$X_{affine}(x) = \boldsymbol{M}x + \boldsymbol{d} \tag{2.5}$$

These transformations preserve collinearity but do not preserve the distance between the points being transformed, as the scales could enlarge or minimize it, and as the shears could shift the points parallel to an axis.

2.3.2.3. Non-rigid Transformations

Both rigid and affine transformations provide global transformation effect, where the same transformation parameters are applied on all points. Non-rigid transformations increase the DOF locally by providing local effect at each point. Non-rigid registration is needed when the structure being registered varies inter- or intra- subject such as soft tissues. Complex differences in objects shapes can be described by simple space deformations where the objects are treated as fluid [168] or elastic [169]. The general non-rigid transformation equation (2.6) is composed from two parts: global transformation, part, usually affine, to align the images, and local transformation part to deform the images locally:

$$X_{non-rigid}(x) = X_{global}(x) + X_{Local}(x) \tag{2.6}$$

In non-rigid registration, every position in S image/surface is mapped into a single corresponding position in T image/surface. Three main techniques are developed for non-rigid image registration: B-spline FFD [170], Demons [171], and large deformation diffeomorphic metric mapping (LDDMM) [172]. The most famous non-rigid surface registration algorithm is Iterative Closest Point algorithm (ICP) [173,174] which has many variants [175-177]. In general, non-rigid registration method is iterative, combining in each iteration an applied similarity criteria between S and T and a calculated geometric transformation. Iterations' transformations can be composed and they have two important characteristics, which are smoothness, to preserve the contour of the deforming object, and invertibility, to allow both forward and backward registration (from T to S). Different similarity metrics are used in non-rigid registration including sum of

square differences (SSD) or cross correlation (CC) for intra- or monomodality registration, joint entropy (JE), mutual information (MI) or normalized mutual information (NMI) for inter- or multimodality registration. Some can be used for both monomodality and multimodality like MI and NMI [178]. For more details a survey can be found in [179,180] for image registration, in [181,182] for surface registration, and in [183] for similarity metrics. Since the non-rigid image transformation used in this work is based on FFD, and since the surfaces in this work are parcellated without deforming them, brief descriptions of FFD and ICP are necessary.

In FFD, a 3D lattice of uniformly spaced control points is embedded into the 3D volume of MRI. Manipulating the lattice will then manipulate the contained 3D volume (see Figure 2.8). Each point in each image experiences a displacement proportional to convolving the control point vectors of the voxel containing it with a B-spline kernel, which will provide local deformations that are globally continuous and smooth. The spacing along each dimension δ_x, δ_y, δ_z specifies the degree of locality for each deformation. By using *i, j, k* as subscripts to index the location of a control point within the lattice $\varphi_{i,j,k}$, the local displacement on any point $x = (x, y, z)^T$ is described by a B-spline tensor product over the local control point as shown in equation (2.7):

$$X_{\text{local}}(x) = \sum_{l=0}^{3} \sum_{m=0}^{3} \sum_{n=0}^{3} B(u)B(v)B(w)\varphi_{i+l,j+m,k+n} \qquad (2.7)$$

where B refers to the cubic B-spline basis functions as in [170], $i = \lfloor x/\delta_x \rfloor - 1$, $j = \lfloor y/\delta_y \rfloor - 1$, $k = \lfloor z/\delta_z \rfloor - 1$, $u = x/\delta_x - \lfloor x/\delta_x \rfloor$, $v = y/\delta_y - \lfloor y/\delta_y \rfloor$, $w = z/\delta_z - \lfloor z/\delta_z \rfloor$.

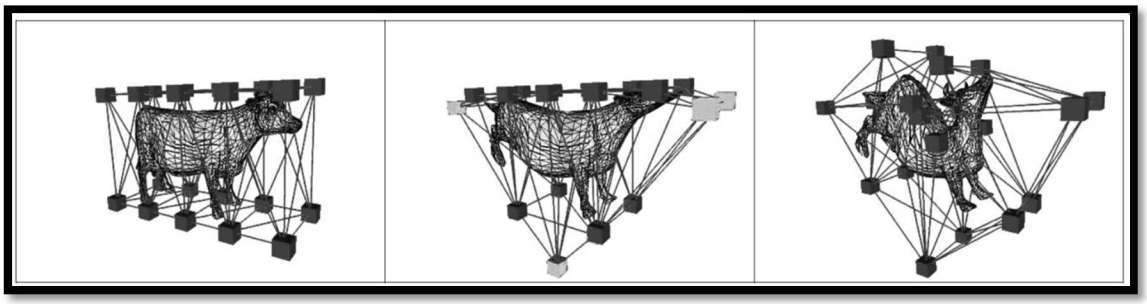

Figure 2.8. Deforming and Pending Cow using FFD (Source: [184]).

In ICP, the least squared distance between points' pairs of two surfaces meshes is minimized to find the best rigid transformation that aligns them together. The linear solution of Horn [185] finds the rigid transformation such that the energy function given in equation (2.8) is minimized:

$$E = \sum_{i=1}^{n} |T_i - \boldsymbol{R}\,(S_i - S_c) - \boldsymbol{d}|^2 \qquad (2.8)$$

where S_c is the centroid of the source mesh. The translation vector $\boldsymbol{d}$ is the offset between the two meshes centroid while the unit quaternion rotation matrix $\boldsymbol{R}$ is the eigenvector corresponding to the largest eigenvalue of the cross-covariant matrix of both meshes after describing all the points with respect to their centroid in each mesh. Different similarity metrics are used to pair n points of T and S. For non-rigid alignment, the process is iterative such that various optimizations are performed in every iteration to pair the points or find the correspondences and use

this pairing to find the best local transformation for each point. Different optimization methods involve different criteria like neighboring point and Jacobean calculation. Therefore, surface non-rigid registration using ICP algorithm is computationally expensive and time consuming.

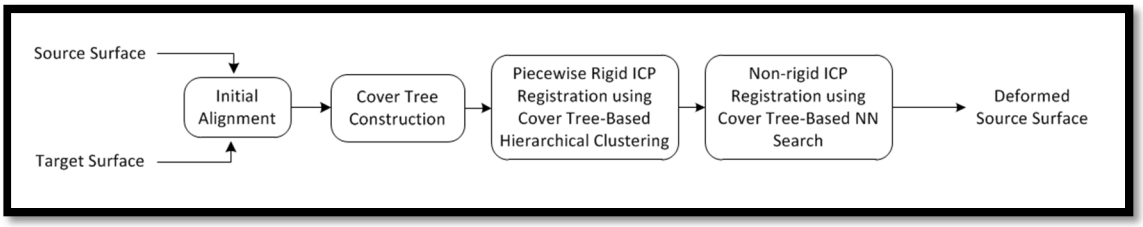

Figure 2.9: Non-rigid registration using cover tree pipeline (Source: [177]).

In our previous work on non-rigid surface registration [177], we proposed a novel non-rigid registration method that computes the correspondences of two deformable surfaces using the cover tree [186]. The aim in that work is to find the correct correspondences without landmark selection and to reduce the computational complexity. As shown in Figure 2.9, the method consists of four steps which are initial alignment, construction of the cover tree, piecewise rigid (p-rigid) ICP registration, and non-rigid ICP registration. In the initial alignment step, the two input surfaces are initially matched by aligning them and scaling the surface S according to the maximum ranges of the points on S and T. After initial alignment, the cover tree is constructed from the points of both surfaces and used for hierarchical clustering and k-NN in the correspondence computation of the p-rigid and non-rigid ICP registration, respectively. The points of the two surfaces are divided into multiple clusters by cutting the cover tree into sub-trees rooted at

nodes of a selected level. The hierarchical clustering based on cover tree helps to establish correspondences of the clusters between two surfaces. For the p-rigid ICP registration, the method finds the correspondence of each source point p among the points in the same cluster which comes from T, q, and has the best correspondence measure given in equation (2.9):

$$\begin{aligned} E_{Corr}(p,q) &= (1-\alpha-\beta)E_{Dist} + \alpha E_{Normal} + \beta E_{Isometric} \\ &= (1-\alpha-\beta)\|p-q\|_2^2 + \alpha n_p \cdot n_q + \beta \sum_k \left| L(p, N_k(p)) - L(q, N_k(q)) \right| \end{aligned} \tag{2.9}$$

The first term E_{Dist} is used to find the closest point by calculating the Euclidean distance between two points. The second term E_{Normal} that indicates the angle between the normal vectors is calculated by inner product of two normalized vectors, n_p and n_q. The third term $E_{Isometric}$ is defined to enforce the two corresponding points that have similar connectivity with the adjacent points N_k. This is measured by calculating the absolute difference between the length L of the connecting edges of p and that of the connecting edges of q.

Once the corresponding point sets on the two surfaces have been determined, each cluster on S is locally transformed to T by minimizing the error between the two point sets. In the non-rigid ICP registration, the candidate correspondences of a given point on S are computed by looking for its k-NN in the cover tree, which are originating from T. A correct correspondence is chosen as the one that has the best correspondence measure among the k nearest points. After determining two correspondent point sets from S and T as P and P', respectively, the deformation D is applied on P to deform it to P' by iteratively optimizing the

energy function E_{DR} given in equation (2.10) that includes a fitting term, a stiffness term, and a Jacobian penalty term:

$$E_{DR}(P', D(P)) = \sum_{i=0}^{N} \omega_i E_{Fit}(p_i', D(p_i)) + \gamma E_{Smooth}(D(p_i)) + \delta E_{Jacobian}(D(p_i)) \quad (2.10)$$

The first term E_{Fit} measures the accuracy of alignment by calculating the distance between P' and $D(P)$. The second error term E_{Smooth} regularizes the deformation by minimizing the sum of differences of the deformation between adjacent points as shown in equation (2.11):

$$E_{Smooth}(D(p_i)) = \sum_{p_j \in N(p_i)} \left\| D(p_j) - D(p_i) \right\| \quad (2.11)$$

The third term $E_{Jacobian}$ regularizes the deformation by assigning penalty to the points with the negative Jacobian determinant. To impose penalty to the points with negative Jacobian and avoid the folding of the deformation, $E_{Jacobian}$ is defined by equation (2.12):

$$E_{Jacobian}(D(p_i)) = c \log(1 - Det(J(D))) \quad (2.12)$$

where $Det(J)$ is the determinant of the Jacobian matrix J, and c is the constant that adjusts the effect of the negative Jacobian term. The constant c is proportional to the distance between p_i and its farthest neighbor. This Jacobian penalty term is applied only for the points with the negative Jacobian. The derivatives of the deformation is normalized by the edge length, $|N(p) - p|$ where $N(p)$ is the adjacent point of p. The Jacobian matrix of the deformation is calculated by equation (2.13):

$$J(T)=\begin{pmatrix} \frac{\partial T_x}{\partial x} & \frac{\partial T_x}{\partial y} \\ \frac{\partial T_y}{\partial x} & \frac{\partial T_y}{\partial y} \end{pmatrix}=\begin{pmatrix} \frac{T_x(N(v))-T_x(v)}{N_x(v)-v_x} & \frac{T_x(N(v))-T_x(v)}{N_y(v)-v_y} \\ \frac{T_y(N(v))-T_y(v)}{N_x(v)-v_x} & \frac{T_y(N(v))-T_y(v)}{N_y(v)-v_y} \end{pmatrix} \tag{2.13}$$

To minimize the E_{DR} between two corresponding point sets P and P', the Levenberg Marquardt optimization algorithm [187] is applied. γ and δ are the parameters that adjust the effect of stiffness term and Jacobian term, respectively. If the stiffness parameter γ is small, the optimization converges quickly to the closest point based on the fitting term. However, the surface mesh becomes very irregular and bumpy. As γ is larger, the deformation is smoother but the optimization becomes slower and the surface may shrink. We set γ to 1. The parameter δ for Jacobian term is set to 1 if the point has a negative Jacobian. Otherwise the value is set to 0. The optimization ends when the termination condition is met. If the reduced error measure after each iteration i, E_{DR}^{i} - E_{DR}^{i-1}, is less than 5% of the error measure E_{DR}^{i}, it is considered that the optimization converges to the optimum. By penalizing the deformation with stiffness term and Jacobian term, the proposed optimization regularizes the deformation so that the deformed surface has smooth deformation with less folding. More details can be found in [177].

Using this method, we analyzed the time complexity of the search to find the correspondence candidates in both stages p-wise registration and non-rigid registration. The correspondence computation time of p-rigid registration was

reduced from $O(n^2)$ to $O(n\frac{1-c^{4d}}{1-c^4})$ and the correspondence computation time of non-rigid registration was reduced to $O(c^{12}\ n\ log\ n)$ according to the following claims:

Claim 1: The correspondence computation using clustering reduces the time complexity of our p-rigid ICP from $O(n^2)$ to $O(nl)$ where l is the number of nodes in the largest cluster.

Claim 2: When applying cover tree-based hierarchical clustering, the number of nodes l in any cluster is upper bounded by $\frac{1-c^{4d}}{1-c^4}$ where c is the expansion constant of the cover tree and d is the depth of the sub-tree that corresponds to a cluster.

Proof:

Each node in the cover tree has at most c^4 children [186]. Assuming the worst case, when the constructed cover tree is balanced and each node has exactly c^4 children, then cutting the cover tree at level i with k nodes will introduce k clusters. Each cluster contains one root node of the sub-tree and all its decedent nodes in all the lower levels from the level i down to the leaves level j. Let d denotes the depth of the sub-tree, i.e. $d = i-j$. The number of the nodes in each cluster is calculated as follows: At level i, d is 0 and each cluster has one node, the root. The total number of nodes at level i is $(c^4)^0 = 1$. At the next level $i-1$, d is 1 and each cluster has at most c^4 nodes which are the children of the root node. The total number of nodes at level $i-1$ is $(c^4)^1 = c^4$. As the level decreases by 1, d increases

by 1 and each cluster at each level has at most $(c^4)^d$ nodes. Therefore, the total number of the nodes in a cluster is calculated using equation (2.14):

$$\sum_{i=0}^{d} c^{4i} = (c^4)^0 + (c^4)^1 + (c^4)^2 + \ldots + (c^4)^d = \frac{1-c^{4d}}{1-c^4} \qquad (2.14)$$

Thus, the number of the nodes l in the largest cluster is upper bounded by $\frac{1-c^{4d}}{1-c^4}$ ■.

Claim 3: The correspondence computation using cover tree-based hierarchical clustering reduces the time complexity of our p-rigid ICP from $O(n^2)$ to $O(n\frac{1-c^{4d}}{1-c^4})$ where c is the expansion constant of the cover tree and d is the depth of the sub-tree that corresponds to a cluster.

Claim 4: The cover tree based NN search reduces the correspondence computation time for non-rigid ICP from $O(n^2)$ to $O(c^{12}\ n \log n)$.

Proof:

Let S and T have the same number of points, n. The time complexity of the cover tree based NN search is $O(c^{12} \log n)$ when the tree is constructed from T. As it takes $O(c^{12} \log n)$ time to find the k-NN for each point on S, the total time complexity for all points on S is $O(c^{12}\ n \log n)$ ■.

Even though this method allowed performing a marker-less registration of two surfaces with less computational time and resulted in accurate deformation, it

is well-known that surface non-rigid registration is generally time consuming and computationally expensive especially with surfaces that have a large number of points. Therefore, we solve the problem of parcellating the brain surfaces of the spatio-temporal atlas 28-44 GA weeks without the need to perform non-rigid registration. In fact, we started tackling the parcellation problem by applying this non-rigid registration method to deform the surfaces and propagate the labels after the deformation, but the problem was solved without the need for expensive computational non-rigid registration, as discussed in Chapter 3.

2.4. Conclusion

The automatic parcellation approaches mentioned in this chapter have been developed for mature brain and are not currently used to automatically and longitudinally parcellate neonatal developing brain atlases at early GA weeks. In fact, if the brain undergoes significant changes in shape, size and structure, as in the case of neonatal brain during early development [24], it has no reliable folding patterns to drive the registration in the case of registration-based parcellation or to rely on in the case of segmentation-based parcellation. Moreover, parcellating it based on a mature brain template introduces a bias since several studies suggested that developing brain analysis needs to be performed independent of mature brain due to significant differences in brain tissue properties, image intensities appearance, and anatomical shapes [30,132,140]. Even though developing brain parcellated atlases reported in this chapter exist in scientific literature, they provide parcellation for a single GA week. No longitudinal parcellation for developing brain that covers early GA weeks exist.

In this dissertation we propose a longitudinal parcellation method for developing brains that is novel, fast, and automatic. The method preserves the surface, without deforming, distorting, or mapping it into a different coordinate system. Also, the method does not rely on any landmark or sulcal depth, and requires only moderate time to perform the parcellation. The parcellation is performed on the brain surface shape three dimensional (3D) coordinate system as opposed to the spherical 2D coordinate system. Also, the parcellation is applied to the whole brain surface as opposed to one hemisphere as in the case of spherical inflation method, and is therefore, suitable to be used with symmetric and asymmetric brain templates. Moreover, the parcellation is done by longitudinally propagating a probabilistic estimation of a labeled neonatal brain atlas at one age of gestation to other gestational weeks using spatial points pairing and temporal points voting without performing the time consuming deformable surface registration.

2.5. Summary

This chapter covers the related work on brain atlases generation and processing, available developing brain atlases, and developed brain parcellation algorithms. It also gives an overview of techniques used throughout the dissertation, such as image/surface registration and parcellation. Also, discussed are the challenges of applying these techniques on the developing brain MRI.

Chapter 3: Methods

Based on:

MH Alassaf, *JK Hahn, "Automatic Parcellation of Longitudinal Cortical Surfaces", SPIE medical imaging. International Society for Optics and Photonics (2015).*

MH Alassaf, *JK Hahn. "Longitudinally Parcellating the Human Developing Brain Cortex". 2015 (In Submission).*

3.1. Introduction

Advances in MRI have facilitated studying brain maturation at the physiological, morphological, and functional levels [24]. Tracking the growth and folds of developing brain regions is important for early detection of disease such as autism, schizophrenia, and epilepsy [9]. Parcellation refers to the process of labeling specific neuroanatomically defined areas using MRI. Originally, cortical parcellation was done manually, a time and labor intensive process [92,94,95], highlighting the need for automation. Automating cortical parcellation has been challenging due to inter-subject cortical geometric heterogeneity, especially in the developing brain as described in Chapter 2.

In this chapter, we present a novel automatic method to parcellate the cortical surface of the neonatal brain at different stages of development. A labeled newborn brain atlas at 41 weeks gestational age (GA) is used to propagate labels of anatomical regions of interest to a spatio-temporal atlas, which provides a dynamic model of brain development at each week between 28-44 GA weeks. The first step involves propagating labels from the cortical volume of the newborn brain to an age-matched cortical surface from the spatio-temporal atlas. Next, we used a novel approach and an energy optimization function to propagate labels across the cortical surfaces of each week of the spatio-temporal atlas by registering successive cortical surfaces. In this procedure, local and global, spatial and

temporal information are incorporated when assigning the labels. As a result, we were able to produce a complete parcellation of 17 neonatal brain surfaces with similar points per labels distributions across weeks.

3.2. Input and Pipeline

In order to label developing cortical structures, we used the three available labeled neonatal brain atlases; the newborn UNC atlas at week 41 GA [74], the ALBERT atlas with 20 newborn infants [70], and the JHU atlas [71], along with the neonatal spatio-temporal brain atlas of weeks 28-44 GA [140] as input. The average age of the ALBERT's 20 subjects is 41 GA week (see Table 3.1 for more details). UNC Atlas parcellation divides the cortex into 90 ROIs, ALBERT atlas parcellation divides the brain into 50 ROIs while JHU atlas divides the brain into 122 ROIs. Details about these ROIs are provided in tables 6.1, 6.2, and 6.3 in Appendix 1.

The proposed method involves three steps (Figure 3.1). Step one involves propagating the labels from the labeled brain atlas to the corresponding age match of the spatio-temporal brain atlas, week 41 as in section 3.3. Second, the labels are propagated from the spatio-temporal atlas volume of week 41 to a constructed WM surface of the same week using proposed volume-surface parcellation, described in section 3.4. Finally, the labels are propagated from the spatio-temporal atlas week 41 surface, among surfaces of the other weeks of the spatio-temporal atlas using the proposed surface-surface parcellation in section 3.5.

3.3. Propagating the Labels in the Volume Space

All UNC, ALBERT, and JHU atlases are provided as 3D volumes of intensities and labels. They need to be registered into the corresponding week, week 41, of the spatio-temporal atlas volume in order to transform the labels into that week. Later in stage two, labels need to be described in surface representation. Stage one of the pipeline is intended to register the volumes.

A labeled volume of a neonate brain atlas parcellation map of week 41 GA, with *C* neuroanatomical regions of interest (ROIs) labels, is registered using FFD [170] to the corresponding week in the spatio-temporal atlas, week 41. This is done by applying FFD registration between the intensity volumes of UNC, ALBERTs, and JHU atlases one at a time as source S, and the intensity volume of week 41 of the spatio-temporal atlas as target T. Then, resultant transformations are used to deform or warp the labels volumes of UNC,

Table 3.1. ALBERT Atlas Subjects Age at Scan.

ALBERT	Gestational Age	Age at scan
1	Term	41.43
2	Term	44.43
3	Term	40.71
4	Term	44.86
5	Term	39.43
6	26.71	41
7	30.57	36.85
8	29.57	36.57
9	26.85	39
10	29	39.85
11	29	39.85
12	28	40.14
13	34.57	43.29
14	29.14	39.14
15	26.85	41.85
16	31.57	43.31
17	26.71	39.57
18	26	41.71
19	32	41.85
20	29	41.29
	Average:	41.36

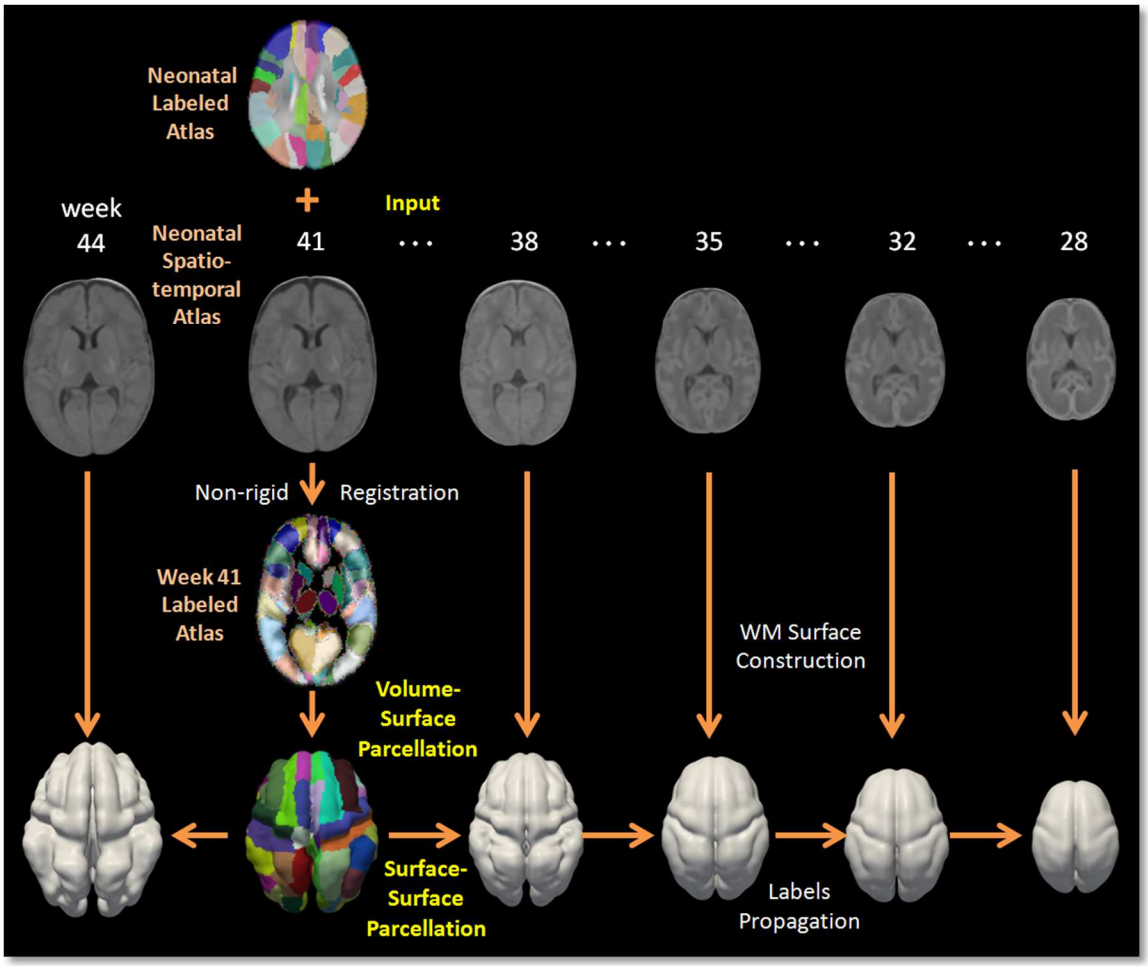

Figure 3.1. Pipeline of the proposed method.

ALBERTs, and JHU atlases into week 41 volume. Hence, the labels are propagated in the volume space as shown in Figure 3.2. In case of the 20 ALBERTs, the normalized transformed label volumes need to be fused together in order to generate one template as shown in Figure 3.3. We used weighted fusing such that each week is assigned a weight based on its temporal location from week 41. The closer weeks to week 41 get higher weights than the distant ones. The weights are specified using equation (3.1):

$$\omega_i = 1 - \left(\frac{1}{longitudinal\ range}\left|\hat{I}^{age} - \bar{I}_i^{age}\right|\right) \tag{3.1}$$

Where $\hat{I}^{age}$ is the average image age, here 41, $\bar{I}_i^{age}$ is image *i* age at scan, longitudinal range is the difference between the first and last time point in the spatio-temporal atlas.

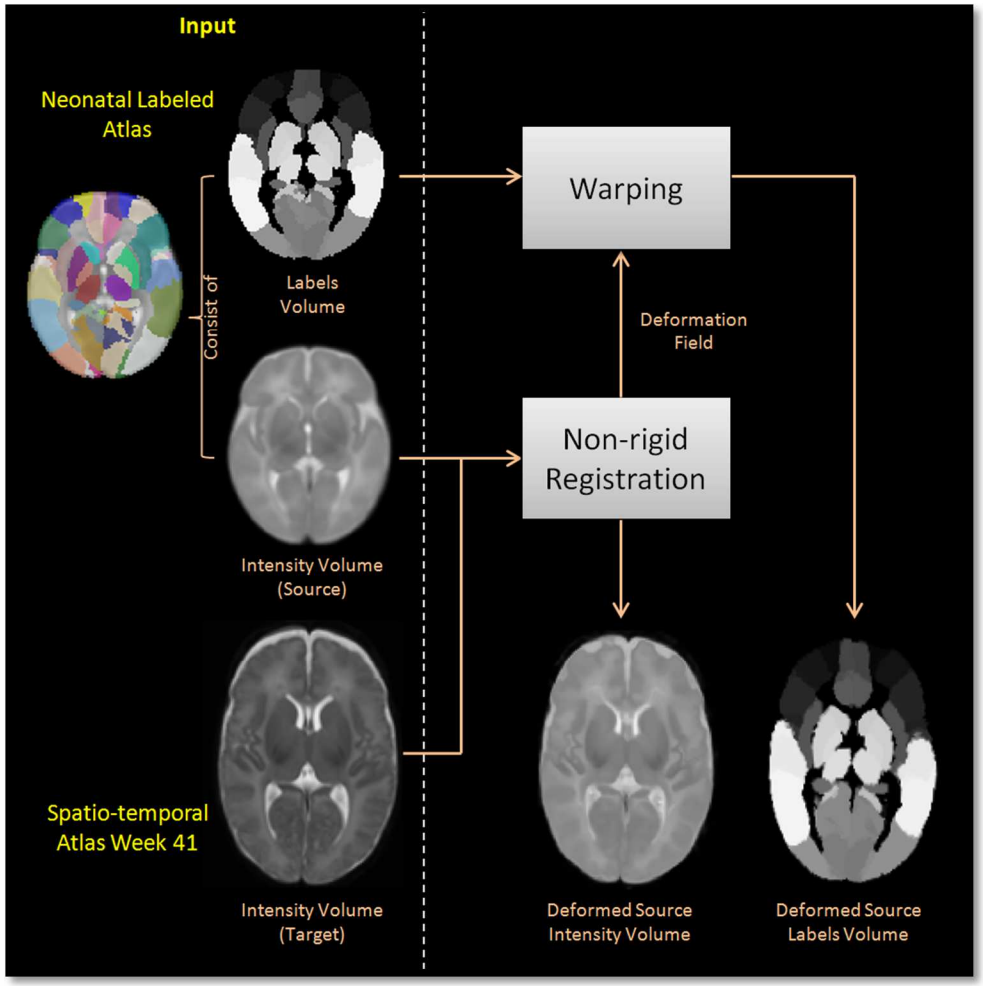

Figure 3.2. Propagating the labels in the volume space.

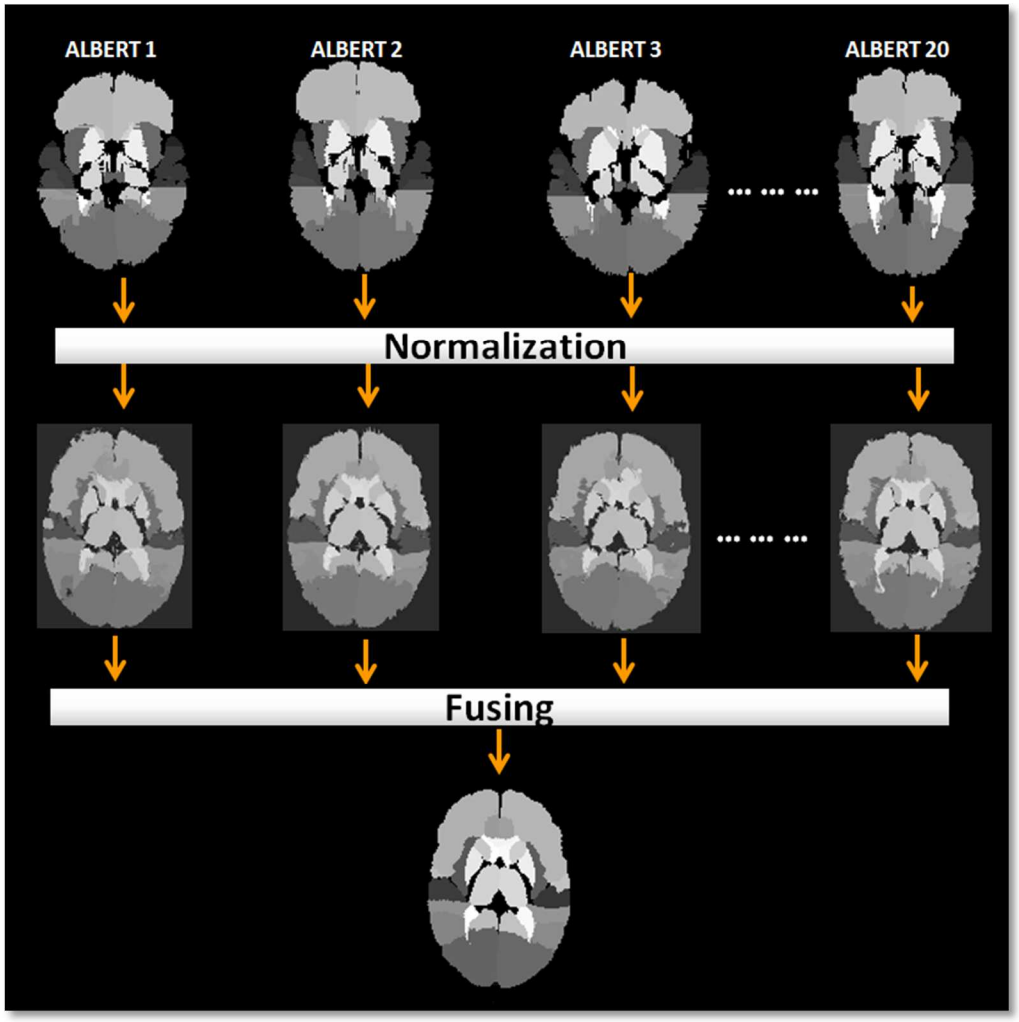

Figure 3.3: ALBERTs' 20 labeled brain normalization and fusing to generate one template.

3.4. Volume-Surface Parcellation

At this stage, week 41 of the spatio-temporal atlas is automatically delineated by labels. A WM surface is constructed from this 41 week intensity volume using Marching Cubes algorithm [167]. To get a smooth surface, the volume is blurred using a Gaussian kernel with $\sigma = 2$ before constructing the surface. The goal of this stage is to find a surface-based representation of the labels from the volume. We start by embedding the surface inside the volume of labels by rigid alignment. Then, for each point p_i on the surface, the

intersection between the surface and the volume determines the label of p_i. Each intersection is located inside a voxel in the volume and the majority of the voxel corners labels is selected as the p_i label. Let Φ be a set that holds the eight corners' labels $f_j, j \in [1,8]$. Labeling p_i is based on C-length weights vector: $w_l, l \in [1, C]$. This weights vector defines a scoring function $p_i \rightarrow w_l.\Phi(f_j)$ and the label associated to point p_i is given by equation (3.2):

$$label(p_i) = argmax_l \; w_l.\Phi(f_j) \tag{3.2}$$

Furthermore, the eight votes are not uniformly distributed among the eight corners. Rather, they are determined based on the location inside the voxel where p_i is located following the trilinear interpolation weighting mechanism. Considering a voxel between two volume grid points $[x_1, y_1, z_1]$ and $[x_2, y_2, z_2]$ as in Figure 3.4:

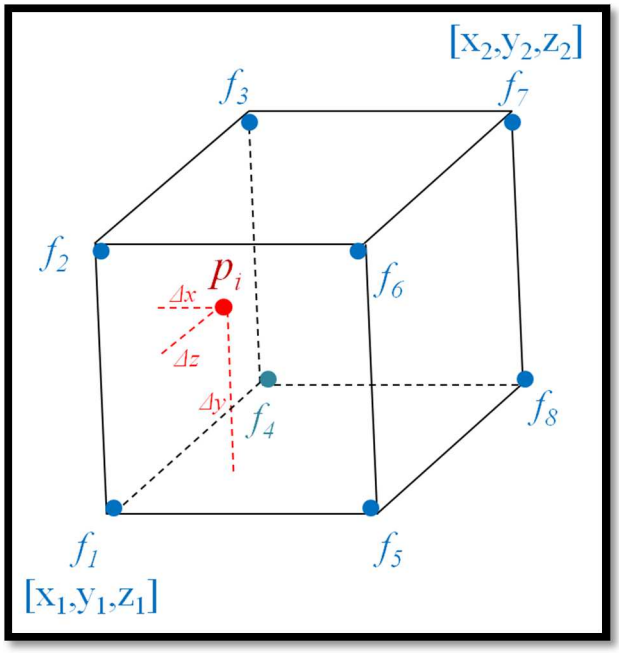

Figure 3.4: Illustration of the localization of a surface point p_i inside a voxel in the volume between two volume grid points $[x_1, y_1, z_1]$ and $[x_2, y_2, z_2]$, the participation of each voxel corner in the voting process is weighted by the location of p_i.

The votes' participation is specified as follows in equations (3.3-3.13):

$$\Delta x = p_i.x - x_1 \tag{3.3}$$

$$\Delta y = p_i.y - y_1 \tag{3.4}$$

$$\Delta z = p_i.z - z_1 \tag{3.5}$$

$$f_1 = (1-\Delta x)*(1-\Delta y)*(1-\Delta z) \tag{3.6}$$

$$f_2 = (1-\Delta x)*\Delta y*(1-\Delta z) \tag{3.7}$$

$$f_3 = (1-\Delta x)*\Delta y*\Delta z \tag{3.8}$$

$$f_4 = (1-\Delta x)*(1-\Delta y)*\Delta z \tag{3.9}$$

$$f_5 = \Delta x*(1-\Delta y)*(1-\Delta z) \tag{3.10}$$

$$f_6 = \Delta x*\Delta y*(1-\Delta z) \tag{3.11}$$

$$f_7 = \Delta x*\Delta y*\Delta z \tag{3.12}$$

$$f_8 = \Delta x*(1-\Delta y)*\Delta z \tag{3.13}$$

If there is no majority, the label of the corner nearest to the intersection point (denoted as *NN*) is participating in the voting more than the other corners labels according to equation (3.14):

$$f_j = \begin{cases} 1 - NN\ distance, & if\ j = NN \\ \frac{NN\ distance}{7}, & otherwise \end{cases} \tag{3.14}$$

Consequently, the label of the *NN* will be selected to be the label of p_i. In this way, jaggies and aliasing artifacts at the boundaries are avoided, ensuring clear boundaries between regions. If p_i intersects the volume in an empty space where no label is defined, a ray is traced from p_i in the direction of its normal vector n_i to find an intersection point p

within a non-empty voxel. Ray tracing [188] advances a fractional distance d from p_i along its normal vector n_i to find new point p as described in equation (3.15):

$$p(d) = p_i + d\, n_i \tag{3.15}$$

This is done iteratively with small d steps until the ray intersects non-empty voxel. Then, this voxel corners' labels are similarly used to assign p_i a label. Illustration of this stage using UNC atlas parcellation map is shown in Figure 3.5.

3.5. Surface-Surface Parcellation

The input to this stage is the labeled atlas surface at week 41 of the spatio-temporal atlas, which plays the role of prior L. The goal is to propagate these labels from the week 41 surface into WM surfaces which are constructed from each week of the spatio-temporal atlas, weeks 28-44 GA. Each surface is represented in an isotropic triangular mesh t of v vertices, e edges, and x triangles, and embedded in a 3D Cartesian space.

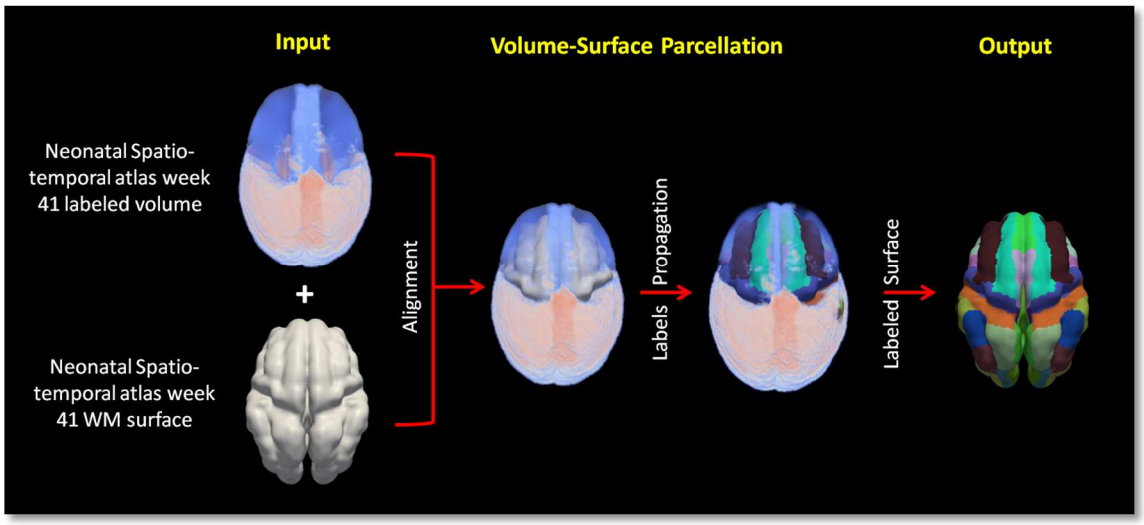

Figure 3.5. Volume-Surface Parcellation: Labels are propagated from the volume to the surface after alignment.

Problem Statement

Automatically and longitudinally labeling the developing brain cortical gyri and sulci problem can be phrased within conditional probability framework. In this framework, for a given observed surface model M, the classification of each point in M depends on its location with respect to the prior information L. Here, the prior L is incorporated in the parcellation of M. Considering the large degree of variability in cortical folding patterns of M, both the priors on L and the conditional probability of observing the surface given the classification can be conveyed within a mapping space. This allows them to be expressed as a function of position on the cortical surface; making them non-stationary. Using this mapping space, the classifiers are distributed and each classifier is responsible for a region with limited number of classes that occur within it. Therefore, a relationship is established between the number of classes falling within a region of space and the accuracy of the mapping system, $P(L(p_i) = l)$. Meaning that, $P(L(p_i) = l) \neq 0$ at each mapped location p_i only for a small number of classes l. In this way, the problem of classifying each surface point into one of C labels is decomposed into a set of tractable problems of classifying the points in each region of the surface model into one of only a small number of labels.

A function $f(p)$ needs to be calculated to define the mapping space $f(p): p \rightarrow x$. This function takes as input a point in the surface p, returning the corresponding location in the prior coordinates x. The returned coordinates are useful in this context only if they are spatially and temporally related to the anatomical location of p. This type of mapping therefore provides the ability to meaningfully relate coordinates temporally. Using the mapping space, the class statistics will vary as function of location.

Mapping Space

During the brain myelination, radial glial cells form the scaffolds where neurons migrate to their cortical destinations [24,53] and cause an increase in the cerebral cortex surface area [53] with total brain tissue volume increasing at the ratio of 22 ml/week [26]. Inspired by the neuronal migrational trajectories (described in section 1.3), which are radial dominant and cortical plate perpendicular [52], and since the cortex globally grows radial with constant rate assumption in early GA development, we can trace the growth of the cortex by linearly registering all weeks' cortical surfaces, identifying the centroid, and shooting rays from the centroid in all directions. Each ray will intersect all surfaces in several points on its way out. Considering a small time interval, these intersection points model the shortest path of growth from one week to its next; hence, a mapping between them. However, to account for the local cortical surface folding that forms the sulci and gyri, a local directional mapping between the points is more desirable. We rely on local pairing between points of consecutive weeks' surfaces to propagate the labels among pairs from labeled surface to unlabeled surface. To map the points locally and also to accelerate the process, we shoot a single ray r_i from each point p_i of the unlabeled surface t along its normal vector direction n_i towards the labeled surface $t\pm1$ rather than shooting all rays from the centroid. In fact, the ray will intersect the labeled surface at some point inside a triangle x_j on that surface mesh. Therefore, defining the mapping function $f(p): p \rightarrow x$.

Denoting the vertices of x_j by v_{j1}, v_{j2}, and v_{j3}, the intersection between a ray originating at p_i having the normalized direction n_i with x_j will occur when the equality in equation (3.16) is satisfied:

$$p_i^t + d\, n_i^t = v_{j1}^{t\pm1} + u\left(v_{j2}^{t\pm1} - v_{j1}^{t\pm1}\right) + s\left(v_{j3}^{t\pm1} - v_{j1}^{t\pm1}\right) \qquad (3.16)$$

We solve in barycentric coordinate for three unknowns: d, u, and s using the linear solution of [189] (see Appendix 2 for more details). After locating x_j, x_j vertices' labels will vote to label p_i and p_i will take the label of the majority. If there is no majority among x_j vertices' labels, p_i will take the label of the closest vertex to the intersection point I_{ij}.

Additionally, due to the fact that one ray can intersect many triangles, a margin around the unlabeled surface is defined to insure that only local intersections within the margin are considered. The benefits of defining a margin are that it will lead to more efficient pairing and accelerates the process. In fact, when two consecutive GA weeks brain surfaces are aligned, some regions of the earlier week surface cover or occlude the later week surface in some locations, and vice versa, as shown in Figure 3.6. This surface overlaying is primarily due to the fact that brain curvature is deforming [24]. The solution of this situation is to look for intersections from each side of the surface via the positive and the negative normal direction as demonstrated in Figure 3.6. In addition, energy optimization function described in equation (3.17) is used to find the best intersection:

$$E_{intersect}\left(p_i^t, x_j^{t\pm1}\right) = E_{dist}\left(p_i^t, x_j^{t\pm1}\right) + E_{normal}\left(n_i^t, xn_j^{t\pm1}\right) \tag{3.17}$$

where p_i^t and n_i^t represent a point and its normal vector on surface t, respectively. And $x_j^{t\pm1}$ and $xn_j^{t\pm1}$ represent a triangle and its normal vector on surface $t\pm1$, respectively. In the first term E_{dist}, the process is optimized by looking for the closest intersected triangle within the described margin, as in equation (3.18):

$$E_{dist}\left(p_i^t, x_j^{t\pm1}\right) = min_j\ distance\left(p_i^t, I_{ij}^{t\pm1}\right) \tag{3.18}$$

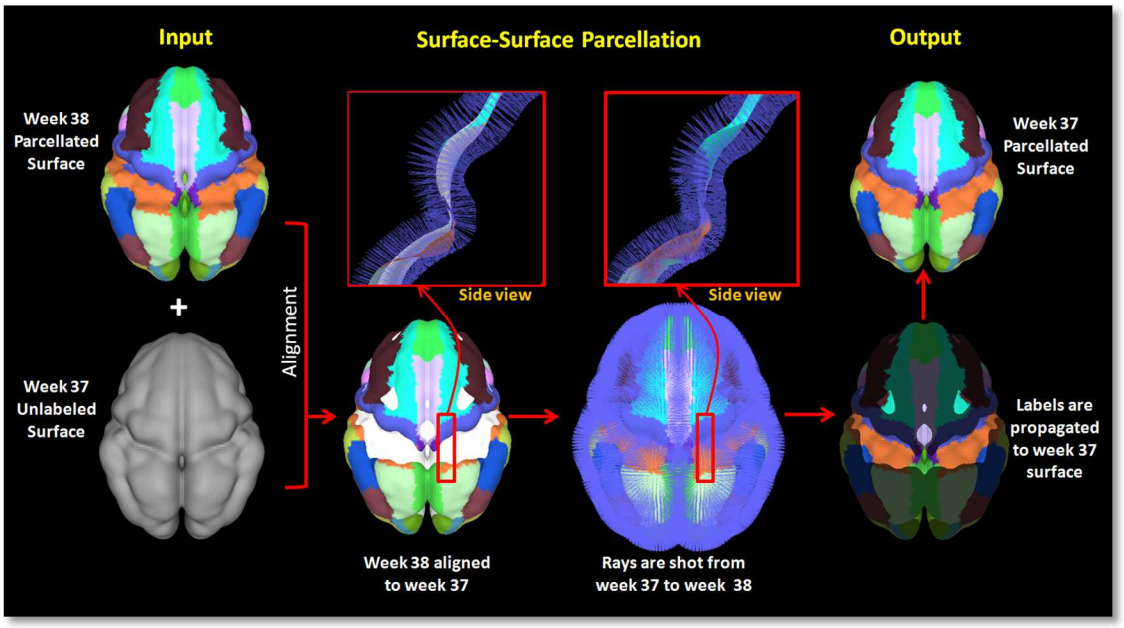

Figure 3.6. Surface-Surface Parcellation: Shooting rays from the unlabeled surface points along their normal vectors and within a margin around the surface toward the labeled surface.

where $I_{ij}^{t\pm1}$ is the intersection point inside the triangle $x_j^{t\pm1}$ with the ray originating from p_i^t. In the second term E_{normal}, the process is optimized by guaranteeing that the selected triangle has the most similar normal vector direction to the point normal vector direction. Therefore, intersections with surface triangles in the opposite direction are avoided, as in equation (3.19):

$$E_{normal}(n_i^t, xn_j^{t\pm1}) = min_j\ (1 - cos(n_i^t, xn_j^{i\pm1})) \tag{3.19}$$

Parcellation

While parcellating the spatio-temporal atlas starting from week *41* and using this parcellation as prior then going in both directions, we build a history of the point-triangle mapping between successive weeks. When we parcellate the surface of *t*, using prior labeled surface of *t±1*, the history information obtained from all weeks *t±2, t±3, t±4* …

etc., are incorporated in the majority voting process such that all previously labeled surfaces participate in giving labels to surface *t* points. The number of points participating in the voting process is specified by the level of priors available at week *t,* starting from week *41* and going in both directions one at a time. We build a tree for each point p_i at time *t* such that p_i will be the root of the tree. In the next tree level, we add 3 nodes, which are the intersected triangle vertices at time $t\pm1$. Each additional level of the tree will have 3^{depth} nodes, which are the intersected triangles vertices at time $t\pm depth$. These nodes are the ones participating in the voting. Let Ω be a set that holds the labels of these nodes. The size of Ω can be expressed using equation (3.20):

$$|\Omega| = \sum_{i=t}^{41} 3^{|i-41|} - 1 \tag{3.20}$$

Now, given the mapping function *f*, and the number of votes participating in the voting process, the probability of assigning class *l* into current point p_i is given by equation (3.21):

$$p(p_i = l) = \frac{\#\ of\ times\ class\ l\ occur\ in\ \Omega}{size\ of\ \Omega} \tag{3.21}$$

After collecting the labels that will participate in the voting process, we can specify the amount of participation of each label based on its temporal location or tree level such that the weeks closer to the current week *t* participate more than distant weeks. Labeling p_i is formulated based on *C*-length weights vector: $\alpha_l^t, l \in [1, C]$. This weights vector defines a relative scoring function based on the longitudinal location t of each point participating in the voting $p_i \rightarrow \alpha_l^t.\Omega\ (p_i^t)$ such that points in $t\pm1$ participate more than points in $t\pm2$, points in $t\pm2$ participate more than points in $t\pm3$, and so on. To specify this temporal participation, time dependent kernel regression [135] is used to estimate the weight of votes

coming from each time. Hence, Gaussian kernel is used to produce the weight α of the votes of the k^{th} time point t as given in equation (3.22):

$$\alpha^t(t_k, t) = \frac{1}{\sigma\sqrt{2\pi}} e^{\frac{-(t_k - t)}{2\sigma^2}} \tag{3.22}$$

Then, the label associated with point p_i is given by equation (3.23):

$$label(p_i^t) = argmax_l \, \alpha_l^k \, \Omega(p_i^k), \; k \in [t+1, 41] \; or \; k \in [41, t-1] \tag{3.23}$$

These votes and their weights will specify the level of certainty when assigning a label to any point. The propagated error will also be quantified based on those votes.

For this Gaussian kernel, the choice of the kernel width σ is important, because it will specify the amount of participation at each level of the tree. We chose $\sigma = 1$. With this choice, the previous 4 times are going to directly affect the prediction of the current label at time t as they will be assigned higher weights than the rest times. According to Markov Chain theory, each state depends only on the states immediately previous in time. Hence, the labels are treated as random variables l_t such that t indicates the time, the future is conditionally depends on the past according to the probability given in equation (3.24):

$$\begin{aligned} &p(L_t = j \,|L_{t\pm1} = \, i_{t\pm1}, L_{t\pm2} = \, i_{t\pm2}, \dots, L_{41} = i_{41}) = \\ &\quad p(L_t = j \mid L_{t\pm1} = \, i_{t\pm1}, L_{t\pm2} = \, i_{t\pm2}, L_{t\pm3} = \, i_{t\pm3}, L_{t\pm4} = \, i_{t\pm4}) \end{aligned} \tag{3.24}$$

Let the discrete values $a_1, \dots, a_t$ denote the variables of a Markov sequence as in equation (3.25):

$$\begin{aligned} &p\big(l_t = a_{i_t} \,\big|l_{t\pm1} = a_{i_{t\pm1}}, l_{t\pm2} = a_{i_{t\pm2}}, \dots, l_{41} = a_{i_{41}}\big) = \\ &\quad p\big(l_t = a_{i_t} \,\big|l_{t\pm1} = a_{i_{t\pm1}}, l_{t\pm2} = a_{i_{t\pm2}}, l_{t\pm3} = a_{i_{t\pm3}}, l_{t\pm4} = a_{i_{t\pm4}}\big) \end{aligned} \tag{3.25}$$

The sequence l_t is called a Markov chain [190]. For Markov chain, the starting state does not affect the long-range predictions.

Additionally, the parcellation is followed by three refinement steps. The first refinement is to fill the gaps. The second refinement is to correct for the parcellation depending on the topology of the surface. The third refinement is to merge small patches with their neighbors as shown in Figure 3.7.

If the ray segment is parallel with the triangles in the defined margin or when u or s is larger than 1, no intersection can be found. Therefore, small gaps, or few points with no assigned label could occur in the parcellated surface. Filling the gaps is solved by adopting a semi-supervised learning approach to propagate the labels between the surface points [191]. In this approach, labels are propagated through the neighbors iteratively until convergence. A C-dimensional vector is defined for each unlabeled point p_i to hold weights for each possible candidate region. Only the weights of the neighboring regions of p_i (e.g. regions of the points that share an edge with p_i in the triangulated surface mesh) are considered and updated. Then, the label of the higher weight region will be given to p_i. This is done iteratively until all unlabeled points are labeled.

Since brain cortex topology consists of sulci and gyri, one automatic, numeric way to capture this topology is by calculating the curvature of the surface. Using the mean curvature (see Figure 3.8), we locate the set Σ of points with maximum/minimum curvature on the surface. Referring to some brain sulci and gyri segmentations, some of these points are located on the boundaries between ROIs. We check to see if these points are surrounded with more than one ROI in a bounded space. If yes, then we determine whether there is

leakage from one ROI to another passing through these points. The leakage is identified by checking for a connected patch around one side of a line formed by points of Σ, where the patch size does not exceed a specified threshold. If we find a leak, we correct for it by pulling the region back to these points, which serve as the boundary between two ROIs, thereby eliminating the leakage.

Shooting rays along the points' normal vectors direction could result in cross intersection due to the fact that the neonatal brain surface curvature is deforming. This results in small patches near borders that belong to neighboring regions after parcellation. The described situation is directly related to the change in the normal vectors direction, especially where the curvature is high among neighboring points. Whenever a small patch with less than a pre-specified threshold number of points is located, we merge it with the neighboring region where the largest border is shared.

3.6. Summary

This chapter presented an approach for propagating a number of neuroanatomical ROIs through 4D atlas of the developing brain. The approach consists of three stages. In the first stage, non-rigid registration of MR images of intensity volumes is performed to propagate the labels into the spatio-temporal atlas at one GA week. In the second stage, intersections between volume, and surface constructed from it are used to propagate the labels from the volume space into the surface space. In the third stage, ray-triangle intersections framework between consecutive weeks' surfaces is described to propagate

the labels among the GA weeks of the spatio-temporal atlas. Experimental results of this approach and evaluation methods are presented in Chapter 4.

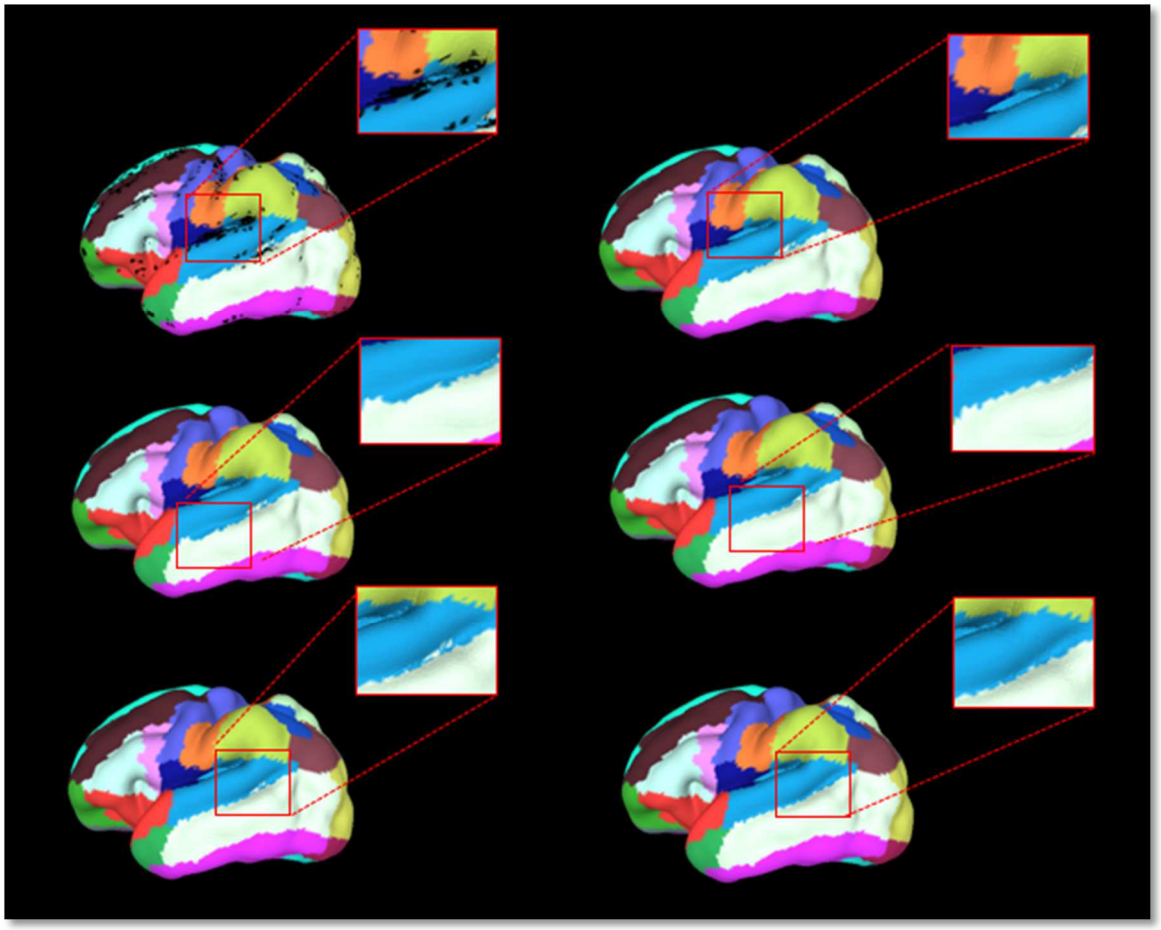

Figure 3.7. Lateral view of parcellated brain and refinements results. First row: Before and after refinement step 1 of filling gaps on left column and right column, respectively. Middle row: Before and after refinement step 2 of correcting for the topology using mean curvature on left column and right column, respectively. Bottom row: Before and after refinement step 3 of merging small patches with neighbors on left column and right column, respectively. Final Refinement Result is shown on the right of the last row.

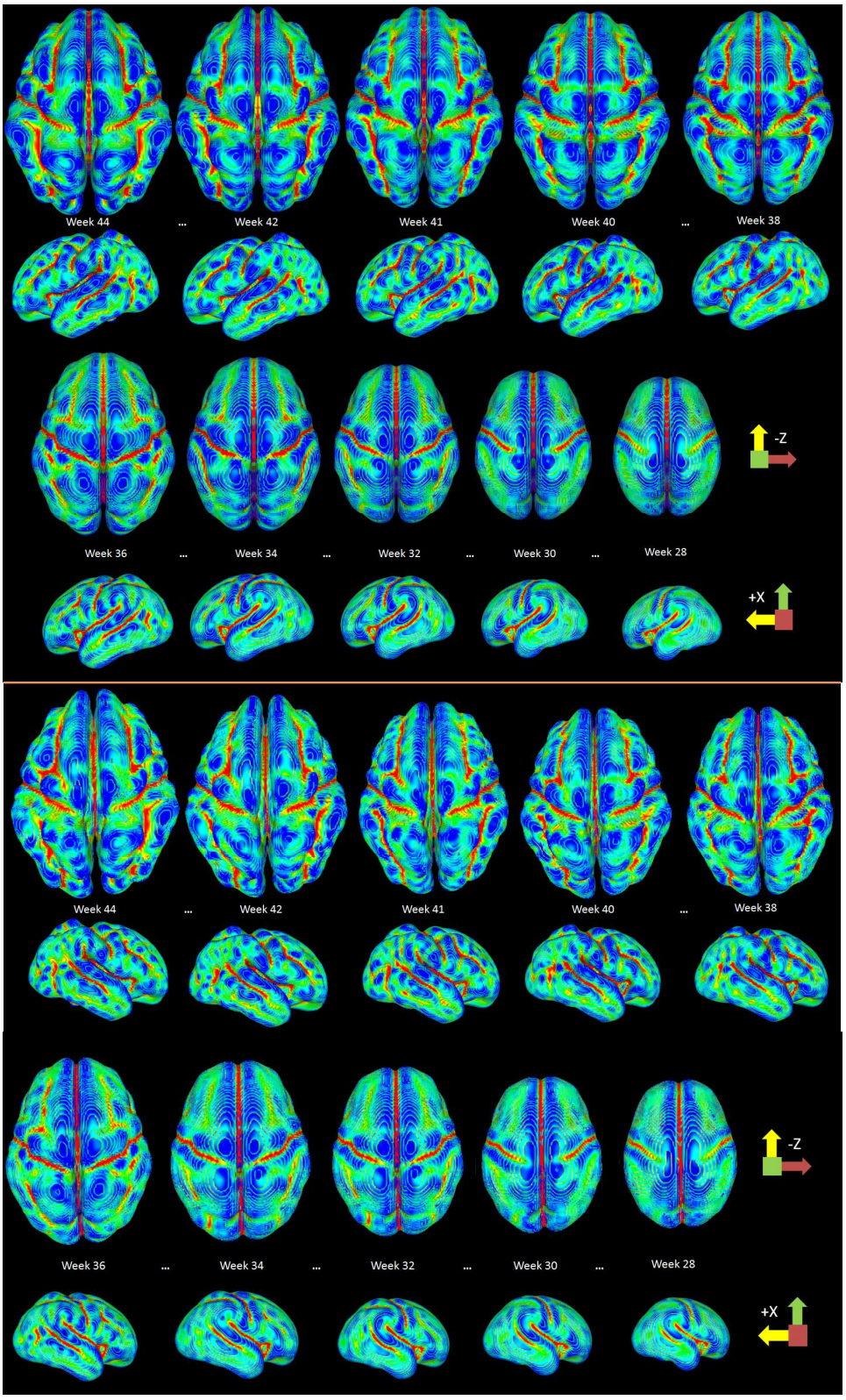

Figure 3.8. Superior and lateral views of the surface mean curvature on selected GA weeks of the spatio-temporal atlas. Top: Symmetric results. Bottom: Asymmetric results.

Chapter 4: Results and Evaluation

4.1. Introduction

This chapter presents the experimental results of the method discussed in Chapter 3 that demonstrate a three-stage parcellation algorithm for 4D atlas of the developing brain. Both final results and individual stages' results are presented in this chapter. Also offered are evaluation methods and discussion. Since there is no available neonatal parcellated atlas that covers weeks 28-44 GA to use as ground truth and for comparison purposes, we designed four experiments to validate the resultant parcellation.

4.2. Experimental Setup

The method described in Chapter 3 has been implemented using C# programming language. The programming and compilation are performed on Microsoft Visual Studio 2012 IDE. The system used is a DELL Precision T7500 Workstation with Intel Xeon 2.27GHz E5607 processor, 54 GB of usable RAM. The operating system is Windows 7 Professional. Two versions of the code are implemented; one without using parallelism, and one with using parallelism in parallel threading [192]. Comparison between performances in term of time is given in Table 4.1.

With regards to the input data, we used the three available datasets on the web for the labeled neonatal atlases; UNC [74], ALBERT [72], and JHU [71]. For the spatio-temporal atlas, we used the only online accessible 4D neonatal atlas that is constructed from the largest number of subjects [140] in order to best represent the population.

4.3. Results and Evaluation

4.3.1. Results

We performed the proposed parcellation on the neonatal spatio-temporal atlas [140] using UNC labeled atlas of C=90 ROIs parcellation map [74], ALBERT labeled atlas of C=50 ROIs parcellation map (44 are cortical ROIs only) [72], and JHU labeled atlas of C=122 ROIs parcellation map [71]. Two versions of each parcellation map are used: one is symmetric and another is asymmetric. In the first stage of propagating the labels in the volume space, the UNC and JHU neonate atlases are non-rigidly registered into week 41 of the spatio-temporal atlas and labels are propagated in the volume domain. For ALBERT atlas, since it consists of 20 parcellated subjects, we need to normalize their volumes into week 41 of the spatio-temporal brain space, then fuse their information to build one template. Each subject is non-rigidly registered to week 41 of the spatio-temporal atlas (which is the average age of ALBERTs as given in Table 3.1) and labels are propagated in the volume domain. Then, fusing is performed using voxel-level majority voting to generate one template (as described in section 3.3), which is used in the stages that follow. Results of the first stage are given in Figure 4.1.

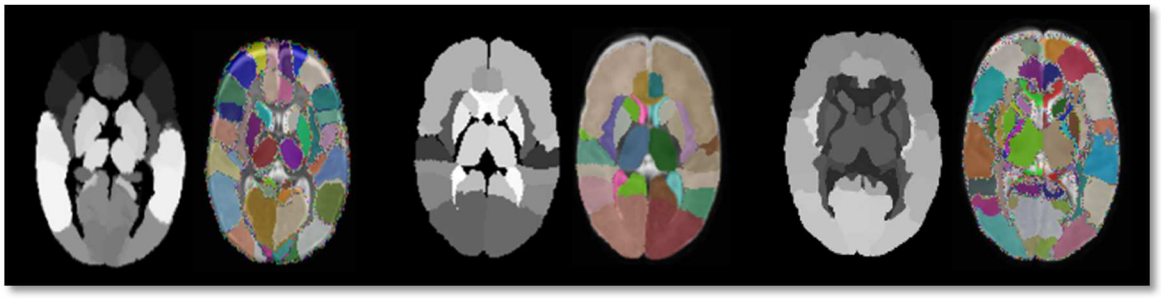

Figure 4.1. Results of first stage: Propagating the labels in the volume space into week 41 of spatio-temporal atlas. Left: Deformed UNC atlas labels. Middle: Deformed ALBERTs atlases labels after majority voting. Right: Deformed JHU atlas labels.

In the volume-surface parcellation stage, the deformed volume of labels of UNC, ALBERT, and JHU are used one at a time to transfer labels into the WM surface of the spatio-temporal atlas at week 41.

For UNC atlas, out of 90 ROIs, three ROIs numbered: 75,76, and 79 in the parcellation map did not initially appear in the volume-surface parcellation results of week 41 because they did not intersect with the constructed cortical surface. Additionally, eight ROIs numbered: 25, 26, 29, 31, 32, 36, 42 and 80 in the parcellation map have a very small number of points assigned to each. Therefore, these regions fade away at different weeks during the propagation because they are considered as small patches and were merged into their neighbors at some longitudinal point in the refinement step as shown in Table 6.5. The remaining 79 ROIs are presented and propagated from week 41 in both directions into the spatio-temporal atlas by proposed surface-surface parcellation.

For ALBERT atlas, 44 cortical ROIs are propagated into the surface after removing the cerebellum and non-cortical structures, which are ROIs numbered: 17, 18, 19, 44, 45, and 48 in the parcellation map as shown in Table 6.7.

For JHU atlas, 49 ROIs did not initially appear in the volume-surface parcellation results of week 41 because they did not intersect with the constructed cortical surface. These ROIs have numbers: [7-16], 21, 23, [25-29], 31, 32, 37, 38, [41-57], [59-66], 102, 119, and 120 in the parcellation map. Also, twelve ROIs numbered: 3, 4, 5, 20, 24, 30, 58, 85, 87, 115, 116 and 118 in the parcellation map had only a small number of points assigned to them. Therefore, these regions fade away at different

weeks during the propagation because they are considered as small patches and were merged into their neighbors in the refinement step as shown in Table 6.9.

The results of this stage in 3D form parcellated surfaces at week 41 GA are embedded in Figure 4.2 and in the supplementary material for interactive illustrations.

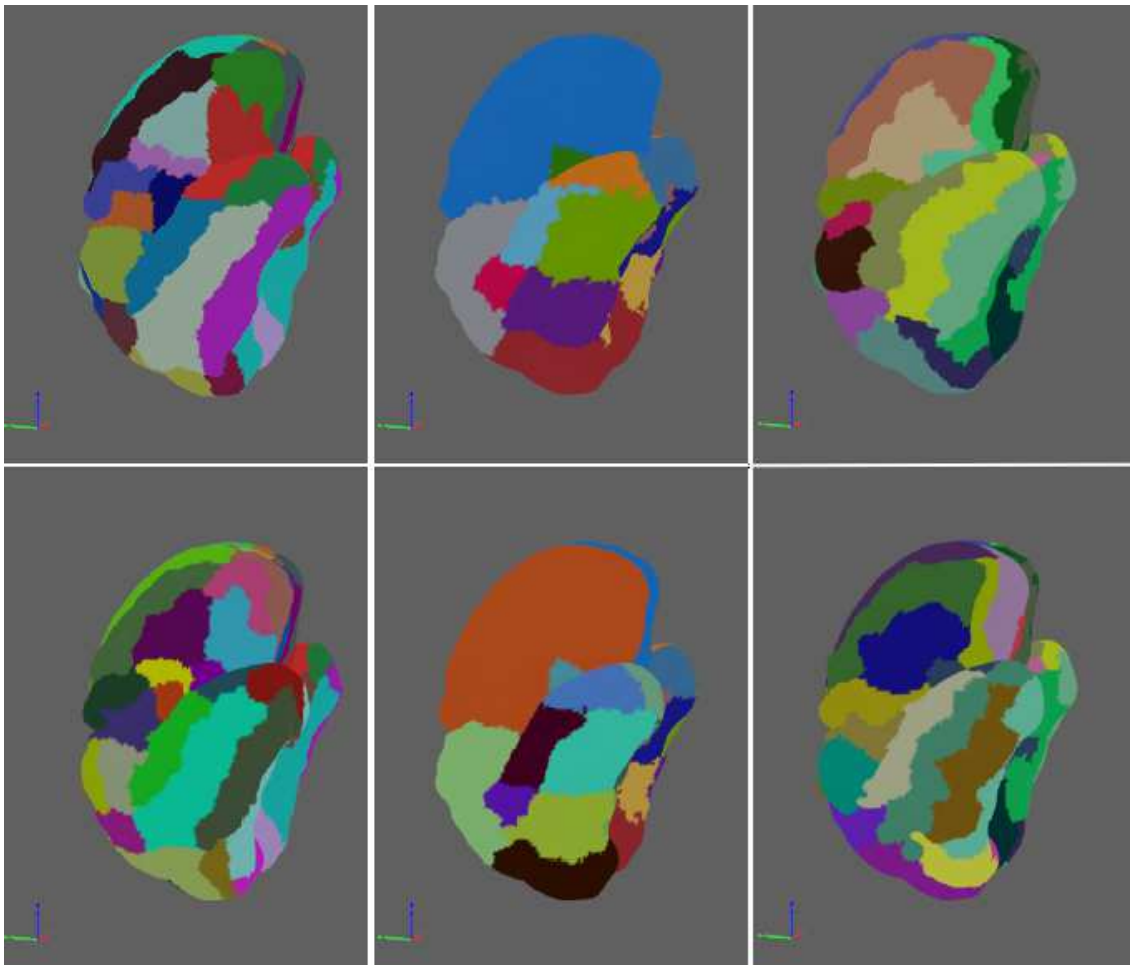

Figure 4.2. 3D results of second stage of volume-surface parcellation. Left: Using UNC atlas labels. Middle: Using ALBERT atlas labels. Right: Using JHU atlas labels. Top: Symmetric. Bottom: Asymmetric.

In the last stage of surface-surface parcellation, labels are propagated into all spatio-temporal atlas weeks. The symmetric and asymmetric results of this stage in selected GA weeks are shown in Figure 4.3 using UNC atlas parcellation map, Figure 4.4 using ALBERT parcellation map, and Figure 4.5 using JHU parcellation map. Visual inspection shows consistent propagation of the labels over time. Processing time is reported in Table 4.1 and depends heavily on the number of points per source surface and the number of triangles per target surface. Because longitudinal brain development and cortical changes in two consecutive GA weeks is minimal and subtle [24,26,193], the ray-triangle intersection process provides rough pairing between the two surfaces as solid ground to propagate the labels among them. It also describes the growth trajectories between successive weeks. The average Euclidian distances of the pairing done by the proposed parcellation across weeks are reported in Table 4.1. The average ranges from 0.26 to 1.02 mm in the symmetric surfaces, and ranges from 0.26 to 1.03 mm in the asymmetric surfaces. This minimal distance between the consecutive surfaces strengthen the proposed parcellation method which rely on the pairing between the consecutive weeks without the need of performing the time-consuming deformable registration.

4.3.2. Evaluation

To our best knowledge, this is the first parcellated atlas of neonatal developing brain that covers GA weeks 28 to 44. For this reason, several approaches are necessary to evaluate the results. We used four evaluation methods on the proposed parcellation. The first approach incorporates ground truth parcellation to assess the validity of the

proposed parcellation method. The second evaluation method includes cross validation on ALBERT's 20 subjects to validate the final result. The third evaluation measures the local growth of individual neuroanatomical regions (labels) over time. The fourth evaluation focuses on comparing the probabilistic distribution of the labels among points across successive weeks. Finally, the utility of the parcellation in capturing the normal growth of perinatal brain individual ROI development is demonstrated in tables 6.4 to 6.9 in Appendix 1.

Table 4.1. Spatio-temporal atlas information: number of points per surface, number of triangles per surface, average pairing distance, and parcellation time starting from week 41 and going in both directions with and without multithreading. Sym.: Symmetric, Asym: Asymmetric

Week	Number of points/Surface		Number of triangles/Surface		Average paring distance (mm)		Time without multithreading (min:sec)		Time with multithreading (min:sec)	
	Sym.	Asym.	Sym.	Asym.	Sym.	Asym.	Sym.	Asym.	Sym.	Asym.
28	35,172	34,872	70,348	69,740	0.58	0.55	11:50	12:40	05:55	5:09
29	37,464	36,926	74,932	73,844	0.96	1.00	14:16	14:22	06:46	5:55
30	40,900	40,522	81,796	81,040	0.77	0.82	16:35	17:15	07:38	6:56
31	43,848	43,706	87,692	87,412	0.70	0.70	17:55	19:47	08:33	7:51
32	46,435	46,448	93,048	92,896	1.02	1.08	20:42	18:02	09:51	9:01
33	50,784	51,264	101,788	102,536	0.69	0.70	22:13	26:38	11:01	10:30
34	53,206	53,784	106,420	107,576	0.93	0.98	25:34	30:47	12:13	12:01
35	56,990	59,240	113,976	118,488	0.64	0.66	30:11	26:50	13:52	14:20
36	60,230	64,180	120,452	128,364	0.26	0.26	30:52	40:15	14:43	15:35
37	60,252	64,752	120,496	129,508	0.85	0.82	35:15	45:47	16:51	17:52
38	69,070	73,280	138,148	146,564	1.02	1.03	45:24	58:13	20:29	22:35
39	78,548	82,254	157,104	164,516	0.49	0.43	50:22	63:58	24:07	24:54
40	76,848	80,770	153,700	161,540	0.55	0.49	50:03	63:28	22:37	25:05
41	78,222	82,310	156,440	164,620	-	-	-	-	-	-
42	86,188	88,924	172,392	177,860	0.86	0.86	59:13	71:53	25:16	27:32
43	85,472	88,694	170,964	177,400	0.41	0.38	60:09	75:27	26:59	29:17
44	88,532	91,070	177,084	182,152	0.31	0.31	63:21	77:10	27:55	30:04

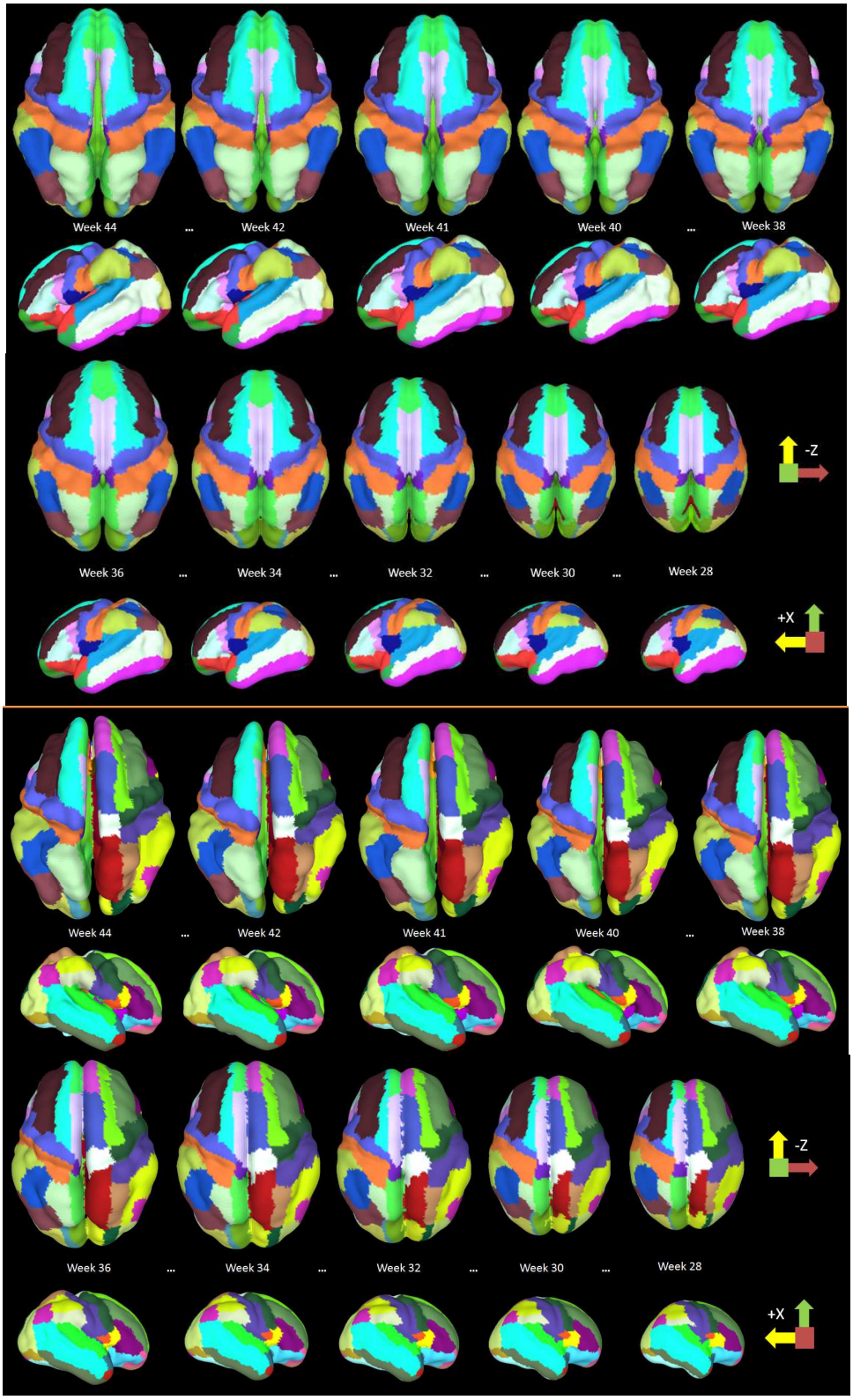

Figure 4.3. Parcellation results using UNC labels map on ten selected GA weeks. Top: Symmetric results. Bottom: Asymmetric results.

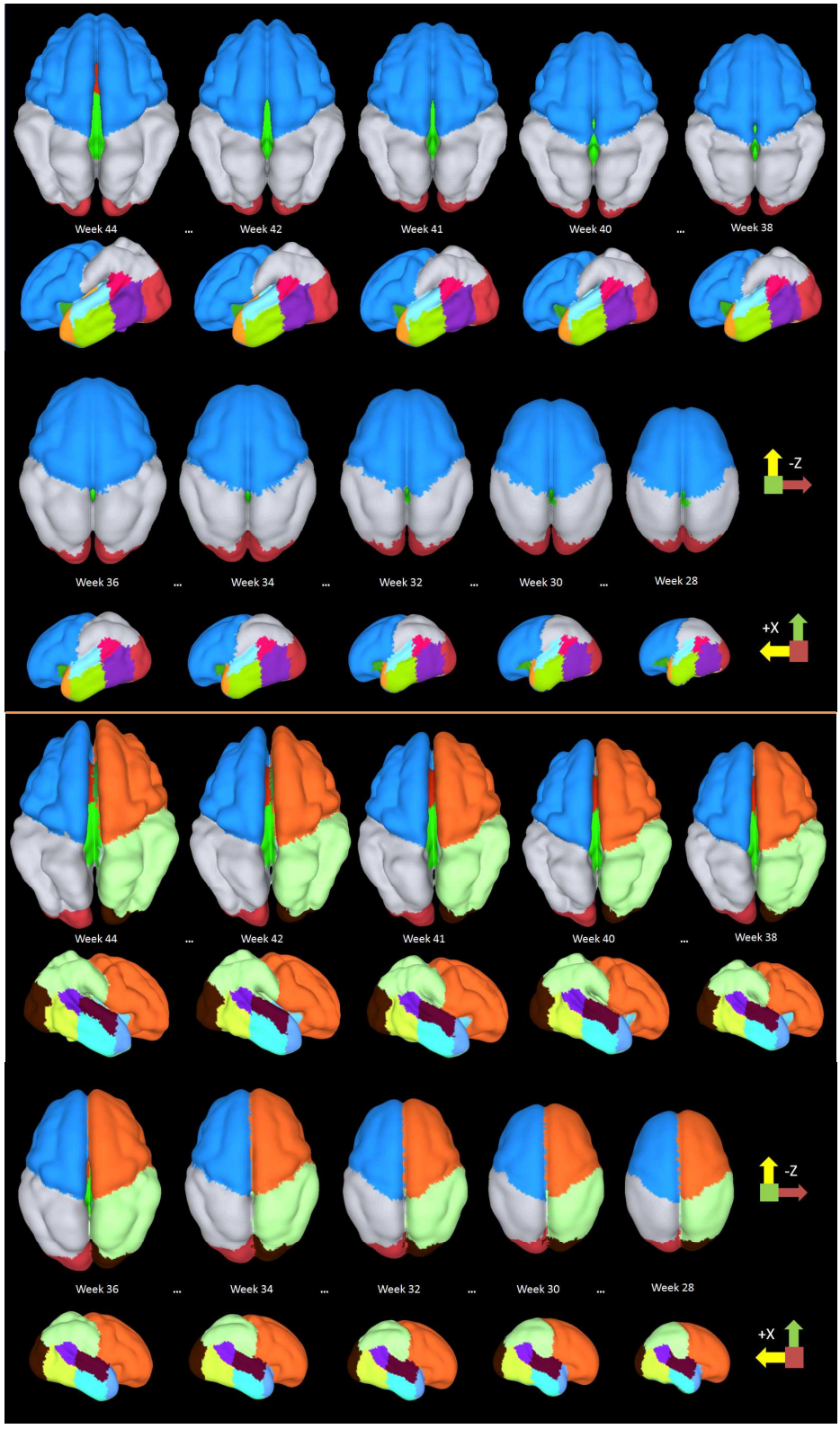

Figure 4.4. Parcellation results using ALBERT labels map on ten selected GA weeks. Top: Symmetric results. Bottom: Asymmetric results.

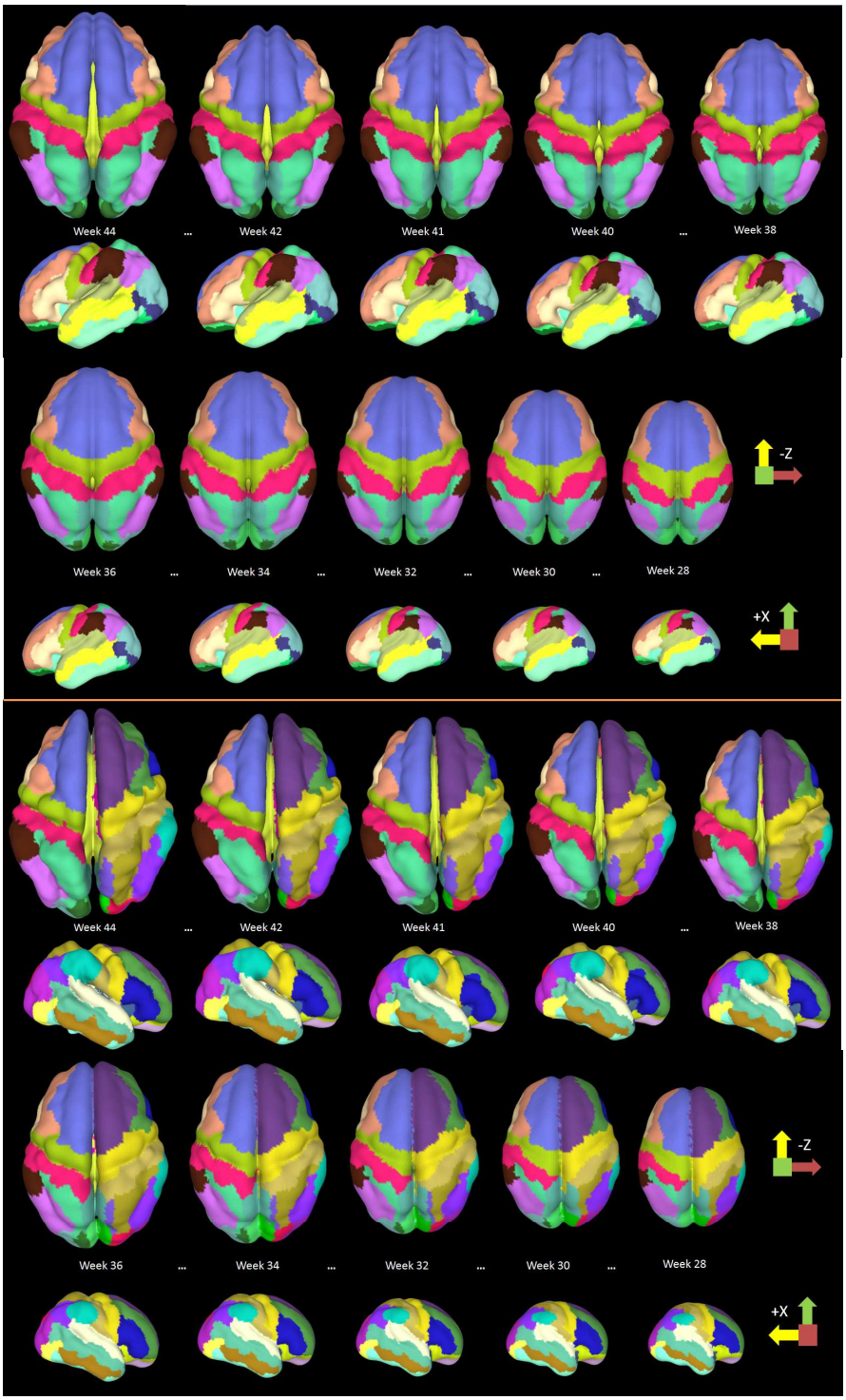

Figure 4.5. Parcellation results using JHU labels map on ten selected GA weeks. Top: Symmetric results. Bottom: Asymmetric results.

First Validation: Spatial and Temporal Consistency using Longitudinal Atlas

We used UNC Infant 0-1-2 parcellated brain atlas [74] to evaluate the proposed longitudinal method. This brain atlas provides full parcellation of the brain at three temporal ages: newborn, 1 year, and 2 years. As ground truth, a parcellated surface is constructed from each time point. Then, labels are propagated from one time point to another; from birth to year 1 and from year 1 to year 2 surfaces and vice versa, using the proposed parcellation method. The result is compared with ground truth point-by-point and by using DICE similarity index [194], which is given in equation (4.1) for any two sets X and Y and measures the overlapping and the agreement of these two sets, hence X and Y stand for the result and the ground truth:

$$2|X \cap Y|/|X| + |Y| \tag{4.1}$$

Having a consistency of 70% to 90%, the propagated labels are compared to ground truth as shown in Table 4.2. This consistency is comparable with the consistency of a similar experiment reported by UNC Infant 0-1-2 brain atlas authors [74]. In fact, the consistency is similar on birth vs. 1 year and is better on 1 vs. 2 years of age (90%). As shown in Figure 4.6, the location of most of the mismatched points is at the borders between regions; the ambiguous locations where precise parcellation could be missed even if it is done manually by an expert. We believe that dramatic changes in the brain shape, geometry, curvature and size between neonates to 1 year then to 2 year old are key reasons why a higher accuracy was not achieved in our validation experiment. These changes in the brain are less in magnitude during a week as opposed to a year. Furthermore, due to significant changes between neonatal and 1-year-old brains, a larger error is reported after propagating the labels starting from neonate towards 2

years old, as indicated in the dark gray shaded cells in Table 4.2. The main reason for this is the differences in the cortical growth rates during the first two years of age, as the cortex grows 1.8 times in average during the first year and 1.2 times in average during the second year [195].

Table 4.2. Dice similaity index of propagating labels among neonate, 1, 2 years old atlas. Left (light gray shaded cells): Starting the propagation from year 2 towards neonate. Right (dark gray shaded cells): Starting propagation from neonate towards year 2.

	From 2 to 1	From 1 to neo.	From neo. to 1	From 1 to 2
DICE score	0.9042	0.8027	0.7297	0.7135

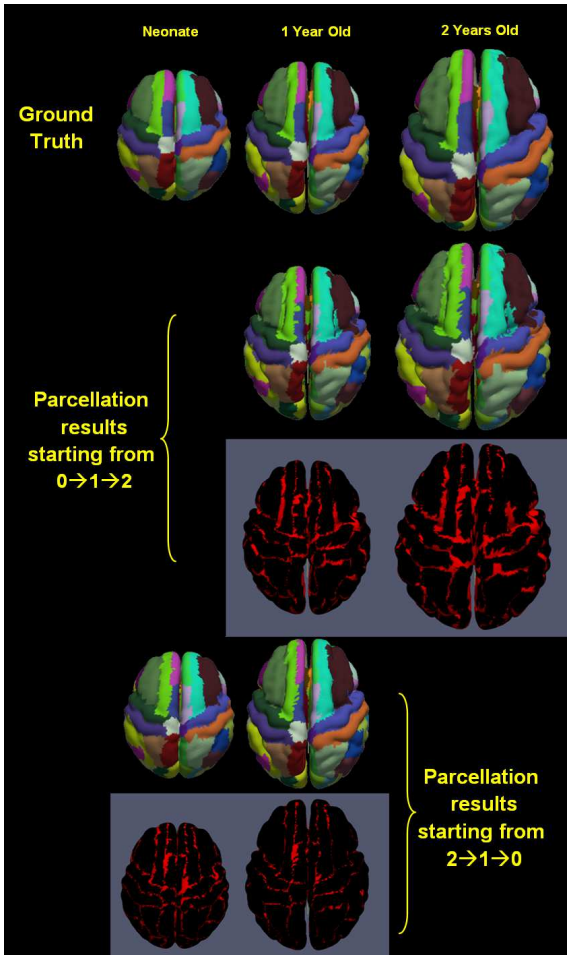

Figure 4.6: The UNC Infant 0-1-2 Atlas validation experiment. Top row: Ground truth parcellation maps. Second and third rows: Proposed method parcellation maps starting from 0 to 1 then to 2 years and the color coded agreement between the ground truth and the proposed method parcellation where error is shown in red. Fourth and fifth rows: Proposed method parcellation maps starting from 2 to 1 then to 0 year old and the color coded agreement between the ground truth and the proposed method parcellation where error is shown in red.

Second Validation: Spatial and Temporal Consistency using Cross validation

The ALBERTs atlas dataset consists of 20 brain MRI scans and their manual parcellation maps. Each brain scan was taken at specific week of gestation as shown Table 3.1. According to Table 4.3, several GA weeks have more than one scan. Therefore, cross validation/leave-one-out/n-folds/jackknife technique can be employed to validate the proposed method. Using this technique, one scan per age is removed from the dataset and called testing scan, the remaining scans are used to create a template by normalizing and fusing them as described in section 3.3, called training set. The new template is used as an input for the proposed parcellation, and its labels are propagated in the spatio-temporal atlas starting from week 41 GA and targeting the testing scan age week. The resultant parcellation of the training set at that age is then compared with the testing scan. The disagreement between the manual and the automated parcellation is quantified point-by-point, whereas this disagreement will report the percentage of error. To further explain how this cross validation was set up, we leave-one-out of each individual week as ground truth, making the testing data size equal to 1 and the training data size 20-1 equal to 19. With the available 20 ALBERTs, we need to perform 5 cross validation experiments where each experiment uses a different age and a randomly selected scan at that age as the testing data according to Table 4.4.

As reported in Table 4.4, parcellation results using the proposed method have 83.79% to 87.08% accuracy with the testing data. The accuracy depends heavily on the randomly selected data for testing. If the leave-one-out scan represents an outlier of the ALBERTs population, the result will be compromised as shown in Figure 4.7. This

compares to the accuracy of a similar experiment reported by FreeSurfer parcellation [92] for adult brain, which reports an accuracy of 79% to 83%.

Table 4.3. ALBERTs atlas information: range of age at scan of 20 neonates brains and number of scans avaliable in the ALBERTs atlas per each age.

Age at scan (week)	36	39	40	41	43	44	Total
Number of scans/age	2	6	2	6	2	2	20

Table 4.4. ALBERTs leave-one-out experiments setup with labels agreements accuracy between the test data and the proposed parcellation result reported in each experiment.

Age at scan (week)	36	39	40	43	44	Training data size	Testing data size	Labels agreement
Number of scans/age	2	6	2	2	2			
Experiment 1	1					19	1	85.93890%
Experiment 2		1				19	1	87.08815%
Experiment 3			1			19	1	83.79138%
Experiment 4				1		19	1	84.88628%
Experiment 5					1	19	1	83.82167%

Third validation: Measuring the Normal Growth

We compared the number of points per label to measure the growth of the brain between weeks. Ultimately, the number of points per region label is expected to fluctuate from one week to another as the brain grows and cells form. The growth of the ROIs fluctuate from one week to another due to the brain structure convolution and sulci and gyri maturation as shown in Appendix 1's tables 6.4 to 6.9. Figure 4.8 shows the growth of two regions reported as good cortical growth biomarkers for the used neonatal spatio-temporal atlas [61] and which is consistent with the growth reported in clinical studies. These regions are: Middle Temporal Gyrus (MTG), and Inferior Temporal Gyrus (ITG).

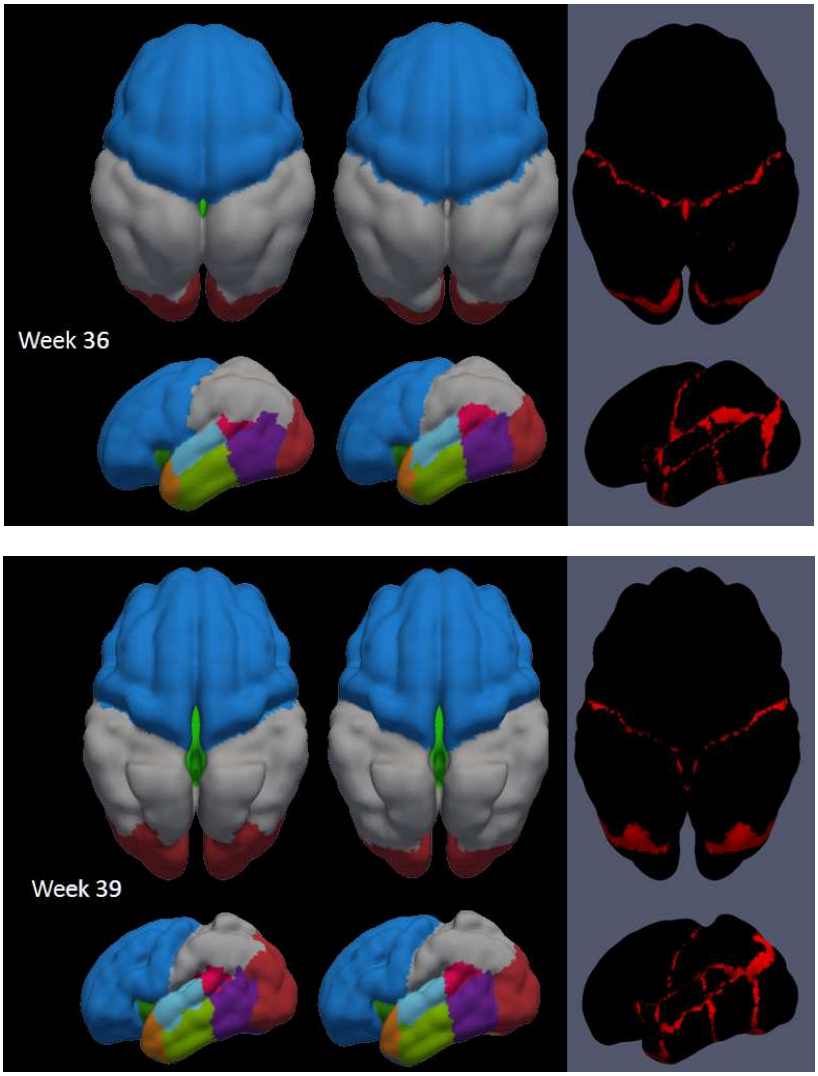

Figure 4.7: The ALBERT Atlas validation experiment. Left column: The leave-one-out per GA week test subject parcellation map as ground truth. Middle column: The parcellation map of proposed method starting from week 41 GA to the corresponding test subject GA week. Right column: The color-coded agreement between the test subject and the proposed method parcellation where error is shown in red.

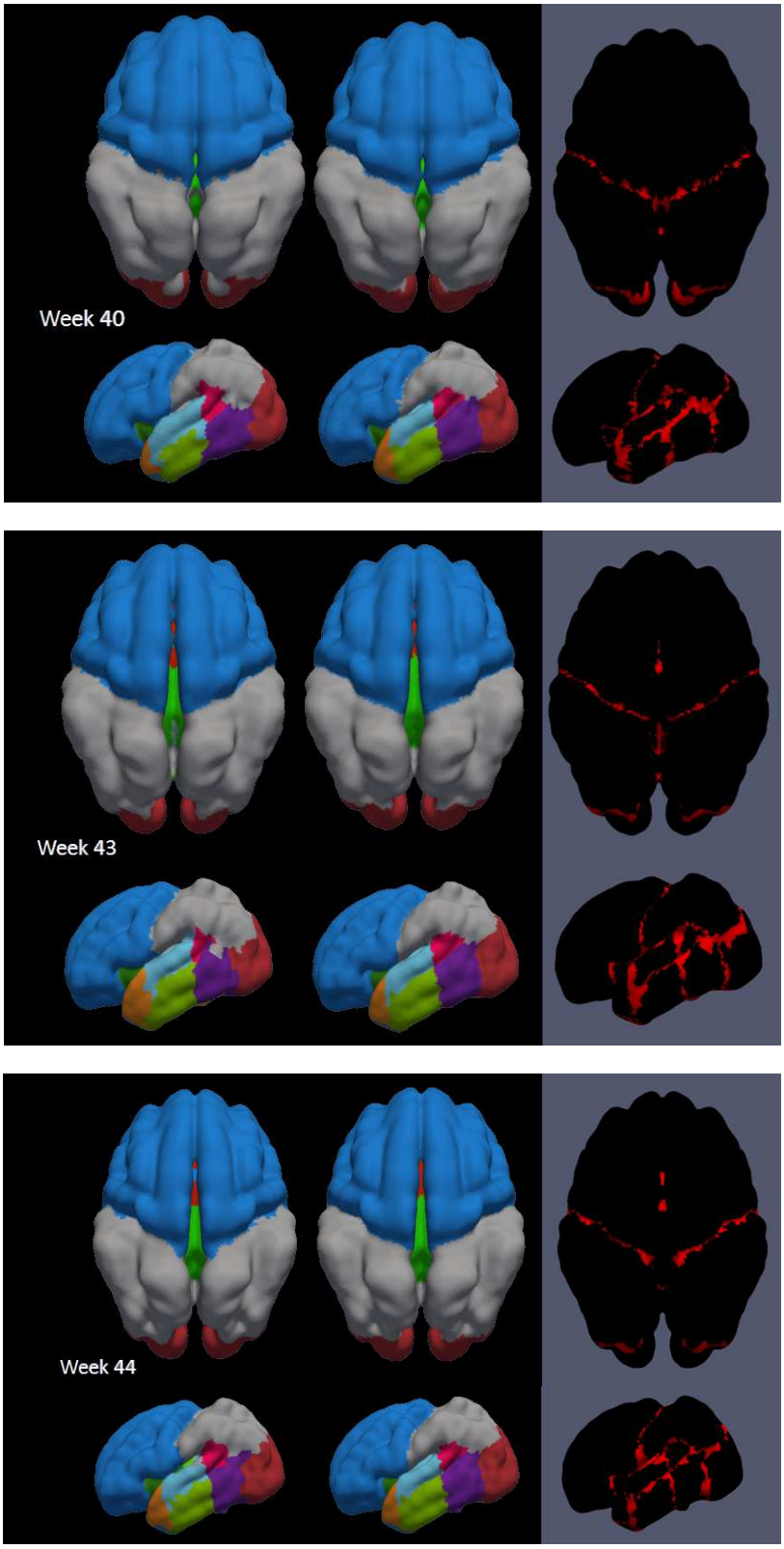

Figure 4.7: *Continued*

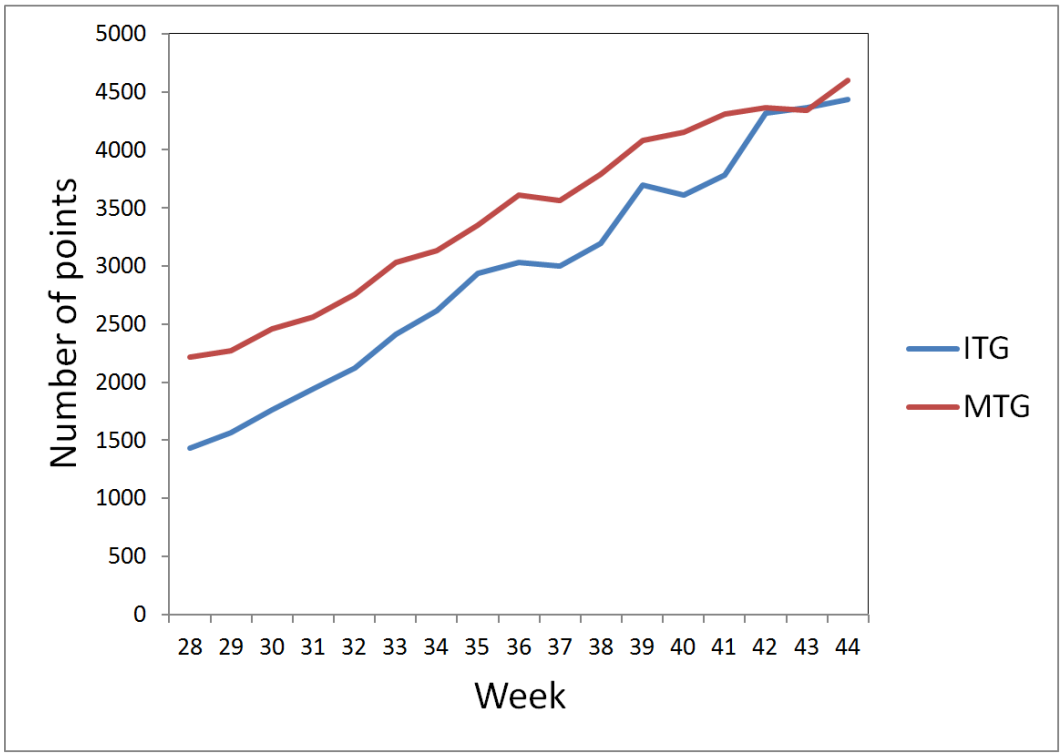

Figure 4.8. The number of points per two biomarker growth regions, (Middle temporal gyrus (MTG), and Inferior temporal gyrus (ITG)) is plotted against age at time of scan.

Fourth Validation: Longitudinal Probabilistic Distribution Consistency

Demonstrating the growth model, the fitting of the propagated labels from a labeled week to a successive unlabeled week is evaluated. The spatial distribution of points per labels of each week after parcellation is quantified by statistical probability. The distribution of the points under each label is maintained with the same probability in all GA week, even though the numbers of surface points (reported in Table 4.1) vary significantly between weeks.

The detailed quantitative information about the growth of each ROI is reported in tables in Appendix 1; including: Tables 6.4 and 6.5 using UNC parcellation map symmetrically and asymmetrically, Tables 6.6 and 6.7 using ALBERT parcellation

map symmetrically and asymmetrically, and Tables 6.8 and 6.9 using JHU parcellation map symmetrically and asymmetrically.

4.4. Limitation

Spatially, one can consider the isotropic concentric brain growth model encoded in the proposed ray-triangle intersection framework a limitation. However, the actual implemented ray-triangle algorithm takes into account the local growth as the rays are shot locally in the direction of their normal vector and are perpendicular to the cortical plate. Therefore, it is not fully isometric and concentric. The local ray-triangle intersection framework is the most relevant model to the growth trajectory, which reflects the behavior of the neuronal migration while the brain is developing. If a detailed model describing the brain ROIs growth trajectories at early development were available, we would more accurately model the brain ROIs growth at early gestational age. Temporally, it is important to mention that when error appears in time t, it will propagate to all times following it, e.g. time $t\pm1$, $t\pm2$, and so on. Currently, to limit this error propagation we incorporated the history of the previous week's parcellated surfaces in the voting process as described in section 3.5. A future project will investigate and address this issue by incorporating the neighboring points in the voting process. Finally, having no ground truth of all GA weeks to compare our result with is a validation limitation, especially in weeks 28 to 35 GA.

4.5. Summary

This chapter described the experimental results of the method of parcellating the developing brain longitudinal cortical surfaces proposed in this dissertation. Two different datasets are used to parcellate the spatio-temporal atlas. The proposed method has three

stages. Individual stages' results are provided along with final results. Also, several evaluations of this parcellation method are discussed. In the next chapter we will conclude the description of this work and propose possible future work.

Chapter 5: Conclusion and Future Work

5.1. Conclusion

The marker-less automatic parcellation method described in this dissertation has been shown to provide a label for each point in the longitudinal cortical surfaces of 17 consecutive GA weeks. Label propagation across neonatal spatio-temporal brain atlas surfaces is phrased within a customized ray-triangle intersection framework. The accuracy of label assignment in the proposed method is leveraged out through the use of local and global, spatial and temporal information. The local information is encoded by modeling the shortest spatial path of growth throughout the 17 weeks as directional rays. The global information is merged into the parcellation by incorporating the history of the voting process in a temporal fashion. The proposed brain parcellation method is applicable when we cannot rely on the surface curvature alone to locate the landmarks or predict the labels, and when the growth is radial, as in the case of developing brains. Having the labels propagated with the same probabilistic distribution into younger GA weeks is appealing, especially with the lack of parcellated brain atlases in early development, such as at week 28 GA. The aim is to parcellate the developing brain, which can be used as a benchmark to assess brain structures development of preterm born children in order to discover functional abnormalities at early age. We ultimately aim to facilitate the acquisition of detailed morphometric information allowing the investigation of correlations between morphological characteristics of neonatal brain regions and specific disorders at early GA.

5.2. Future Work

The long-term future work includes extending this method to the use of other labeled neonatal brain atlases and to parcellate different neonatal and fetal brain spatio-temporal atlases. Also, we intend to perform cortical region analysis, find the gyrification indices on the developing brain and accelerate the parcellation by making use of GPU computation. In addition, we intend to investigate more ways to quantify the propagated error.

6. Appendix 1

Table 6.1. Index of the UNC infant-AAL atlas ROIs' names and colors. Sym.: Symmetric, Asym.: Asymmetric.

Index	Color (Sym.)	Color (Asym.)	Region	Abbreviation
1			Precentral gyrus left	PreCG-L
2			Precentral gyrus right	PreCG-R
3			Superior frontal gyrus (dorsal) left	SFGdor-L
4			Superior frontal gyrus (dorsal) right	SFGdor-R
5			Orbitofrontal cortex (superior) left	ORBsupb-L
6			Orbitofrontal cortex (superior) right	ORBsupb-R
7			Middle frontal gyrus left	MFG-L
8			Middle frontal gyrus right	MFG-R
9			Orbitofrontal cortex (middle) left	ORBmid-L
10			Orbitofrontal cortex (middle) right	ORBmid-R
11			Inferior frontal gyrus (opercular) left	IFGoperc-L
12			Inferior frontal gyrus (opercular) right	IFGoperc-R
13			Inferior frontal gyrus (triangular) left	IFGtriang-L
14			Inferior frontal gyrus (triangular) right	IFGtriang-R
15			Orbitofrontal cortex (inferior) left	ORBinf-L
16			Orbitofrontal cortex (inferior) right	ORBinf-R
17			Rolandic operculum left	ROL-L
18			Rolandic operculum right	ROL-R
19			Supplementary motor area left	SMA-L
20			Supplementary motor area right	SMA-R
21			Olfactory left	OLF-L
22			Olfactory right	OLF-R
23			Superior frontal gyrus (medial) left	SFGmed-L
24			Superior frontal gyrus (medial) right	SFGmed-R
25			Orbitofrontal cortex (medial) left	ORBmed-L
26			Orbitofrontal cortex (medial) right	ORBmed-R
27			Rectus gyrus left	REC-L
28			Rectus gyrus right	REC-R
29			Insula left	INS-L
30			Insula right	INS-R
31			Anterior cingulate gyrus left	ACG-L
32			Anterior cingulate gyrus right	ACG-R
33			Middle cingulate gyrus left	MCG-L

34		Middle cingulate gyrus right	MCG-R
35		Posterior cingulate gyrus left	PCG-L
36		Posterior cingulate gyrus right	PCG-R
37		Hippocampus left	HIP-L
38		Hippocampus right	HIP-R
39		ParaHippocampal gyrus left	PHG-L
40		ParaHippocampal gyrus right	PHG-R
41		Amygdala left	AMYG-L
42		Amygdala right	AMYG-R
43		Calcarine cortex left	CAL-L
44		Calcarine cortex right	CAL-R
45		Cuneus left	CUN-L
46		Cuneus right	CUN-R
47		Lingual gyrus left	LING-L
48		Lingual gyrus right	LING-R
49		Superior occipital gyrus left	SOG-L
50		Superior occipital gyrus right	SOG-R
51		Middle occipital gyrus left	MOG-L
52		Middle occipital gyrus right	MOG-R
53		Inferior occipital gyrus left	IOG-L
54		Inferior occipital gyrus right	IOG-R
55		Fusiform gyrus left	FFG-L
56		Fusiform gyrus right	FFG-R
57		Postcentral gyrus left	PoCG-L
58		Postcentral gyrus right	PoCG-R
59		Superior parietal gyrus left	SPG-L
60		Superior parietal gyrus right	SPG-R
61		Inferior parietal lobule left	IPL-L
62		Inferior parietal lobule right	IPL-R
63		Supramarginal gyrus left	SMG-L
64		Supramarginal gyrus right	SMG-R
65		Angular gyrus left	ANG-L
66		Angular gyrus right	ANG-R
67		Precuneus left	PCUN-L
68		Precuneus right	PCUN-R
69		Paracentral lobule left	PCL-L
70		Paracentral lobule right	PCL-R
71		Caudate left	CAU-L
72		Caudate right	CAU-R
73		Putamen left	PUT-L
74		Putamen right	PUT-R

75		Pallidum left	PAL-L
76		Pallidum right	PAL-R
77		Thalamus left	THA-L
78		Thalamus right	THA-R
79		Heschl gyrus left	HES-L
80		Heschl gyrus right	HES-R
81		Superior temporal gyrus left	STG-L
82		Superior temporal gyrus right	STG-R
83		Temporal pole (superior) left	TPOsup-L
84		Temporal pole (superior) right	TPOsup-R
85		Middle temporal gyrus left	MTG-L
86		Middle temporal gyrus right	MTG-R
87		Temporal pole (middle) left	TPOmid-L
88		Temporal pole (middle) right	TPOmid-R
89		Inferior temporal gyrus left	ITG-L
90		Inferior temporal gyrus right	ITG-R

Table 6.2. Index of the ALBERT atlas ROIs' names and colors. Sym.: Symmetric, Asym.: Asymmetric.

Index	Color (Sym.)	Color (Asym.)	Region
1			Hippocampus right
2			Hippocampus left
3			Amygdala right
4			Amygdala left
5			Anterior temporal lobe, medial part right
6			Anterior temporal lobe, medial part left
7			Anterior temporal lobe, lateral part right
8			Anterior temporal lobe, lateral part left
9			Gyri parahippocampalis et ambiens anterior part right
10			Gyri parahippocampalis et ambiens anterior part left
11			Superior temporal gyrus, middle part right
12			Superior temporal gyrus, middle part left
13			Medial and inferior temporal gyri anterior part right
14			Medial and inferior temporal gyri anterior part left
15			Lateral occipitotemporal gyrus, gyrus fusiformis anterior part right
16			Lateral occipitotemporal gyrus, gyrus fusiformis anterior part left
17			Cerebellum right
18			Cerebellum left
19			Brainstem, spans the midline
20			Insula left
21			Insula right
22			Occipital lobe left
23			Occipital lobe right
24			Gyri parahippocampalis et ambiens posterior part left
25			Gyri parahippocampalis et ambiens posterior part right
26			Lateral occipitotemporal gyrus, gyrus fusiformis posterior part left
27			Lateral occipitotemporal gyrus, gyrus fusiformis posterior part right
28			Medial and inferior temporal gyri posterior part left
29			Medial and inferior temporal gyri posterior part right
30			Superior temporal gyrus, posterior part left
31			Superior temporal gyrus, posterior part right
32			Cingulate gyrus, anterior part left
33			Cingulate gyrus, anterior part right
34			Cingulate gyrus, posterior part left

35		Cingulate gyrus, posterior part right
36		Frontal lobe left
37		Frontal lobe right
38		Parietal lobe left
39		Parietal lobe right
40		Caudate nucleus left
41		Caudate nucleus right
42		Thalamus left
43		Thalamus right
44		Subthalamic nucleus left
45		Subthalamic nucleus right
46		Lentiform Nucleus left
47		Lentiform Nucleus right
48		Corpus Callosum
49		Lateral Ventricle right
50		Lateral Ventricle left

Table 6.3. Index of the JHU atlas ROIs' names and colors. Sym.: Symmetric, Asym.: Asymmetric.

Index	Color (Sym.)	Color (Asym.)	Region	Location
1			corpus callosum	left
2			corpus callosum	right
3			anterior limb of internal capsule	left
4			anterior limb of internal capsule	right
5			posterior limb of internal capsule	left
6			posterior limb of internal capsule	right
7			retrolenticular part of internal capsule	left
8			retrolenticular part of internal capsule	right
9			anterior corona radiata	left
10			anterior corona radiata	right
11			superior corona radiata	left
12			superior corona radiata	right
13			posterior corona radiata	left
14			posterior corona radiata	right
15			cingulum cingular part	left
16			cingulum cingular part	right
17			cingulum hippocampal part	left
18			cingulum hippocampal part	right
19			fornix	left
20			fornix	right
21			stria terminalis	left
22			stria terminalis	right
23			tapetum	left
24			tapetum	right
25			superior longitudinal fasciculus	left
26			superior longitudinal fasciculus	right
27			external capsule	left
28			external capsule	right
29			posterior thalamic radiation	left
30			posterior thalamic radiation	right
31			sagittal stratum	left
32			sagittal stratum	right
33			thalamus	left
34			Thalamus	right
35			Putamen	left
36			Putamen	right
37			globus pallidus	left
38			globus pallidus	right

39		caudate nucleus	left
40		caudate nucleus	right
41		cerebral peduncle	left
42		cerebral peduncle	right
43		superior fronto-occipital fasciculus	left
44		superior fronto-occipital fasciculus	right
45		inferior fronto-occipital fasciculus	left
46		inferior fronto-occipital fasciculus	right
47		corticospinal tract	left
48		corticospinal tract	right
49		superior cerebellar peduncle	left
50		superior cerebellar peduncle	right
51		middle cerebellar peduncle	left
52		middle cerebellar peduncle	right
53		inferior cerebellar peduncle	left
54		inferior cerebellar peduncle	right
55		pontine crossing tract	left
56		pontine crossing tract	right
57		uncinate fasciculus	left
58		uncinate fasciculus	right
59		midbrain	left
60		midbrain	right
61		pons	left
62		pons	right
63		medial lemniscus	left
64		medial lemniscus	right
65		medulla oblongata	left
66		medulla oblongata	right
67		superior frontal gyrus	left
68		superior frontal gyrus	right
69		middle frontal gyrus	left
70		middle frontal gyrus	right
71		inferior frontal gyrus	left
72		inferior frontal gyrus	right
73		medial fronto-orbaital gyrus	left
74		medial fronto-orbaital gyrus	right
75		lateral fronto-orbital gyrus	left
76		lateral fronto-orbital gyrus	right
77		gyrus rectus	left
78		gyrus rectus	right
79		precentral gyrus	left

80		precentral gyrus	right
81		postcentral gyrus	left
82		postcentral gyrus	right
83		superior parietal gyrus	left
84		superior parietal gyrus	right
85		precuneus	left
86		precuneus	right
87		cingular gyrus	left
88		cingular gyrus	right
89		supramarginal gyrus	left
90		supramarginal gyrus	right
91		angular gyrus	left
92		angular gyrus	right
93		superior temporal gyrus	left
94		superior temporal gyrus	right
95		middle temporal gyrus	left
96		middle temporal gyrus	right
97		inferior temporal gyrus	left
98		inferior temporal gyrus	right
99		fusiform gyrus	left
100		fusiform gyrus	right
101		parahippocampal gyrus	left
102		parahippocampal gyrus	right
103		entrhinal cortex	left
104		entrhinal cortex	right
105		superior occipital gyrus	left
106		superior occipital gyrus	right
107		middle occipital gyrus	left
108		middle occipital gyrus	right
109		inferior occipital gyrus	left
110		inferior occipital gyrus	right
111		cuneus	left
112		cuneus	right
113		lyngual gyrus	left
114		lyngual gyrus	right
115		amygdala	left
116		amygdala	right
117		hippocampus	left
118		hippocampus	right
119		cerebellar hemisphere	left
120		cerebellar hemisphere	right

121		insular cortex	left
122		insular cortex	right

Table 6.4. Longitudinal Probabilistic Distribution of Points per ROIs using Symmetric UNC Parcellation Map with 90 ROIs given as: Number of points per ROI (Percentage on surface %)

Week /ROI#	28	29	30	31	32	33	34	35	36	37	38	39	40	41	42	43	44
1 & 2	1031(2.931%)	1087(2.901%)	1190(2.91%)	1266(2.887%)	1409(3.028%)	1570(3.085%)	1708(3.21%)	1916(3.362%)	1978(3.284%)	2092(3.472%)	2497(3.615%)	2721(3.464%)	2734(3.558%)	2757(3.525%)	2963(3.438%)	2838(3.32%)	2907(3.284%)
3 & 4	1073(3.051%)	1180(3.15%)	1349(3.298%)	1527(3.482%)	1807(3.884%)	2128(4.181%)	2290(4.304%)	2648(4.646%)	2824(4.689%)	2881(4.782%)	3183(4.608%)	3573(4.549%)	3467(4.512%)	3657(4.675%)	4334(5.029%)	4173(4.882%)	4248(4.798%)
5 & 6	547(1.555%)	614(1.639%)	695(1.699%)	772(1.761%)	823(1.769%)	907(1.782%)	984(1.849%)	1077(1.89%)	1123(1.865%)	1073(1.781%)	1161(1.681%)	1324(1.686%)	1293(1.683%)	1352(1.728%)	1578(1.831%)	1540(1.802%)	1652(1.866%)
7 & 8	2769(7.873%)	2909(7.765%)	3209(7.846%)	3442(7.85%)	3627(7.796%)	3893(7.649%)	4085(7.678%)	4351(7.635%)	4460(7.405%)	4495(7.46%)	4715(6.826%)	5126(6.526%)	5024(6.538%)	5073(6.485%)	5395(6.26%)	5357(6.268%)	5547(6.266%)
9 & 10	376(1.069%)	456(1.217%)	561(1.372%)	677(1.544%)	738(1.586%)	831(1.633%)	956(1.797%)	1151(2.02%)	1218(2.022%)	1187(1.97%)	1307(1.892%)	1542(1.963%)	1541(2.005%)	1587(2.029%)	1729(2.006%)	1736(2.031%)	1778(2.008%)
11 & 12	718(2.041%)	709(1.892%)	724(1.77%)	715(1.631%)	705(1.515%)	694(1.364%)	668(1.255%)	689(1.209%)	658(1.092%)	674(1.119%)	762(1.103%)	790(1.006%)	816(1.062%)	815(1.042%)	860(0.998%)	900(1.053%)	927(1.047%)
13 & 14	756(2.149%)	826(2.205%)	926(2.264%)	968(2.208%)	1054(2.265%)	1135(2.23%)	1230(2.312%)	1330(2.334%)	1437(2.386%)	1415(2.348%)	1596(2.311%)	1775(2.26%)	1731(2.252%)	1658(2.12%)	1686(1.956%)	1808(2.115%)	1802(2.035%)
15 & 16	1632(4.64%)	1683(4.492%)	1734(4.24%)	1751(3.993%)	1773(3.811%)	1793(3.523%)	1834(3.447%)	1834(3.218%)	1879(3.12%)	1819(3.019%)	1941(2.81%)	2132(2.714%)	2118(2.756%)	2075(2.653%)	2100(2.437%)	2228(2.607%)	2255(2.547%)
17 & 18	522(1.484%)	542(1.447%)	572(1.399%)	586(1.336%)	588(1.264%)	587(1.153%)	590(1.109%)	614(1.077%)	533(0.885%)	557(0.924%)	615(0.89%)	880(1.12%)	804(1.046%)	558(0.713%)	948(1.1%)	991(1.159%)	950(1.073%)
19 & 20	730(2.076%)	769(2.053%)	787(1.924%)	780(1.779%)	816(1.754%)	896(1.76%)	872(1.639%)	873(1.532%)	1027(1.705%)	1077(1.787%)	1510(2.186%)	1935(2.463%)	1891(2.461%)	2006(2.564%)	2225(2.582%)	2296(2.686%)	2408(2.72%)
21 & 22	427(1.214%)	441(1.177%)	467(1.142%)	467(1.065%)	469(1.008%)	451(0.886%)	440(0.827%)	467(0.819%)	456(0.757%)	407(0.675%)	361(0.523%)	366(0.466%)	338(0.44%)	338(0.432%)	337(0.391%)	309(0.362%)	302(0.341%)
23 & 24	860(2.445%)	902(2.408%)	954(2.333%)	957(2.183%)	995(2.139%)	971(1.908%)	1033(1.942%)	1153(2.023%)	1151(1.911%)	1137(1.887%)	1330(1.926%)	1754(2.233%)	1652(2.115%)	1778(2.273%)	2107(2.445%)	2061(2.411%)	2415(2.728%)
25 & 26	93(0.264%)	97(0.259%)	101(0.247%)	106(0.242%)	106(0.228%)	109(0.214%)	115(0.216%)	126(0.221%)	123(0.204%)	126(0.209%)	137(0.198%)	267(0.34%)	282(0.367%)	309(0.395%)	422(0.49%)	407(0.476%)	486(0.549%)
27 & 28	222(0.631%)	252(0.673%)	291(0.711%)	301(0.686%)	340(0.731%)	371(0.729%)	360(0.677%)	382(0.67%)	386(0.641%)	380(0.631%)	380(0.55%)	424(0.54%)	393(0.511%)	395(0.505%)	404(0.469%)	403(0.471%)	398(0.45%)
29 & 30	0(0%)	0(0%)	0(0%)	0(0%)	0(0%)	0(0%)	0(0%)	0(0%)	0(0%)	46(0.076%)	181(0.262%)	200(0.255%)	197(0.256%)	196(0.251%)	184(0.213%)	174(0.204%)	159(0.18%)
31 & 32	0(0%)	0(0%)	0(0%)	0(0%)	0(0%)	0(0%)	0(0%)	0(0%)	0(0%)	0(0%)	354(0.513%)	750(0.955%)	739(0.962%)	823(1.052%)	919(1.066%)	909(1.064%)	1110(1.254%)
33 & 34	164(0.466%)	362(0.966%)	502(1.227%)	523(1.193%)	489(1.051%)	443(0.87%)	405(0.761%)	220(0.386%)	527(0.875%)	488(0.81%)	1130(1.636%)	1436(1.828%)	1361(1.771%)	1323(1.691%)	1310(1.52%)	1588(1.858%)	1684(1.902%)
35 & 36	217(0.617%)	253(0.675%)	260(0.636%)	242(0.552%)	215(0.462%)	190(0.373%)	156(0.293%)	164(0.288%)	169(0.281%)	192(0.319%)	186(0.269%)	166(0.211%)	165(0.215%)	172(0.22%)	164(0.19%)	159(0.186%)	150(0.169%)
37 & 38	560(1.592%)	684(1.826%)	727(1.778%)	805(1.836%)	817(1.756%)	946(1.859%)	903(1.697%)	897(1.574%)	957(1.589%)	942(1.563%)	1074(1.555%)	1114(1.418%)	1085(1.412%)	1164(1.488%)	1285(1.491%)	1278(1.495%)	1308(1.477%)
39 & 40	1511(4.296%)	1614(4.308%)	1635(3.998%)	1676(3.822%)	1664(3.576%)	1640(3.222%)	1586(2.981%)	1491(2.616%)	1460(2.424%)	1423(2.362%)	1293(1.872%)	1244(1.584%)	1218(1.585%)	1188(1.519%)	1050(1.218%)	1011(1.183%)	992(1.12%)
41 & 42	292(0.83%)	317(0.846%)	334(0.817%)	341(0.778%)	405(0.87%)	438(0.861%)	437(0.821%)	417(0.732%)	407(0.676%)	428(0.71%)	389(0.563%)	326(0.415%)	346(0.45%)	306(0.391%)	264(0.306%)	276(0.323%)	276(0.312%)
43 & 44	616(1.751%)	682(1.82%)	847(2.071%)	994(2.267%)	1027(2.207%)	1393(2.737%)	1402(2.635%)	1391(2.441%)	1703(2.827%)	1640(2.722%)	2160(3.127%)	2510(3.195%)	2479(3.226%)	2726(3.485%)	3284(3.81%)	2975(3.481%)	3049(3.444%)
45 & 46	509(1.447%)	546(1.457%)	630(1.54%)	768(1.752%)	861(1.851%)	1070(2.102%)	1224(2.3%)	1453(2.55%)	1489(2.472%)	1467(2.435%)	1715(2.483%)	1920(2.444%)	1943(2.528%)	1804(2.306%)	1934(2.244%)	1921(2.248%)	1924(2.173%)

47 & 48	2119(6.025%)	2207(5.891%)	2301(5.626%)	2411(5.499%)	2511(5.397%)	2609(5.126%)	2714(5.101%)	2681(4.704%)	2529(4.199%)	2532(4.202%)	2601(3.766%)	2644(3.366%)	2406(3.131%)	2477(3.167%)	2424(2.812%)	2203(2.577%)	2203(2.488%)
49 & 50	0(0%)	0(0%)	150(0.367%)	179(0.408%)	229(0.492%)	292(0.574%)	368(0.692%)	466(0.818%)	512(0.85%)	489(0.812%)	676(0.979%)	971(1.236%)	769(1.001%)	852(1.089%)	951(1.103%)	814(0.952%)	918(1.037%)
51 & 52	990(2.815%)	1045(2.789%)	1060(2.592%)	1202(2.741%)	1259(2.706%)	1504(2.955%)	1630(3.064%)	1789(3.139%)	1865(3.096%)	1857(3.082%)	2111(3.056%)	2340(2.979%)	2167(2.82%)	2297(2.937%)	2356(2.734%)	2316(2.71%)	2475(2.796%)
53 & 54	87(0.247%)	106(0.283%)	152(0.372%)	201(0.458%)	238(0.512%)	335(0.658%)	440(0.827%)	536(0.941%)	577(0.958%)	572(0.949%)	729(1.055%)	976(1.243%)	885(1.152%)	1040(1.33%)	1144(1.327%)	1033(1.209%)	1044(1.179%)
55 & 56	1065(3.028%)	1309(3.494%)	1490(3.643%)	1647(3.756%)	1744(3.748%)	1967(3.865%)	2185(4.107%)	2353(4.129%)	2497(4.146%)	2621(4.35%)	2840(4.112%)	3321(4.228%)	3202(4.167%)	3394(4.339%)	3315(3.846%)	3123(3.654%)	3057(3.453%)
57 & 58	1413(4.017%)	1466(3.913%)	1599(3.91%)	1699(3.875%)	1801(3.871%)	1919(3.77%)	2036(3.827%)	2236(3.923%)	2284(3.792%)	2324(3.857%)	2503(3.624%)	2505(3.189%)	2514(3.271%)	2381(3.044%)	2478(2.875%)	2495(2.919%)	2484(2.806%)
59 & 60	288(0.819%)	319(0.851%)	364(0.89%)	436(0.994%)	545(1.171%)	685(1.346%)	769(1.445%)	997(1.749%)	1173(1.948%)	1306(2.168%)	1641(2.376%)	2040(2.597%)	1838(2.392%)	2101(2.686%)	2436(2.826%)	2287(2.676%)	2388(2.697%)
61 & 62	897(2.55%)	933(2.49%)	959(2.345%)	989(2.256%)	1039(2.233%)	1077(2.116%)	1111(2.088%)	1189(2.086%)	1196(1.986%)	1236(2.051%)	1379(1.997%)	1536(1.955%)	1548(2.014%)	1538(1.966%)	1765(2.048%)	1732(2.026%)	1795(2.028%)
63 & 64	579(1.646%)	640(1.708%)	765(1.87%)	856(1.952%)	979(2.104%)	1023(2.01%)	1140(2.143%)	1329(2.332%)	1445(2.399%)	1465(2.431%)	1611(2.332%)	1852(2.358%)	1953(2.541%)	2033(2.599%)	2296(2.664%)	2545(2.978%)	2547(2.877%)
65 & 66	870(2.474%)	899(2.4%)	968(2.367%)	1107(2.525%)	1223(2.629%)	1368(2.688%)	1443(2.712%)	1588(2.786%)	1686(2.799%)	1651(2.74%)	1783(2.581%)	1936(2.465%)	1909(2.484%)	1958(2.503%)	2090(2.425%)	2063(2.414%)	2131(2.407%)
67 & 68	1151(3.272%)	1187(3.168%)	1298(3.174%)	1440(3.284%)	1525(3.278%)	1673(3.287%)	1703(3.201%)	1696(2.976%)	1964(3.261%)	2027(3.364%)	2722(3.941%)	3150(4.01%)	3097(4.03%)	3200(4.091%)	3268(3.792%)	3299(3.86%)	3369(3.805%)
69 & 70	149(0.424%)	165(0.44%)	185(0.452%)	214(0.488%)	214(0.46%)	247(0.485%)	241(0.453%)	242(0.425%)	261(0.433%)	240(0.398%)	271(0.392%)	276(0.351%)	252(0.328%)	261(0.334%)	247(0.287%)	259(0.303%)	280(0.316%)
71 & 72	622(1.768%)	693(1.85%)	741(1.812%)	807(1.844%)	794(1.707%)	953(1.872%)	1124(2.113%)	1227(2.153%)	1438(2.388%)	1351(2.242%)	1595(2.309%)	1925(2.451%)	2094(2.725%)	1902(2.432%)	2389(2.772%)	2235(2.615%)	2390(2.7%)
73 & 74	1012(2.877%)	1119(2.987%)	1254(3.066%)	1364(3.111%)	1404(3.018%)	1586(3.116%)	1650(3.101%)	1675(2.939%)	1864(3.095%)	1800(2.987%)	2006(2.904%)	2145(2.731%)	2193(2.854%)	2219(2.837%)	2433(2.823%)	2546(2.979%)	2651(2.994%)
75 & 76	0(0%)	0(0%)	0(0%)	0(0%)	0(0%)	0(0%)	0(0%)	0(0%)	0(0%)	0(0%)	0(0%)	0(0%)	0(0%)	0(0%)	0(0%)	0(0%)	0(0%)
77 & 78	718(2.041%)	709(1.892%)	760(1.858%)	826(1.884%)	862(1.853%)	912(1.792%)	924(1.737%)	968(1.699%)	985(1.635%)	968(1.607%)	1067(1.545%)	1236(1.574%)	1187(1.545%)	1296(1.657%)	1589(1.844%)	1385(1.62%)	1490(1.683%)
79 & 80	0(0%)	0(0%)	0(0%)	0(0%)	0(0%)	0(0%)	0(0%)	0(0%)	0(0%)	0(0%)	0(0%)	0(0%)	0(0%)	0(0%)	0(0%)	0(0%)	0(0%)
81 & 82	1300(3.696%)	1331(3.553%)	1468(3.589%)	1535(3.501%)	1577(3.39%)	1625(3.193%)	1587(2.983%)	1756(3.081%)	1772(2.942%)	1764(2.928%)	2819(4.081%)	3462(4.407%)	3480(4.528%)	2804(3.585%)	3537(4.104%)	3355(3.925%)	3636(4.107%)
83 & 84	550(1.564%)	588(1.57%)	644(1.575%)	723(1.649%)	804(1.728%)	910(1.788%)	995(1.87%)	1214(2.13%)	1458(2.421%)	1504(2.496%)	1816(2.629%)	2150(2.737%)	2111(2.747%)	2241(2.865%)	3207(3.721%)	3408(3.987%)	3418(3.861%)
85 & 86	1223(3.477%)	1355(3.617%)	1573(3.846%)	1765(4.025%)	2004(4.307%)	2314(4.547%)	2552(4.796%)	2859(5.017%)	3222(5.349%)	3271(5.429%)	3561(5.156%)	3941(5.017%)	4114(5.353%)	4308(5.507%)	4407(5.113%)	4308(5.04%)	4366(4.932%)
87 & 88	199(0.566%)	221(0.59%)	274(0.67%)	359(0.819%)	475(1.021%)	592(1.163%)	692(1.301%)	800(1.404%)	942(1.564%)	996(1.653%)	1109(1.606%)	1342(1.709%)	1389(1.807%)	1451(1.855%)	1580(1.833%)	1575(1.843%)	1601(1.808%)
89 & 90	3765(10.705%)	3685(9.836%)	3857(9.43%)	3922(8.945%)	3989(8.574%)	4171(8.195%)	4135(7.772%)	4260(7.475%)	4084(6.781%)	3804(6.313%)	3690(5.342%)	3894(4.957%)	3515(4.574%)	3783(4.836%)	4158(4.824%)	4553(5.327%)	4951(5.592%)

Table 6.5. Longitudinal Probabilistic Distribution of Points per ROIs using Asymmetric UNC Parcellation Map with 90 ROIs given as: Number of points per ROI (Percentage on surface %)

Week /ROI#	28	29	30	31	32	33	34	35	36	37	38	39	40	41	42	43	44
1	504(1.445%)	527(1.427%)	577(1.424%)	617(1.412%)	673(1.449%)	780(1.522%)	821(1.526%)	911(1.538%)	938(1.462%)	967(1.493%)	1136(1.55%)	1223(1.487%)	1229(1.522%)	1247(1.515%)	1346(1.514%)	1400(1.578%)	1459(1.602%)
2	419(1.202%)	440(1.192%)	507(1.251%)	547(1.252%)	605(1.303%)	686(1.338%)	741(1.378%)	845(1.426%)	894(1.393%)	947(1.463%)	1019(1.391%)	1142(1.388%)	1131(1.4%)	1167(1.418%)	1264(1.421%)	1253(1.413%)	1293(1.42%)
3	461(1.322%)	495(1.341%)	583(1.439%)	666(1.524%)	776(1.671%)	927(1.808%)	980(1.822%)	1121(1.892%)	1159(1.806%)	1170(1.807%)	1279(1.745%)	1368(1.663%)	1347(1.668%)	1394(1.694%)	1462(1.644%)	1462(1.648%)	1488(1.634%)
4	295(0.846%)	329(0.891%)	382(0.943%)	433(0.991%)	492(1.059%)	600(1.17%)	666(1.238%)	810(1.367%)	922(1.437%)	933(1.441%)	1130(1.542%)	1407(1.711%)	1344(1.664%)	1434(1.742%)	1875(2.109%)	1821(2.053%)	1840(2.02%)
5	257(0.737%)	287(0.777%)	340(0.839%)	323(0.739%)	362(0.779%)	407(0.794%)	441(0.82%)	483(0.815%)	484(0.754%)	461(0.712%)	498(0.68%)	576(0.7%)	561(0.695%)	593(0.72%)	603(0.678%)	611(0.689%)	622(0.683%)
6	193(0.553%)	231(0.626%)	274(0.676%)	332(0.76%)	376(0.81%)	393(0.767%)	425(0.79%)	497(0.839%)	499(0.777%)	472(0.729%)	528(0.721%)	649(0.789%)	601(0.744%)	639(0.776%)	804(0.904%)	745(0.84%)	836(0.918%)
7	1318(3.78%)	1375(3.724%)	1489(3.675%)	1571(3.594%)	1637(3.524%)	1728(3.371%)	1823(3.389%)	1910(3.224%)	1972(3.073%)	1969(3.041%)	2069(2.823%)	2261(2.749%)	2196(2.719%)	2196(2.668%)	2325(2.615%)	2277(2.567%)	2354(2.585%)
8	1327(3.805%)	1382(3.743%)	1489(3.675%)	1611(3.686%)	1703(3.666%)	1862(3.632%)	1951(3.627%)	2093(3.533%)	2134(3.325%)	2120(3.274%)	2182(2.978%)	2341(2.846%)	2321(2.874%)	2326(2.826%)	2335(2.626%)	2414(2.722%)	2387(2.621%)
9	153(0.439%)	186(0.504%)	211(0.521%)	240(0.549%)	254(0.547%)	301(0.587%)	334(0.621%)	396(0.668%)	429(0.668%)	423(0.653%)	471(0.643%)	549(0.667%)	553(0.685%)	573(0.696%)	670(0.753%)	669(0.754%)	696(0.764%)
10	208(0.596%)	225(0.609%)	281(0.693%)	317(0.725%)	346(0.745%)	416(0.811%)	478(0.889%)	550(0.928%)	593(0.924%)	585(0.903%)	659(0.899%)	796(0.968%)	773(0.957%)	820(0.996%)	925(1.04%)	949(1.07%)	971(1.066%)
11	187(0.536%)	196(0.531%)	205(0.506%)	199(0.455%)	212(0.456%)	216(0.421%)	200(0.372%)	204(0.344%)	213(0.332%)	214(0.33%)	230(0.314%)	228(0.277%)	224(0.277%)	221(0.268%)	231(0.26%)	250(0.282%)	243(0.267%)
12	372(1.067%)	370(1.002%)	376(0.928%)	413(0.945%)	413(0.889%)	435(0.849%)	431(0.801%)	448(0.756%)	486(0.757%)	425(0.656%)	430(0.587%)	373(0.453%)	361(0.447%)	367(0.446%)	337(0.379%)	356(0.401%)	354(0.389%)
13	495(1.419%)	532(1.441%)	591(1.458%)	617(1.412%)	650(1.399%)	691(1.348%)	724(1.346%)	793(1.339%)	833(1.298%)	794(1.226%)	875(1.194%)	994(1.208%)	1027(1.272%)	1007(1.223%)	1056(1.188%)	1114(1.256%)	1119(1.229%)
14	407(1.167%)	437(1.183%)	483(1.192%)	490(1.121%)	531(1.143%)	596(1.163%)	621(1.155%)	683(1.153%)	725(1.13%)	716(1.106%)	743(1.014%)	831(1.01%)	800(0.99%)	868(1.055%)	822(0.924%)	859(0.968%)	861(0.945%)
15	847(2.429%)	879(2.38%)	916(2.261%)	938(2.146%)	963(2.073%)	952(1.857%)	1000(1.859%)	1034(1.745%)	1055(1.644%)	1023(1.58%)	975(1.331%)	1080(1.313%)	1065(1.319%)	1085(1.318%)	1114(1.253%)	1169(1.318%)	1186(1.302%)
16	450(1.29%)	488(1.322%)	532(1.313%)	567(1.297%)	609(1.311%)	658(1.284%)	720(1.339%)	795(1.342%)	844(1.315%)	811(1.252%)	891(1.216%)	1001(1.217%)	1020(1.263%)	1048(1.273%)	1038(1.167%)	1078(1.215%)	1085(1.191%)
17	42(0.12%)	46(0.125%)	58(0.143%)	60(0.137%)	70(0.151%)	72(0.14%)	81(0.151%)	82(0.138%)	83(0.129%)	84(0.13%)	293(0.4%)	503(0.612%)	532(0.659%)	347(0.422%)	553(0.622%)	370(0.417%)	330(0.362%)
18	56(0.161%)	65(0.176%)	64(0.158%)	65(0.149%)	72(0.155%)	83(0.162%)	91(0.169%)	106(0.179%)	118(0.184%)	105(0.162%)	120(0.164%)	148(0.18%)	159(0.197%)	178(0.216%)	237(0.267%)	234(0.264%)	222(0.244%)
19	431(1.236%)	454(1.229%)	474(1.17%)	470(1.075%)	524(1.128%)	638(1.245%)	594(1.104%)	670(1.131%)	901(1.404%)	1034(1.597%)	1125(1.535%)	1183(1.438%)	1184(1.466%)	1192(1.448%)	1331(1.497%)	1251(1.41%)	1283(1.409%)
20	382(1.095%)	385(1.043%)	390(0.962%)	422(0.966%)	442(0.952%)	482(0.94%)	581(1.08%)	789(1.332%)	819(1.276%)	858(1.325%)	860(1.174%)	833(1.013%)	820(1.015%)	825(1.002%)	832(0.936%)	859(0.968%)	892(0.979%)
21	195(0.559%)	207(0.561%)	208(0.513%)	205(0.469%)	211(0.454%)	211(0.412%)	206(0.383%)	224(0.378%)	212(0.33%)	215(0.332%)	240(0.328%)	234(0.284%)	221(0.274%)	227(0.276%)	226(0.254%)	221(0.249%)	211(0.232%)
22	415(1.19%)	441(1.194%)	333(0.821%)	324(0.741%)	321(0.691%)	309(0.603%)	307(0.571%)	299(0.505%)	301(0.469%)	314(0.485%)	309(0.422%)	309(0.376%)	310(0.384%)	304(0.369%)	288(0.324%)	285(0.321%)	287(0.315%)
23	424(1.216%)	453(1.227%)	491(1.212%)	524(1.199%)	586(1.262%)	665(1.297%)	700(1.302%)	866(1.462%)	933(1.454%)	943(1.456%)	1402(1.913%)	1743(2.119%)	1673(2.071%)	1669(2.028%)	1960(2.204%)	1865(2.103%)	1915(2.103%)

24	336(0.964%)	346(0.937%)	381(0.94%)	440(1.007%)	476(1.025%)	526(1.026%)	565(1.05%)	683(1.153%)	747(1.164%)	741(1.144%)	1017(1.388%)	1169(1.421%)	1155(1.43%)	1189(1.445%)	1147(1.29%)	1116(1.258%)	1115(1.224%)
25	0(0%)	0(0%)	0(0%)	100(0.229%)	96(0.207%)	114(0.222%)	122(0.227%)	154(0.26%)	172(0.268%)	165(0.255%)	250(0.341%)	350(0.426%)	348(0.431%)	306(0.372%)	377(0.424%)	435(0.49%)	449(0.493%)
26	0(0%)	0(0%)	0(0%)	0(0%)	0(0%)	51(0.099%)	65(0.121%)	92(0.155%)	100(0.156%)	102(0.158%)	297(0.405%)	421(0.512%)	400(0.495%)	563(0.684%)	606(0.681%)	472(0.532%)	499(0.548%)
27	202(0.579%)	235(0.636%)	260(0.642%)	298(0.682%)	318(0.685%)	352(0.687%)	365(0.679%)	414(0.699%)	433(0.675%)	406(0.627%)	440(0.6%)	491(0.597%)	463(0.573%)	457(0.555%)	609(0.685%)	543(0.612%)	563(0.618%)
28	286(0.82%)	297(0.804%)	324(0.8%)	292(0.668%)	303(0.652%)	294(0.574%)	301(0.56%)	311(0.525%)	288(0.449%)	284(0.439%)	274(0.374%)	276(0.336%)	278(0.344%)	293(0.356%)	304(0.342%)	322(0.363%)	313(0.344%)
29	0(0%)	0(0%)	0(0%)	0(0%)	0(0%)	0(0%)	0(0%)	0(0%)	0(0%)	41(0.063%)	174(0.237%)	164(0.199%)	171(0.212%)	163(0.198%)	251(0.282%)	262(0.295%)	252(0.277%)
30	260(0.746%)	204(0.552%)	202(0.498%)	211(0.483%)	220(0.474%)	238(0.464%)	235(0.437%)	240(0.405%)	188(0.293%)	195(0.301%)	211(0.288%)	214(0.26%)	188(0.233%)	218(0.265%)	214(0.241%)	217(0.245%)	210(0.231%)
31	0(0%)	0(0%)	0(0%)	0(0%)	0(0%)	0(0%)	0(0%)	0(0%)	273(0.425%)	434(0.67%)	645(0.888%)	745(0.906%)	706(0.874%)	677(0.823%)	721(0.811%)	866(0.976%)	970(1.065%)
32	0(0%)	0(0%)	0(0%)	0(0%)	0(0%)	0(0%)	0(0%)	0(0%)	193(0.301%)	393(0.607%)	607(0.828%)	674(0.819%)	703(0.87%)	697(0.847%)	665(0.748%)	722(0.814%)	722(0.793%)
33	216(0.619%)	227(0.615%)	330(0.814%)	334(0.764%)	365(0.786%)	317(0.618%)	420(0.781%)	628(1.06%)	870(1.356%)	847(1.308%)	928(1.266%)	992(1.206%)	976(1.208%)	846(1.028%)	970(1.091%)	986(1.112%)	1097(1.205%)
34	0(0%)	108(0.292%)	121(0.299%)	152(0.348%)	179(0.385%)	218(0.425%)	221(0.411%)	312(0.527%)	790(1.231%)	868(1.34%)	1125(1.535%)	1282(1.559%)	1320(1.634%)	1417(1.722%)	1249(1.405%)	1273(1.435%)	1329(1.459%)
35	502(1.44%)	460(1.246%)	511(1.261%)	571(1.306%)	553(1.191%)	511(0.997%)	512(0.952%)	417(0.704%)	448(0.698%)	434(0.67%)	483(0.659%)	482(0.586%)	457(0.566%)	456(0.554%)	533(0.599%)	522(0.588%)	542(0.595%)
36	0(0%)	0(0%)	0(0%)	0(0%)	0(0%)	0(0%)	0(0%)	0(0%)	0(0%)	0(0%)	0(0%)	0(0%)	0(0%)	60(0.073%)	56(0.063%)	0(0%)	0(0%)
37	0(0%)	55(0.149%)	153(0.378%)	176(0.403%)	183(0.394%)	222(0.433%)	216(0.402%)	248(0.419%)	269(0.419%)	271(0.419%)	375(0.512%)	457(0.556%)	451(0.558%)	521(0.633%)	574(0.645%)	565(0.637%)	563(0.618%)
38	157(0.45%)	267(0.723%)	316(0.78%)	354(0.81%)	434(0.934%)	506(0.987%)	465(0.865%)	507(0.856%)	588(0.916%)	517(0.798%)	564(0.77%)	498(0.605%)	503(0.623%)	507(0.616%)	541(0.608%)	558(0.629%)	587(0.645%)
39	986(2.827%)	982(2.659%)	941(2.322%)	949(2.171%)	976(2.101%)	951(1.855%)	926(1.722%)	886(1.496%)	851(1.326%)	833(1.286%)	734(1.002%)	683(0.83%)	667(0.826%)	695(0.844%)	595(0.669%)	567(0.639%)	535(0.587%)
40	955(2.739%)	974(2.638%)	959(2.367%)	997(2.281%)	997(2.146%)	997(1.945%)	1041(1.936%)	924(1.56%)	886(1.38%)	858(1.325%)	757(1.033%)	697(0.847%)	724(0.896%)	699(0.849%)	615(0.692%)	625(0.705%)	623(0.684%)
41	110(0.315%)	132(0.357%)	153(0.378%)	169(0.387%)	186(0.4%)	206(0.402%)	208(0.387%)	225(0.38%)	242(0.377%)	247(0.381%)	186(0.254%)	188(0.229%)	189(0.234%)	164(0.199%)	165(0.186%)	170(0.192%)	169(0.186%)
42	0(0%)	0(0%)	0(0%)	0(0%)	0(0%)	0(0%)	0(0%)	82(0.138%)	81(0.126%)	77(0.119%)	70(0.096%)	67(0.081%)	64(0.079%)	71(0.086%)	61(0.069%)	61(0.069%)	52(0.057%)
43	96(0.275%)	111(0.301%)	156(0.385%)	232(0.531%)	247(0.532%)	415(0.81%)	555(1.032%)	682(1.151%)	908(1.415%)	955(1.475%)	1309(1.786%)	1520(1.848%)	1442(1.785%)	1479(1.797%)	1826(2.053%)	1768(1.993%)	1874(2.058%)
44	99(0.284%)	105(0.284%)	141(0.348%)	160(0.366%)	233(0.502%)	469(0.915%)	646(1.201%)	759(1.281%)	1003(1.563%)	940(1.452%)	1157(1.579%)	1384(1.683%)	1411(1.747%)	1540(1.871%)	1657(1.863%)	1673(1.886%)	1700(1.867%)
45	351(1.007%)	357(0.967%)	417(1.029%)	458(1.048%)	490(1.055%)	526(1.026%)	545(1.013%)	633(1.069%)	641(0.999%)	658(1.016%)	918(1.253%)	1058(1.286%)	1055(1.306%)	1014(1.232%)	1051(1.182%)	1050(1.184%)	1059(1.163%)
46	523(1.5%)	572(1.549%)	634(1.565%)	566(1.295%)	637(1.371%)	638(1.245%)	626(1.164%)	661(1.116%)	739(1.151%)	759(1.172%)	828(1.13%)	888(1.08%)	903(1.118%)	907(1.102%)	834(0.938%)	861(0.971%)	879(0.965%)
47	1261(3.616%)	1350(3.656%)	1390(3.43%)	1530(3.501%)	1536(3.307%)	1714(3.343%)	1696(3.153%)	1819(3.071%)	1790(2.789%)	1787(2.76%)	1839(2.51%)	1891(2.299%)	1803(2.232%)	1873(2.276%)	1792(2.015%)	1666(1.878%)	1634(1.794%)
48	833(2.389%)	875(2.37%)	1019(2.515%)	1167(2.67%)	1149(2.474%)	1261(2.46%)	1303(2.423%)	1469(2.48%)	1489(2.32%)	1462(2.258%)	1471(2.007%)	1481(1.801%)	1345(1.665%)	1399(1.7%)	1277(1.436%)	1288(1.452%)	1290(1.416%)

49	143(0.41%)	143(0.387%)	168(0.415%)	206(0.471%)	226(0.487%)	299(0.583%)	363(0.675%)	452(0.763%)	500(0.779%)	494(0.763%)	674(0.92%)	864(1.05%)	742(0.919%)	783(0.951%)	829(0.932%)	774(0.873%)	839(0.921%)
50	77(0.221%)	79(0.214%)	98(0.242%)	126(0.288%)	142(0.306%)	182(0.355%)	218(0.405%)	283(0.478%)	337(0.525%)	325(0.502%)	454(0.62%)	650(0.79%)	527(0.652%)	564(0.685%)	666(0.749%)	610(0.688%)	687(0.754%)
51	573(1.643%)	624(1.69%)	719(1.774%)	811(1.856%)	876(1.886%)	1017(1.984%)	1096(2.038%)	1197(2.021%)	1254(1.954%)	1246(1.924%)	1357(1.852%)	1515(1.842%)	1428(1.768%)	1524(1.852%)	1608(1.808%)	1521(1.715%)	1641(1.802%)
52	515(1.477%)	537(1.454%)	610(1.505%)	670(1.533%)	715(1.539%)	827(1.613%)	913(1.698%)	1018(1.718%)	1056(1.645%)	1042(1.609%)	1164(1.588%)	1372(1.668%)	1283(1.588%)	1323(1.607%)	1391(1.564%)	1445(1.629%)	1473(1.617%)
53	136(0.39%)	161(0.436%)	188(0.464%)	202(0.462%)	220(0.474%)	274(0.534%)	286(0.532%)	298(0.503%)	323(0.503%)	326(0.503%)	354(0.483%)	409(0.497%)	374(0.463%)	401(0.487%)	435(0.489%)	429(0.484%)	420(0.461%)
54	125(0.358%)	130(0.352%)	154(0.38%)	188(0.43%)	205(0.441%)	257(0.501%)	315(0.586%)	377(0.636%)	396(0.617%)	405(0.625%)	486(0.663%)	614(0.746%)	590(0.73%)	642(0.78%)	722(0.812%)	704(0.794%)	737(0.809%)
55	1114(3.195%)	1088(2.946%)	1078(2.666%)	1157(2.647%)	1196(2.575%)	1300(2.536%)	1353(2.516%)	1442(2.434%)	1437(2.239%)	1420(2.193%)	1461(1.994%)	1608(1.955%)	1542(1.909%)	1639(1.991%)	1609(1.809%)	1628(1.836%)	1834(2.014%)
56	1188(3.407%)	1228(3.326%)	1308(3.228%)	1255(2.871%)	1259(2.711%)	1397(2.725%)	1434(2.666%)	1574(2.657%)	1559(2.429%)	1542(2.381%)	1545(2.108%)	1688(2.052%)	1728(2.139%)	1750(2.126%)	1762(1.981%)	1689(1.904%)	1693(1.859%)
57	885(2.538%)	923(2.5%)	1006(2.483%)	1083(2.478%)	1116(2.403%)	1121(2.187%)	1174(2.183%)	1244(2.1%)	1184(1.845%)	1195(1.846%)	1284(1.752%)	1284(1.561%)	1265(1.566%)	1183(1.437%)	1200(1.349%)	1158(1.306%)	1168(1.283%)
58	704(2.019%)	725(1.963%)	743(1.834%)	765(1.75%)	775(1.669%)	806(1.572%)	834(1.551%)	923(1.558%)	921(1.435%)	963(1.487%)	1107(1.511%)	1187(1.443%)	1305(1.616%)	1254(1.524%)	1230(1.383%)	1155(1.302%)	1212(1.331%)
59	221(0.634%)	227(0.615%)	254(0.627%)	296(0.677%)	336(0.723%)	388(0.757%)	421(0.783%)	502(0.847%)	562(0.876%)	591(0.913%)	655(0.894%)	770(0.936%)	766(0.948%)	794(0.965%)	885(0.995%)	871(0.982%)	869(0.954%)
60	135(0.387%)	152(0.412%)	173(0.427%)	205(0.469%)	224(0.482%)	260(0.507%)	295(0.548%)	377(0.636%)	453(0.706%)	513(0.792%)	682(0.931%)	878(1.067%)	850(1.052%)	1008(1.225%)	1141(1.283%)	1101(1.241%)	1156(1.269%)
61	628(1.801%)	656(1.777%)	686(1.693%)	722(1.652%)	759(1.634%)	803(1.566%)	833(1.549%)	902(1.523%)	937(1.461%)	938(1.449%)	1030(1.406%)	1158(1.408%)	1197(1.482%)	1233(1.498%)	1469(1.652%)	1478(1.666%)	1512(1.66%)
62	532(1.526%)	533(1.443%)	567(1.399%)	579(1.325%)	592(1.275%)	612(1.194%)	633(1.177%)	672(1.134%)	676(1.053%)	680(1.05%)	758(1.034%)	814(0.99%)	859(1.064%)	827(1.005%)	895(1.006%)	871(0.982%)	897(0.985%)
63	165(0.473%)	187(0.506%)	224(0.553%)	251(0.574%)	295(0.635%)	295(0.575%)	331(0.615%)	361(0.609%)	397(0.619%)	413(0.638%)	480(0.655%)	533(0.648%)	539(0.667%)	551(0.669%)	583(0.656%)	672(0.758%)	686(0.753%)
64	364(1.044%)	386(1.045%)	456(1.125%)	519(1.187%)	573(1.234%)	696(1.358%)	775(1.441%)	843(1.423%)	909(1.416%)	923(1.425%)	997(1.361%)	1092(1.328%)	1071(1.326%)	1056(1.283%)	1361(1.531%)	1348(1.52%)	1383(1.519%)
65	224(0.642%)	223(0.604%)	256(0.632%)	291(0.666%)	328(0.706%)	370(0.722%)	400(0.744%)	446(0.753%)	490(0.763%)	502(0.775%)	556(0.759%)	611(0.743%)	565(0.7%)	603(0.733%)	634(0.713%)	612(0.69%)	624(0.685%)
66	497(1.425%)	507(1.373%)	553(1.365%)	603(1.38%)	650(1.399%)	721(1.406%)	777(1.445%)	869(1.467%)	943(1.469%)	944(1.458%)	1032(1.408%)	1160(1.411%)	1118(1.384%)	1132(1.375%)	1216(1.367%)	1215(1.37%)	1237(1.358%)
67	554(1.589%)	605(1.638%)	622(1.535%)	703(1.608%)	861(1.854%)	1068(2.083%)	1024(1.904%)	1333(2.25%)	1669(2.6%)	1724(2.662%)	2006(2.737%)	2285(2.778%)	2192(2.714%)	2355(2.861%)	2564(2.883%)	2411(2.718%)	2372(2.605%)
68	643(1.844%)	710(1.923%)	773(1.908%)	873(1.997%)	1054(2.269%)	895(1.746%)	815(1.515%)	866(1.462%)	953(1.485%)	994(1.535%)	1181(1.612%)	1273(1.548%)	1240(1.535%)	1344(1.633%)	1330(1.496%)	1308(1.475%)	1314(1.443%)
69	268(0.769%)	284(0.769%)	359(0.886%)	377(0.863%)	387(0.833%)	515(1.005%)	437(0.813%)	490(0.827%)	465(0.725%)	507(0.783%)	518(0.707%)	539(0.655%)	478(0.592%)	490(0.595%)	500(0.562%)	459(0.518%)	472(0.518%)
70	91(0.261%)	93(0.252%)	150(0.37%)	259(0.593%)	113(0.243%)	263(0.513%)	317(0.589%)	170(0.287%)	165(0.257%)	175(0.27%)	154(0.21%)	164(0.199%)	139(0.172%)	130(0.158%)	130(0.146%)	126(0.142%)	134(0.147%)
71	201(0.576%)	198(0.536%)	339(0.837%)	378(0.865%)	408(0.878%)	536(1.046%)	592(1.101%)	683(1.153%)	805(1.254%)	760(1.174%)	928(1.266%)	1171(1.424%)	1239(1.534%)	1137(1.381%)	1508(1.696%)	1425(1.607%)	1527(1.677%)
72	473(1.356%)	569(1.541%)	631(1.557%)	735(1.682%)	740(1.593%)	862(1.681%)	940(1.748%)	917(1.548%)	1018(1.586%)	1017(1.571%)	1125(1.535%)	1248(1.517%)	1339(1.658%)	1288(1.565%)	1493(1.679%)	1376(1.551%)	1494(1.64%)
73	256(0.734%)	353(0.956%)	424(1.046%)	471(1.078%)	467(1.005%)	562(1.096%)	579(1.077%)	609(1.028%)	702(1.094%)	657(1.015%)	771(1.052%)	852(1.036%)	879(1.088%)	895(1.087%)	987(1.11%)	1043(1.176%)	1074(1.179%)

74	463(1.328%)	517(1.4%)	592(1.461%)	633(1.448%)	694(1.494%)	781(1.523%)	781(1.452%)	835(1.41%)	949(1.479%)	918(1.418%)	1062(1.449%)	1170(1.422%)	1203(1.489%)	1238(1.504%)	1350(1.518%)	1360(1.533%)	1405(1.543%)
75	0(0%)	0(0%)	0(0%)	0(0%)	0(0%)	0(0%)	0(0%)	0(0%)	0(0%)	0(0%)	0(0%)	0(0%)	0(0%)	0(0%)	0(0%)	0(0%)	0(0%)
76	0(0%)	0(0%)	0(0%)	0(0%)	0(0%)	0(0%)	0(0%)	0(0%)	0(0%)	0(0%)	0(0%)	0(0%)	0(0%)	0(0%)	0(0%)	0(0%)	0(0%)
77	187(0.536%)	139(0.376%)	139(0.343%)	149(0.341%)	178(0.383%)	198(0.386%)	220(0.409%)	212(0.358%)	194(0.302%)	190(0.293%)	206(0.281%)	189(0.23%)	178(0.22%)	164(0.199%)	174(0.196%)	183(0.206%)	199(0.219%)
78	155(0.444%)	153(0.414%)	203(0.501%)	205(0.469%)	217(0.467%)	224(0.437%)	236(0.439%)	255(0.43%)	254(0.396%)	239(0.369%)	245(0.334%)	232(0.282%)	207(0.256%)	215(0.261%)	198(0.223%)	223(0.251%)	216(0.237%)
79	0(0%)	0(0%)	0(0%)	0(0%)	0(0%)	0(0%)	0(0%)	0(0%)	0(0%)	0(0%)	0(0%)	0(0%)	0(0%)	0(0%)	0(0%)	0(0%)	0(0%)
80	0(0%)	0(0%)	0(0%)	0(0%)	0(0%)	0(0%)	0(0%)	0(0%)	0(0%)	0(0%)	42(0.057%)	101(0.123%)	79(0.098%)	97(0.118%)	42(0.047%)	78(0.088%)	0(0%)
81	400(1.147%)	404(1.094%)	430(1.061%)	450(1.03%)	475(1.023%)	527(1.028%)	556(1.034%)	671(1.133%)	720(1.122%)	724(1.118%)	1092(1.49%)	1373(1.669%)	1320(1.634%)	1085(1.318%)	1691(1.902%)	1857(2.094%)	1962(2.154%)
82	605(1.735%)	638(1.728%)	704(1.737%)	724(1.657%)	798(1.718%)	855(1.668%)	894(1.662%)	1009(1.703%)	1119(1.744%)	1176(1.816%)	1653(2.256%)	2256(2.743%)	2206(2.731%)	2113(2.567%)	2587(2.909%)	2495(2.813%)	2741(3.01%)
83	183(0.525%)	209(0.566%)	228(0.563%)	259(0.593%)	289(0.622%)	351(0.685%)	371(0.69%)	416(0.702%)	499(0.778%)	525(0.811%)	636(0.868%)	753(0.915%)	722(0.894%)	732(0.889%)	828(0.931%)	869(0.98%)	887(0.974%)
84	713(2.045%)	728(1.972%)	751(1.853%)	763(1.746%)	779(1.677%)	786(1.533%)	768(1.428%)	759(1.281%)	915(1.426%)	992(1.532%)	1131(1.543%)	1340(1.629%)	1306(1.617%)	1357(1.649%)	1512(1.7%)	1744(1.966%)	1728(1.897%)
85	1368(3.923%)	1375(3.724%)	1468(3.623%)	1504(3.441%)	1566(3.372%)	1635(3.189%)	1632(3.034%)	1691(2.854%)	1764(2.749%)	1748(2.7%)	1843(2.515%)	1960(2.383%)	1997(2.472%)	2005(2.436%)	2001(2.25%)	2017(2.274%)	2099(2.305%)
86	1026(2.942%)	1087(2.944%)	1168(2.882%)	1267(2.899%)	1352(2.911%)	1490(2.907%)	1531(2.847%)	1664(2.809%)	1813(2.825%)	1863(2.877%)	2065(2.818%)	2208(2.684%)	2252(2.788%)	2310(2.806%)	2360(2.654%)	2360(2.661%)	2395(2.63%)
87	61(0.175%)	78(0.211%)	110(0.271%)	130(0.297%)	154(0.332%)	197(0.384%)	260(0.483%)	318(0.537%)	371(0.578%)	375(0.579%)	423(0.577%)	527(0.641%)	523(0.648%)	559(0.679%)	620(0.697%)	652(0.735%)	675(0.741%)
88	103(0.295%)	110(0.298%)	132(0.326%)	164(0.375%)	189(0.407%)	262(0.511%)	285(0.53%)	340(0.574%)	396(0.617%)	434(0.67%)	522(0.712%)	641(0.779%)	630(0.78%)	695(0.844%)	817(0.919%)	859(0.968%)	847(0.93%)
89	523(1.5%)	610(1.652%)	729(1.799%)	781(1.787%)	858(1.847%)	943(1.839%)	1009(1.876%)	1141(1.926%)	1166(1.817%)	1161(1.793%)	1218(1.662%)	1399(1.701%)	1343(1.663%)	1458(1.771%)	1634(1.838%)	1657(1.868%)	1622(1.781%)
90	1362(3.906%)	1470(3.981%)	1667(4.114%)	1845(4.221%)	1976(4.254%)	2055(4.009%)	2137(3.973%)	2326(3.926%)	2373(3.697%)	2254(3.481%)	2260(3.084%)	2522(3.066%)	2375(2.94%)	2438(2.962%)	2638(2.967%)	2811(3.169%)	2879(3.161%)

Table 6.6. Longitudinal Probabilistic Distribution of Points per ROIs using Symmetric ALBERT Parcellation Map with 50 ROIs given as: Number of points per ROI (Percentage on surface %)

Week /ROI#	28	29	30	31	32	33	34	35	36	37	38	39	40	41	42	43	44
1 & 2	159(0.452%)	176(0.47%)	189(0.462%)	150(0.342%)	164(0.352%)	187(0.367%)	189(0.355%)	173(0.304%)	186(0.309%)	199(0.33%)	216(0.313%)	281(0.358%)	308(0.401%)	379(0.485%)	425(0.493%)	429(0.502%)	485(0.548%)
3 & 4	0(0%)	0(0%)	0(0%)	74(0.169%)	132(0.284%)	167(0.328%)	176(0.331%)	206(0.361%)	253(0.42%)	245(0.407%)	268(0.388%)	289(0.368%)	336(0.437%)	325(0.415%)	309(0.359%)	317(0.371%)	278(0.314%)
5 & 6	452(1.285%)	523(1.396%)	591(1.445%)	701(1.599%)	769(1.653%)	900(1.768%)	967(1.817%)	1197(2.1%)	1342(2.228%)	1367(2.269%)	1621(2.347%)	1879(2.392%)	1851(2.409%)	1927(2.464%)	2035(2.361%)	2091(2.446%)	2335(2.637%)
7 & 8	486(1.382%)	494(1.319%)	565(1.381%)	615(1.403%)	701(1.507%)	771(1.515%)	901(1.693%)	993(1.742%)	1148(1.906%)	1149(1.907%)	1249(1.808%)	1441(1.835%)	1398(1.819%)	1476(1.887%)	2384(2.766%)	2568(3.004%)	2565(2.897%)
9 & 10	1993(5.666%)	2055(5.485%)	2083(5.093%)	2119(4.833%)	2131(4.58%)	2077(4.081%)	2063(3.877%)	1994(3.499%)	1945(3.229%)	1903(3.158%)	1721(2.492%)	1599(2.036%)	1555(2.023%)	1509(1.929%)	1400(1.624%)	1330(1.556%)	1321(1.492%)
11 & 12	650(1.848%)	660(1.762%)	736(1.8%)	822(1.875%)	834(1.793%)	881(1.731%)	928(1.744%)	1100(1.93%)	1078(1.79%)	1093(1.814%)	1887(2.732%)	2688(3.422%)	2804(3.649%)	1927(2.464%)	2808(3.258%)	2665(3.118%)	2835(3.202%)
13 & 14	1517(4.313%)	1593(4.252%)	1800(4.401%)	1901(4.335%)	2020(4.342%)	2262(4.444%)	2358(4.432%)	2601(4.564%)	2683(4.455%)	2666(4.425%)	2785(4.032%)	3127(3.981%)	3069(3.994%)	3275(4.187%)	3616(4.195%)	3668(4.291%)	3667(4.142%)
15 & 16	671(1.908%)	758(2.023%)	794(1.941%)	873(1.991%)	931(2.001%)	1027(2.018%)	1073(2.017%)	1089(1.911%)	1122(1.863%)	1116(1.852%)	1177(1.704%)	1256(1.599%)	1251(1.628%)	1297(1.658%)	1323(1.535%)	1351(1.581%)	1336(1.509%)
17 & 18	0(0%)	0(0%)	0(0%)	0(0%)	0(0%)	0(0%)	0(0%)	0(0%)	0(0%)	0(0%)	0(0%)	0(0%)	0(0%)	0(0%)	0(0%)	0(0%)	0(0%)
19 & 20	559(1.589%)	524(1.399%)	528(1.291%)	498(1.136%)	501(1.077%)	473(0.929%)	471(0.885%)	497(0.872%)	583(0.968%)	700(1.162%)	961(1.391%)	1034(1.316%)	1026(1.335%)	899(1.149%)	883(1.025%)	908(1.062%)	892(1.008%)
21 & 22	4826(13.721%)	5204(13.891%)	5846(14.293%)	6586(15.02%)	6920(14.873%)	8076(15.868%)	8783(16.508%)	9352(16.41%)	9647(16.017%)	9631(15.985%)	10957(15.864%)	12606(16.049%)	11718(15.248%)	12355(15.795%)	12827(14.883%)	12207(14.282%)	12586(14.216%)
23 & 24	602(1.712%)	606(1.618%)	606(1.482%)	632(1.441%)	630(1.354%)	630(1.238%)	630(1.184%)	634(1.112%)	768(1.275%)	778(1.291%)	876(1.268%)	832(1.059%)	761(0.99%)	744(0.951%)	798(0.926%)	851(0.996%)	857(0.968%)
25 & 26	817(2.323%)	876(2.338%)	912(2.23%)	925(2.11%)	937(2.014%)	1016(1.996%)	1033(1.942%)	1099(1.928%)	1082(1.796%)	1127(1.87%)	1152(1.668%)	1243(1.582%)	1212(1.577%)	1281(1.638%)	1266(1.469%)	1242(1.453%)	1218(1.376%)
27 & 28	2115(6.013%)	2167(5.784%)	2312(5.653%)	2364(5.391%)	2490(5.352%)	2694(5.293%)	2725(5.122%)	2851(5.003%)	3035(5.039%)	3028(5.026%)	3153(4.565%)	3436(4.374%)	3347(4.355%)	3580(4.577%)	3625(4.206%)	3658(4.28%)	3803(4.296%)
29 & 30	400(1.137%)	398(1.062%)	451(1.103%)	487(1.111%)	567(1.219%)	571(1.122%)	584(1.098%)	680(1.193%)	741(1.23%)	724(1.202%)	851(1.232%)	905(1.152%)	955(1.243%)	947(1.211%)	956(1.109%)	955(1.117%)	1031(1.165%)
31 & 32	0(0%)	0(0%)	0(0%)	0(0%)	0(0%)	0(0%)	0(0%)	0(0%)	0(0%)	0(0%)	634(0.918%)	1014(1.291%)	1010(1.314%)	984(1.258%)	995(1.154%)	1073(1.255%)	1265(1.429%)
33 & 34	154(0.438%)	355(0.948%)	511(1.249%)	537(1.225%)	510(1.096%)	531(1.043%)	476(0.895%)	269(0.472%)	667(1.107%)	602(0.999%)	890(1.289%)	977(1.244%)	910(1.184%)	826(1.056%)	785(0.911%)	853(0.998%)	897(1.013%)
35 & 36	11561(32.87%)	12307(32.85%)	13451(32.888%)	14175(32.328%)	15129(32.517%)	16228(31.885%)	17076(32.094%)	18530(32.514%)	19210(31.894%)	19230(31.916%)	21440(31.041%)	24542(31.245%)	24043(31.286%)	24787(31.688%)	27437(31.834%)	27493(32.166%)	28510(32.203%)
37 & 38	6011(17.09%)	6403(17.091%)	6873(16.804%)	7375(16.819%)	7959(17.107%)	8559(16.817%)	8799(16.538%)	9734(17.08%)	10269(17.05%)	10475(17.385%)	12324(17.843%)	13737(17.489%)	13439(17.488%)	13757(17.587%)	14960(17.357%)	14892(17.423%)	15314(17.298%)
39 & 40	114(0.324%)	117(0.312%)	154(0.377%)	176(0.401%)	182(0.391%)	281(0.552%)	380(0.714%)	359(0.63%)	457(0.759%)	386(0.641%)	535(0.775%)	725(0.923%)	899(1.17%)	797(1.019%)	1130(1.311%)	1054(1.233%)	1099(1.241%)
41 & 42	855(2.431%)	897(2.394%)	933(2.281%)	1010(2.303%)	1049(2.255%)	1215(2.387%)	1260(2.368%)	1308(2.295%)	1403(2.329%)	1351(2.242%)	1449(2.098%)	1527(1.944%)	1508(1.962%)	1529(1.955%)	1624(1.884%)	1634(1.912%)	1643(1.856%)
43 & 44	0(0%)	0(0%)	0(0%)	0(0%)	0(0%)	0(0%)	0(0%)	0(0%)	0(0%)	0(0%)	0(0%)	0(0%)	0(0%)	0(0%)	0(0%)	0(0%)	0(0%)
45 & 46	710(2.019%)	808(2.157%)	954(2.333%)	1042(2.376%)	1093(2.349%)	1226(2.409%)	1271(2.389%)	1293(2.269%)	1451(2.409%)	1398(2.32%)	1613(2.335%)	1795(2.285%)	1837(2.39%)	1872(2.393%)	2118(2.457%)	2223(2.601%)	2336(2.639%)

47 & 48	155(0.441%)	150(0.4%)	162(0.396%)	161(0.367%)	145(0.312%)	126(0.248%)	115(0.216%)	117(0.205%)	101(0.168%)	98(0.163%)	82(0.119%)	88(0.112%)	97(0.126%)	81(0.104%)	71(0.082%)	83(0.097%)	77(0.087%)
49 & 50	365(1.038%)	393(1.049%)	449(1.098%)	625(1.425%)	641(1.378%)	886(1.741%)	948(1.782%)	914(1.604%)	1059(1.758%)	986(1.636%)	1229(1.779%)	1527(1.944%)	1514(1.97%)	1668(2.132%)	2413(2.8%)	1927(2.255%)	2182(2.465%)

Table 6.7. Longitudinal Probabilistic Distribution of Points per ROIs using Asymmetric ALBERT Parcellation Map with 50 ROIs given as: Number of points per ROI (Percentage on surface %)

Week \ROI #	28	29	30	31	32	33	34	35	36	37	38	39	40	41	42	43	44
1	0(0%)	0(0%)	0(0%)	0(0%)	0(0%)	0(0%)	0(0%)	0(0%)	0(0%)	0(0%)	0(0%)	0(0%)	41(0.051 %)	110(0.13 4%)	46(0.052 %)	0(0%)	0(0%)
2	0(0%)	0(0%)	0(0%)	0(0%)	0(0%)	0(0%)	0(0%)	0(0%)	0(0%)	0(0%)	0(0%)	67(0.081 %)	140(0.17 3%)	202(0.24 5%)	236(0.26 5%)	264(0.29 8%)	272(0.29 9%)
3	0(0%)	0(0%)	0(0%)	0(0%)	42(0.09 %)	124(0.2 42%)	130(0.2 42%)	133(0.22 5%)	157(0.24 5%)	164(0.25 3%)	173(0.23 6%)	176(0.21 4%)	179(0.22 2%)	142(0.17 3%)	195(0.21 9%)	235(0.26 5%)	230(0.25 3%)
4	102(0.29 2%)	112(0.3 03%)	130(0.3 21%)	130(0.2 97%)	144(0.3 1%)	186(0.3 63%)	230(0.4 28%)	305(0.51 5%)	318(0.49 5%)	256(0.39 5%)	260(0.35 5%)	256(0.31 1%)	130(0.16 1%)	130(0.15 8%)	191(0.21 5%)	195(0.22 %)	192(0.21 1%)
5	267(0.76 6%)	299(0.8 1%)	345(0.8 51%)	395(0.9 04%)	449(0.9 67%)	511(0.9 97%)	581(1.0 8%)	690(1.16 5%)	764(1.19 %)	779(1.20 3%)	900(1.22 8%)	1045(1.2 7%)	1017(1.2 59%)	1038(1.2 61%)	1049(1.1 8%)	1080(1.2 18%)	1197(1.3 14%)
6	177(0.50 8%)	193(0.5 23%)	212(0.5 23%)	252(0.5 77%)	310(0.6 67%)	365(0.7 12%)	393(0.7 31%)	474(0.8 %)	571(0.89 %)	596(0.92 %)	728(0.99 3%)	855(1.03 9%)	841(1.04 1%)	844(1.02 5%)	923(1.03 8%)	909(1.02 5%)	957(1.05 1%)
7	335(0.96 1%)	351(0.9 51%)	390(0.9 62%)	410(0.9 38%)	431(0.9 28%)	494(0.9 64%)	555(1.0 32%)	610(1.03 %)	676(1.05 3%)	699(1.08 %)	750(1.02 3%)	870(1.05 8%)	836(1.03 5%)	876(1.06 4%)	1239(1.3 93%)	1254(1.4 14%)	1237(1.3 58%)
8	231(0.66 2%)	256(0.6 93%)	293(0.7 23%)	331(0.7 57%)	356(0.7 66%)	419(0.8 17%)	521(0.9 69%)	529(0.89 3%)	618(0.96 3%)	583(0.9 %)	731(0.99 8%)	772(0.93 9%)	752(0.93 1%)	890(1.08 1%)	977(1.09 9%)	1173(1.3 23%)	1144(1.2 56%)
9	1045(2.9 97%)	1094(2. 963%)	1121(2. 766%)	1169(2. 675%)	1181(2. 543%)	1173(2. 288%)	1159(2. 155%)	1114(1.8 8%)	1009(1.5 72%)	989(1.52 7%)	912(1.24 5%)	848(1.03 1%)	840(1.04 %)	774(0.94 %)	817(0.91 9%)	811(0.91 4%)	818(0.89 8%)
10	802(2.3 %)	819(2.2 18%)	777(1.9 17%)	822(1.8 81%)	859(1.8 49%)	900(1.7 56%)	847(1.5 75%)	862(1.45 5%)	835(1.30 1%)	834(1.28 8%)	776(1.05 9%)	685(0.83 3%)	730(0.90 4%)	646(0.78 5%)	588(0.66 1%)	600(0.67 6%)	581(0.63 8%)
11	475(1.36 2%)	474(1.2 84%)	529(1.3 05%)	544(1.2 45%)	571(1.2 29%)	609(1.1 88%)	589(1.0 95%)	647(1.09 2%)	654(1.01 9%)	638(0.98 5%)	685(0.93 5%)	737(0.89 6%)	690(0.85 4%)	708(0.86 %)	703(0.79 1%)	739(0.83 3%)	757(0.83 1%)
12	516(1.48 %)	538(1.4 57%)	570(1.4 07%)	570(1.3 04%)	617(1.3 28%)	630(1.2 29%)	641(1.1 92%)	704(1.18 8%)	698(1.08 8%)	777(1.2 %)	1109(1.5 13%)	1463(1.7 79%)	1428(1.7 68%)	1401(1.7 02%)	1707(1.9 2%)	1522(1.7 16%)	1573(1.7 27%)
13	499(1.43 1%)	555(1.5 03%)	641(1.5 82%)	711(1.6 27%)	793(1.7 07%)	905(1.7 65%)	1000(1. 859%)	1120(1.8 91%)	1167(1.8 18%)	1132(1.7 48%)	1194(1.6 29%)	1365(1.6 59%)	1324(1.6 39%)	1397(1.6 97%)	1651(1.8 57%)	1715(1.9 34%)	1693(1.8 59%)
14	730(2.09 3%)	791(2.1 42%)	893(2.2 04%)	980(2.2 42%)	1048(2. 256%)	1158(2. 259%)	1204(2. 239%)	1373(2.3 18%)	1455(2.2 67%)	1455(2.2 47%)	1543(2.1 06%)	1714(2.0 84%)	1752(2.1 69%)	1826(2.2 18%)	1939(2.1 81%)	1989(2.2 43%)	1993(2.1 88%)
15	411(1.17 9%)	392(1.0 62%)	364(0.8 98%)	393(0.8 99%)	359(0.7 73%)	391(0.7 63%)	345(0.6 41%)	376(0.63 5%)	377(0.58 7%)	370(0.57 1%)	399(0.54 4%)	426(0.51 8%)	448(0.55 5%)	465(0.56 5%)	472(0.53 1%)	470(0.53 %)	462(0.50 7%)
16	796(2.28 3%)	832(2.2 53%)	887(2.1 89%)	869(1.9 88%)	877(1.8 88%)	870(1.6 97%)	883(1.6 42%)	869(1.46 7%)	840(1.30 9%)	756(1.16 8%)	685(0.93 5%)	731(0.88 9%)	647(0.80 1%)	647(0.78 6%)	661(0.74 3%)	652(0.73 5%)	660(0.72 5%)
17	0(0%)	0(0%)	0(0%)	0(0%)	0(0%)	0(0%)	0(0%)	0(0%)	0(0%)	0(0%)	0(0%)	0(0%)	0(0%)	0(0%)	0(0%)	0(0%)	0(0%)
18	0(0%)	0(0%)	0(0%)	0(0%)	0(0%)	0(0%)	0(0%)	0(0%)	0(0%)	0(0%)	0(0%)	0(0%)	0(0%)	0(0%)	0(0%)	0(0%)	0(0%)
19	0(0%)	0(0%)	0(0%)	0(0%)	0(0%)	0(0%)	0(0%)	0(0%)	0(0%)	0(0%)	0(0%)	0(0%)	0(0%)	0(0%)	0(0%)	0(0%)	0(0%)
20	113(0.32 4%)	88(0.23 8%)	215(0.5 31%)	228(0.5 22%)	264(0.5 68%)	287(0.5 6%)	302(0.5 62%)	319(0.53 8%)	380(0.59 2%)	426(0.65 8%)	473(0.64 5%)	657(0.79 9%)	651(0.80 6%)	642(0.78 %)	697(0.78 4%)	799(0.90 1%)	752(0.82 6%)
21	0(0%)	0(0%)	0(0%)	0(0%)	0(0%)	0(0%)	0(0%)	0(0%)	0(0%)	46(0.071 %)	179(0.24 4%)	170(0.20 7%)	173(0.21 4%)	336(0.40 8%)	313(0.35 2%)	326(0.36 8%)	353(0.38 8%)
22	2027(5.8 13%)	2172(5. 882%)	2552(6. 298%)	2762(6. 319%)	3085(6. 642%)	3599(7. 021%)	4017(7. 469%)	4541(7.6 65%)	4949(7.7 11%)	4834(7.4 65%)	5465(7.4 58%)	6327(7.6 92%)	5912(7.3 2%)	6131(7.4 49%)	6173(6.9 42%)	6170(6.9 57%)	6347(6.9 69%)
23	1791(5.1 36%)	1917(5. 191%)	2166(5. 345%)	2473(5. 658%)	2729(5. 875%)	3317(6. 47%)	3590(6. 675%)	4132(6.9 75%)	4392(6.8 43%)	4369(6.7 47%)	5011(6.8 38%)	5748(6.9 88%)	5288(6.5 47%)	5618(6.8 25%)	5723(6.4 36%)	5383(6.0 69%)	5573(6.1 19%)

24	311(0.892%)	352(0.953%)	394(0.972%)	423(0.968%)	376(0.81%)	411(0.802%)	418(0.777%)	432(0.729%)	441(0.687%)	374(0.578%)	379(0.517%)	353(0.429%)	381(0.472%)	416(0.505%)	399(0.449%)	425(0.479%)	451(0.495%)
25	451(1.293%)	488(1.322%)	455(1.123%)	506(1.158%)	378(0.814%)	377(0.735%)	372(0.692%)	387(0.653%)	412(0.642%)	409(0.632%)	438(0.598%)	414(0.503%)	406(0.503%)	408(0.496%)	427(0.48%)	398(0.449%)	376(0.413%)
26	337(0.966%)	340(0.921%)	354(0.874%)	375(0.858%)	381(0.82%)	425(0.829%)	443(0.824%)	491(0.829%)	495(0.771%)	520(0.803%)	541(0.738%)	606(0.737%)	636(0.787%)	646(0.785%)	636(0.715%)	659(0.743%)	620(0.681%)
27	336(0.964%)	379(1.026%)	414(1.022%)	423(0.968%)	433(0.932%)	451(0.88%)	479(0.891%)	487(0.822%)	487(0.759%)	486(0.751%)	496(0.677%)	536(0.652%)	540(0.669%)	579(0.703%)	576(0.648%)	585(0.66%)	599(0.658%)
28	1163(3.335%)	1201(3.252%)	1317(3.25%)	1376(3.148%)	1451(3.124%)	1534(2.992%)	1535(2.854%)	1650(2.785%)	1723(2.685%)	1722(2.659%)	1835(2.504%)	1920(2.334%)	1941(2.403%)	1965(2.387%)	1997(2.246%)	2048(2.309%)	2087(2.292%)
29	905(2.595%)	917(2.483%)	991(2.446%)	1021(2.336%)	1092(2.351%)	1184(2.31%)	1218(2.265%)	1280(2.161%)	1348(2.1%)	1354(2.091%)	1383(1.887%)	1494(1.816%)	1472(1.822%)	1565(1.901%)	1590(1.788%)	1584(1.786%)	1603(1.76%)
30	129(0.37%)	136(0.368%)	165(0.407%)	186(0.426%)	214(0.461%)	243(0.474%)	271(0.504%)	326(0.55%)	336(0.524%)	361(0.558%)	514(0.701%)	618(0.751%)	595(0.737%)	681(0.827%)	747(0.84%)	715(0.806%)	864(0.949%)
31	236(0.677%)	242(0.655%)	265(0.654%)	279(0.638%)	311(0.67%)	324(0.632%)	331(0.615%)	371(0.626%)	409(0.637%)	387(0.598%)	440(0.6%)	468(0.569%)	490(0.607%)	473(0.575%)	465(0.523%)	454(0.512%)	538(0.591%)
32	0(0%)	24(0.065%)	222(0.548%)	136(0.311%)	143(0.308%)	65(0.127%)	143(0.266%)	94(0.159%)	576(0.897%)	478(0.738%)	611(0.834%)	695(0.845%)	680(0.842%)	690(0.838%)	575(0.647%)	570(0.643%)	567(0.623%)
33	0(0%)	0(0%)	0(0%)	0(0%)	0(0%)	0(0%)	0(0%)	0(0%)	250(0.39%)	199(0.307%)	288(0.393%)	331(0.402%)	358(0.443%)	335(0.407%)	450(0.506%)	483(0.545%)	549(0.603%)
34	0(0%)	0(0%)	0(0%)	0(0%)	0(0%)	0(0%)	0(0%)	158(0.267%)	489(0.762%)	565(0.873%)	696(0.95%)	749(0.911%)	774(0.958%)	735(0.893%)	708(0.796%)	734(0.828%)	770(0.846%)
35	0(0%)	0(0%)	0(0%)	0(0%)	0(0%)	0(0%)	0(0%)	0(0%)	116(0.181%)	89(0.137%)	96(0.131%)	99(0.12%)	110(0.136%)	139(0.169%)	141(0.159%)	148(0.167%)	147(0.161%)
36	6096(17.481%)	6371(17.253%)	6849(16.902%)	7308(16.721%)	7698(16.573%)	8564(16.706%)	9066(16.856%)	10182(17.188%)	10807(16.839%)	11130(17.189%)	12296(16.779%)	13773(16.744%)	13500(16.714%)	13936(16.931%)	14869(16.721%)	15067(16.988%)	15403(16.913%)
37	6183(17.731%)	6552(17.744%)	7118(17.566%)	7558(17.293%)	8117(17.475%)	8907(17.375%)	9228(17.158%)	10442(17.627%)	10924(17.021%)	11329(17.496%)	12785(17.447%)	14340(17.434%)	14185(17.562%)	13872(16.853%)	15371(17.286%)	15245(17.188%)	15604(17.134%)
38	2970(8.517%)	3134(8.487%)	3377(8.334%)	3806(8.708%)	4051(8.722%)	4295(8.378%)	4409(8.198%)	4705(7.942%)	5070(7.9%)	5175(7.992%)	5812(7.931%)	6717(8.166%)	6666(8.253%)	6866(8.342%)	7388(8.308%)	7359(8.297%)	7471(8.204%)
39	3020(8.66%)	3176(8.601%)	3464(8.548%)	3807(8.71%)	4097(8.821%)	4509(8.796%)	4759(8.848%)	5152(8.697%)	5578(8.691%)	5773(8.916%)	7169(9.783%)	7924(9.634%)	7738(9.58%)	7423(9.018%)	8641(9.717%)	8640(9.741%)	8966(9.845%)
40	151(0.433%)	152(0.412%)	153(0.378%)	196(0.448%)	201(0.433%)	248(0.484%)	288(0.535%)	268(0.452%)	396(0.617%)	335(0.517%)	393(0.536%)	462(0.562%)	528(0.654%)	539(0.655%)	666(0.749%)	595(0.671%)	665(0.73%)
41	178(0.51%)	219(0.593%)	226(0.558%)	322(0.737%)	339(0.73%)	394(0.769%)	430(0.799%)	364(0.614%)	394(0.614%)	295(0.456%)	390(0.532%)	496(0.603%)	572(0.708%)	543(0.66%)	729(0.82%)	698(0.787%)	739(0.811%)
42	443(1.27%)	488(1.322%)	628(1.55%)	692(1.583%)	739(1.591%)	811(1.582%)	789(1.467%)	845(1.426%)	953(1.485%)	808(1.248%)	598(0.816%)	591(0.719%)	579(0.717%)	611(0.742%)	592(0.666%)	600(0.676%)	585(0.642%)
43	519(1.488%)	569(1.541%)	663(1.636%)	792(1.812%)	830(1.787%)	989(1.929%)	930(1.729%)	873(1.474%)	1002(1.561%)	982(1.517%)	1115(1.522%)	1124(1.366%)	1043(1.291%)	1035(1.257%)	1053(1.184%)	1044(1.177%)	1032(1.133%)
44	0(0%)	0(0%)	0(0%)	0(0%)	0(0%)	0(0%)	0(0%)	0(0%)	0(0%)	0(0%)	0(0%)	0(0%)	0(0%)	0(0%)	0(0%)	0(0%)	0(0%)
45	0(0%)	0(0%)	0(0%)	0(0%)	0(0%)	0(0%)	0(0%)	0(0%)	0(0%)	0(0%)	0(0%)	0(0%)	0(0%)	0(0%)	0(0%)	0(0%)	0(0%)
46	405(1.161%)	461(1.248%)	419(1.034%)	461(1.055%)	510(1.098%)	583(1.137%)	588(1.093%)	620(1.047%)	716(1.116%)	676(1.044%)	807(1.101%)	923(1.122%)	914(1.132%)	954(1.159%)	1075(1.209%)	1145(1.291%)	1185(1.301%)
47	348(0.998%)	406(1.099%)	489(1.207%)	533(1.22%)	534(1.15%)	560(1.092%)	572(1.064%)	598(1.009%)	694(1.081%)	667(1.03%)	745(1.017%)	811(0.986%)	832(1.03%)	779(0.946%)	918(1.032%)	965(1.088%)	1011(1.11%)
48	0(0%)	0(0%)	0(0%)	0(0%)	0(0%)	0(0%)	0(0%)	0(0%)	0(0%)	0(0%)	0(0%)	0(0%)	0(0%)	0(0%)	0(0%)	0(0%)	0(0%)
49	0(0%)	0(0%)	0(0%)	0(0%)	0(0%)	0(0%)	0(0%)	140(0.236%)	194(0.302%)	228(0.352%)	318(0.434%)	505(0.614%)	548(0.678%)	749(0.91%)	1000(1.125%)	783(0.883%)	873(0.959%)

50	374(1.072%)	436(1.181%)	474(1.17%)	467(1.069%)	438(0.943%)	452(0.882%)	528(0.982%)	577(0.974%)	510(0.795%)	707(1.092%)	1162(1.586%)	1393(1.694%)	1463(1.811%)	1548(1.881%)	1611(1.812%)	1464(1.651%)	1574(1.728%)

Table 6.8. Longitudinal Probabilistic Distribution of Points per ROIs using Symmetric JHU Parcellation Map with 122 ROIs given as: Number of points per ROI (Percentage on surface %)

Week\ ROI#	28	29	30	31	32	33	34	35	36	37	38	39	40	41	42	43	44
1 & 2	133(0.378%)	140(0.374%)	144(0.352%)	146(0.333%)	146(0.314%)	143(0.281%)	150(0.282%)	159(0.279%)	161(0.267%)	179(0.297%)	240(0.347%)	285(0.363%)	262(0.341%)	330(0.422%)	438(0.508%)	363(0.425%)	408(0.461%)
3 & 4	0(0%)	0(0%)	51(0.125%)	81(0.185%)	80(0.172%)	135(0.265%)	156(0.293%)	147(0.258%)	214(0.355%)	180(0.299%)	258(0.374%)	335(0.426%)	323(0.42%)	329(0.421%)	395(0.458%)	421(0.493%)	517(0.584%)
5 & 6	221(0.628%)	226(0.603%)	258(0.631%)	273(0.623%)	302(0.649%)	319(0.627%)	318(0.598%)	335(0.588%)	343(0.569%)	345(0.573%)	371(0.537%)	397(0.505%)	404(0.526%)	403(0.515%)	414(0.48%)	471(0.551%)	474(0.535%)
7 & 8	0(0%)	0(0%)	0(0%)	0(0%)	0(0%)	0(0%)	0(0%)	0(0%)	0(0%)	0(0%)	0(0%)	0(0%)	0(0%)	0(0%)	0(0%)	0(0%)	0(0%)
9 & 10	0(0%)	0(0%)	0(0%)	0(0%)	0(0%)	0(0%)	0(0%)	0(0%)	0(0%)	0(0%)	0(0%)	0(0%)	0(0%)	0(0%)	0(0%)	0(0%)	0(0%)
11 & 12	0(0%)	0(0%)	0(0%)	0(0%)	0(0%)	0(0%)	0(0%)	0(0%)	0(0%)	0(0%)	0(0%)	0(0%)	0(0%)	0(0%)	0(0%)	0(0%)	0(0%)
13 & 14	0(0%)	0(0%)	0(0%)	0(0%)	0(0%)	0(0%)	0(0%)	0(0%)	0(0%)	0(0%)	0(0%)	0(0%)	0(0%)	0(0%)	0(0%)	0(0%)	0(0%)
15 & 16	0(0%)	0(0%)	0(0%)	0(0%)	0(0%)	0(0%)	0(0%)	0(0%)	0(0%)	0(0%)	0(0%)	0(0%)	0(0%)	0(0%)	0(0%)	0(0%)	0(0%)
17 & 18	763(2.169%)	818(2.183%)	769(1.88%)	789(1.799%)	799(1.717%)	802(1.576%)	719(1.351%)	691(1.212%)	640(1.063%)	630(1.046%)	610(0.883%)	577(0.735%)	541(0.704%)	565(0.722%)	531(0.616%)	507(0.593%)	510(0.576%)
19 & 20	557(1.584%)	572(1.527%)	570(1.394%)	653(1.489%)	667(1.434%)	724(1.423%)	793(1.49%)	831(1.458%)	890(1.478%)	861(1.429%)	837(1.212%)	821(1.045%)	836(1.088%)	815(1.042%)	787(0.913%)	741(0.867%)	765(0.864%)
21 & 22	0(0%)	0(0%)	0(0%)	0(0%)	0(0%)	0(0%)	0(0%)	0(0%)	0(0%)	0(0%)	0(0%)	0(0%)	0(0%)	0(0%)	0(0%)	0(0%)	0(0%)
23 & 24	0(0%)	0(0%)	0(0%)	0(0%)	0(0%)	0(0%)	0(0%)	0(0%)	0(0%)	0(0%)	0(0%)	72(0.092%)	49(0.064%)	107(0.137%)	216(0.251%)	143(0.167%)	190(0.215%)
25 & 26	0(0%)	0(0%)	0(0%)	0(0%)	0(0%)	0(0%)	0(0%)	0(0%)	0(0%)	0(0%)	0(0%)	0(0%)	0(0%)	0(0%)	0(0%)	0(0%)	0(0%)
27 & 28	0(0%)	0(0%)	0(0%)	0(0%)	0(0%)	0(0%)	0(0%)	0(0%)	0(0%)	0(0%)	0(0%)	0(0%)	0(0%)	0(0%)	0(0%)	0(0%)	0(0%)
29 & 30	0(0%)	0(0%)	0(0%)	0(0%)	0(0%)	0(0%)	0(0%)	0(0%)	0(0%)	0(0%)	0(0%)	0(0%)	0(0%)	0(0%)	0(0%)	0(0%)	0(0%)
31 & 32	0(0%)	0(0%)	0(0%)	0(0%)	0(0%)	0(0%)	0(0%)	0(0%)	0(0%)	0(0%)	0(0%)	0(0%)	0(0%)	0(0%)	0(0%)	0(0%)	0(0%)
33 & 34	565(1.606%)	630(1.682%)	684(1.672%)	756(1.724%)	770(1.655%)	921(1.81%)	951(1.787%)	1024(1.797%)	1078(1.79%)	1080(1.792%)	1247(1.805%)	1318(1.678%)	1312(1.707%)	1306(1.67%)	1392(1.615%)	1391(1.627%)	1383(1.562%)
35 & 36	393(1.117%)	454(1.212%)	507(1.24%)	563(1.284%)	603(1.296%)	697(1.369%)	739(1.389%)	799(1.402%)	940(1.561%)	918(1.524%)	1076(1.558%)	1093(1.392%)	1122(1.46%)	1153(1.474%)	1297(1.505%)	1360(1.591%)	1380(1.559%)
37 & 38	0(0%)	0(0%)	0(0%)	0(0%)	0(0%)	0(0%)	0(0%)	0(0%)	0(0%)	0(0%)	0(0%)	0(0%)	0(0%)	0(0%)	0(0%)	0(0%)	0(0%)
39 & 40	329(0.935%)	354(0.945%)	371(0.907%)	423(0.965%)	412(0.886%)	534(1.049%)	650(1.222%)	643(1.128%)	781(1.297%)	690(1.145%)	945(1.368%)	1349(1.717%)	1532(1.994%)	1380(1.764%)	1980(2.297%)	1785(2.088%)	1916(2.164%)
41 & 42	0(0%)	0(0%)	0(0%)	0(0%)	0(0%)	0(0%)	0(0%)	0(0%)	0(0%)	0(0%)	0(0%)	0(0%)	0(0%)	0(0%)	0(0%)	0(0%)	0(0%)
43 & 44	0(0%)	0(0%)	0(0%)	0(0%)	0(0%)	0(0%)	0(0%)	0(0%)	0(0%)	0(0%)	0(0%)	0(0%)	0(0%)	0(0%)	0(0%)	0(0%)	0(0%)
45 & 46	129(0.367%)	139(0.371%)	164(0.401%)	176(0.401%)	184(0.395%)	155(0.305%)	150(0.282%)	138(0.242%)	139(0.231%)	144(0.239%)	128(0.185%)	124(0.158%)	133(0.173%)	125(0.16%)	118(0.137%)	115(0.135%)	123(0.139%)

47 & 48	0(0%)	0(0%)	0(0%)	0(0%)	0(0%)	0(0%)	0(0%)	0(0%)	0(0%)	0(0%)	0(0%)	0(0%)	0(0%)	0(0%)	0(0%)	0(0%)	0(0%)
49 & 50	0(0%)	0(0%)	0(0%)	0(0%)	0(0%)	0(0%)	0(0%)	0(0%)	0(0%)	0(0%)	0(0%)	0(0%)	0(0%)	0(0%)	0(0%)	0(0%)	0(0%)
51 & 52	0(0%)	0(0%)	0(0%)	0(0%)	0(0%)	0(0%)	0(0%)	0(0%)	0(0%)	0(0%)	0(0%)	0(0%)	0(0%)	0(0%)	0(0%)	0(0%)	0(0%)
53 & 54	0(0%)	0(0%)	0(0%)	0(0%)	0(0%)	0(0%)	0(0%)	0(0%)	0(0%)	0(0%)	0(0%)	0(0%)	0(0%)	0(0%)	0(0%)	0(0%)	0(0%)
55 & 56	0(0%)	0(0%)	0(0%)	0(0%)	0(0%)	0(0%)	0(0%)	0(0%)	0(0%)	0(0%)	0(0%)	0(0%)	0(0%)	0(0%)	0(0%)	0(0%)	0(0%)
57 & 58	0(0%)	0(0%)	0(0%)	0(0%)	0(0%)	0(0%)	0(0%)	0(0%)	0(0%)	0(0%)	0(0%)	0(0%)	0(0%)	0(0%)	0(0%)	0(0%)	0(0%)
59 & 60	0(0%)	0(0%)	0(0%)	0(0%)	0(0%)	0(0%)	0(0%)	0(0%)	0(0%)	0(0%)	0(0%)	0(0%)	0(0%)	0(0%)	0(0%)	0(0%)	0(0%)
61 & 62	0(0%)	0(0%)	0(0%)	0(0%)	0(0%)	0(0%)	0(0%)	0(0%)	0(0%)	0(0%)	0(0%)	0(0%)	0(0%)	0(0%)	0(0%)	0(0%)	0(0%)
63 & 64	0(0%)	0(0%)	0(0%)	0(0%)	0(0%)	0(0%)	0(0%)	0(0%)	0(0%)	0(0%)	0(0%)	0(0%)	0(0%)	0(0%)	0(0%)	0(0%)	0(0%)
65 & 66	0(0%)	0(0%)	0(0%)	0(0%)	0(0%)	0(0%)	0(0%)	0(0%)	0(0%)	0(0%)	0(0%)	0(0%)	0(0%)	0(0%)	0(0%)	0(0%)	0(0%)
67 & 68	3022(8.592%)	3194(8.526%)	3437(8.403%)	3601(8.212%)	3945(8.479%)	4229(8.309%)	4471(8.403%)	4886(8.573%)	5070(8.418%)	5177(8.592%)	5872(8.502%)	7142(9.093%)	6808(8.859%)	7417(9.482%)	8506(9.869%)	8620(10.085%)	8905(10.059%)
69 & 70	2870(8.16%)	3066(8.184%)	3451(8.438%)	3771(8.6%)	3999(8.595%)	4376(8.598%)	4682(8.8%)	5138(9.016%)	5340(8.866%)	5300(8.796%)	5739(8.309%)	6295(8.014%)	6279(8.171%)	6374(8.149%)	6757(7.84%)	6649(7.779%)	6853(7.741%)
71 & 72	1484(4.219%)	1571(4.193%)	1783(4.359%)	1834(4.183%)	1964(4.221%)	2086(4.099%)	2233(4.197%)	2384(4.183%)	2481(4.119%)	2406(3.993%)	2605(3.772%)	2920(3.717%)	2929(3.811%)	2958(3.782%)	3174(3.683%)	3440(4.025%)	3456(3.904%)
73 & 74	602(1.712%)	659(1.759%)	701(1.714%)	755(1.722%)	800(1.719%)	840(1.65%)	912(1.714%)	968(1.699%)	1014(1.684%)	975(1.618%)	1045(1.513%)	1185(1.509%)	1167(1.519%)	1192(1.524%)	1359(1.577%)	1295(1.515%)	1343(1.517%)
75 & 76	1058(3.008%)	1153(3.078%)	1218(2.978%)	1290(2.942%)	1338(2.876%)	1412(2.774%)	1431(2.69%)	1591(2.792%)	1635(2.715%)	1612(2.675%)	1746(2.528%)	1928(2.455%)	1823(2.372%)	1721(2.2%)	1932(2.242%)	1927(2.255%)	1980(2.236%)
77 & 78	956(2.718%)	1040(2.776%)	1143(2.795%)	1158(2.641%)	1207(2.594%)	1261(2.478%)	1248(2.346%)	1321(2.318%)	1291(2.143%)	1264(2.098%)	1281(1.855%)	1430(1.821%)	1364(1.775%)	1454(1.859%)	1555(1.804%)	1596(1.867%)	1752(1.979%)
79 & 80	1401(3.983%)	1494(3.988%)	1552(3.795%)	1612(3.676%)	1750(3.761%)	1915(3.763%)	1980(3.721%)	2143(3.76%)	2213(3.674%)	2318(3.847%)	2802(4.057%)	3021(3.846%)	2953(3.843%)	2936(3.753%)	3210(3.724%)	3070(3.592%)	3136(3.542%)
81 & 82	1319(3.75%)	1373(3.665%)	1529(3.738%)	1679(3.829%)	1813(3.897%)	1974(3.878%)	2103(3.953%)	2295(4.027%)	2371(3.937%)	2411(4.002%)	2643(3.827%)	2639(3.36%)	2604(3.389%)	2551(3.261%)	2614(3.033%)	2642(3.091%)	2688(3.036%)
83 & 84	552(1.569%)	590(1.575%)	662(1.619%)	792(1.806%)	902(1.939%)	1039(2.041%)	1126(2.116%)	1364(2.393%)	1579(2.622%)	1726(2.865%)	2108(3.052%)	2566(3.267%)	2376(3.092%)	2564(3.278%)	2908(3.374%)	2733(3.198%)	2822(3.188%)
85 & 86	989(2.812%)	1029(2.747%)	1049(2.565%)	1085(2.474%)	1185(2.547%)	1243(2.442%)	1196(2.248%)	1298(2.278%)	1284(2.132%)	1346(2.234%)	1656(2.398%)	1976(2.516%)	2020(2.629%)	1981(2.533%)	2132(2.474%)	2080(2.434%)	2173(2.454%)
87 & 88	582(1.655%)	828(2.21%)	1017(2.487%)	1096(2.5%)	1030(2.214%)	1237(2.43%)	1125(2.114%)	877(1.539%)	1562(2.593%)	1525(2.531%)	2762(3.999%)	3615(4.602%)	3502(4.557%)	3410(4.359%)	3597(4.173%)	3739(4.375%)	4240(4.789%)
89 & 90	451(1.282%)	487(1.3%)	592(1.447%)	650(1.482%)	754(1.621%)	809(1.59%)	920(1.729%)	1113(1.953%)	1250(2.075%)	1256(2.085%)	1408(2.039%)	1678(2.136%)	1806(2.35%)	1919(2.453%)	2217(2.572%)	2382(2.787%)	2379(2.687%)
91 & 92	1617(4.597%)	1668(4.452%)	1769(4.325%)	1899(4.331%)	2018(4.337%)	2164(4.252%)	2303(4.328%)	2488(4.366%)	2574(4.274%)	2571(4.267%)	2747(3.977%)	2968(3.779%)	2941(3.827%)	3020(3.861%)	3282(3.808%)	3211(3.757%)	3315(3.744%)
93 & 94	1548(4.401%)	1623(4.332%)	1782(4.357%)	1953(4.454%)	2017(4.335%)	2199(4.321%)	2240(4.21%)	2552(4.478%)	2592(4.304%)	2639(4.38%)	3921(5.677%)	4974(6.332%)	4956(6.449%)	4056(5.185%)	5944(6.897%)	5945(6.955%)	6153(6.95%)
95 & 96	968(2.752%)	1031(2.752%)	1221(2.985%)	1316(3.001%)	1506(3.237%)	1674(3.289%)	1846(3.47%)	2100(3.685%)	2511(4.169%)	2580(4.282%)	2916(4.222%)	3440(4.379%)	3573(4.649%)	3680(4.705%)	3999(4.64%)	4057(4.747%)	4077(4.605%)

97 & 98	3515(9.994%)	3496(9.332%)	3691(9.024%)	3724(8.493%)	3806(8.18%)	4040(7.938%)	4063(7.636%)	4259(7.473%)	4090(6.791%)	3799(6.305%)	3710(5.371%)	3949(5.027%)	3521(4.582%)	3866(4.942%)	4266(4.95%)	4658(5.45%)	5102(5.763%)
99 & 100	975(2.772%)	1132(3.022%)	1313(3.21%)	1495(3.41%)	1655(3.557%)	1875(3.684%)	2078(3.906%)	2323(4.076%)	2412(4.005%)	2543(4.221%)	2614(3.785%)	2948(3.753%)	2983(3.882%)	3089(3.949%)	3011(3.494%)	2875(3.364%)	2729(3.083%)
101 & 102	0(0%)	0(0%)	0(0%)	0(0%)	0(0%)	0(0%)	0(0%)	0(0%)	0(0%)	0(0%)	0(0%)	0(0%)	0(0%)	0(0%)	0(0%)	0(0%)	0(0%)
103 & 104	565(1.606%)	597(1.594%)	583(1.425%)	605(1.38%)	636(1.367%)	600(1.179%)	603(1.133%)	535(0.939%)	586(0.973%)	607(1.007%)	652(0.944%)	583(0.742%)	577(0.751%)	601(0.768%)	449(0.521%)	420(0.491%)	396(0.447%)
105 & 106	45(0.128%)	99(0.264%)	135(0.33%)	175(0.399%)	215(0.462%)	272(0.534%)	343(0.645%)	442(0.776%)	493(0.819%)	497(0.825%)	717(1.038%)	992(1.263%)	821(1.068%)	869(1.111%)	916(1.063%)	845(0.989%)	922(1.041%)
107 & 108	1431(4.069%)	1513(4.039%)	1747(4.271%)	1978(4.511%)	2162(4.647%)	2572(5.053%)	2786(5.236%)	3071(5.389%)	3230(5.363%)	3176(5.271%)	3672(5.316%)	4176(5.316%)	3840(4.997%)	4080(5.216%)	4266(4.95%)	4084(4.778%)	4380(4.947%)
109 & 110	593(1.686%)	687(1.834%)	815(1.993%)	946(2.157%)	1018(2.188%)	1171(2.301%)	1280(2.406%)	1427(2.504%)	1500(2.49%)	1542(2.559%)	1662(2.406%)	1958(2.493%)	1884(2.452%)	2070(2.646%)	2013(2.336%)	1897(2.219%)	1947(2.199%)
111 & 112	927(2.636%)	931(2.485%)	989(2.418%)	1063(2.424%)	1124(2.416%)	1286(2.527%)	1312(2.466%)	1446(2.537%)	1566(2.6%)	1533(2.544%)	1862(2.696%)	2049(2.609%)	2109(2.744%)	2099(2.683%)	2215(2.57%)	2213(2.589%)	2207(2.493%)
113 & 114	2487(7.071%)	2644(7.057%)	2844(6.954%)	3001(6.844%)	3101(6.665%)	3345(6.572%)	3625(6.813%)	3619(6.35%)	3674(6.1%)	3657(6.07%)	4023(5.825%)	4325(5.506%)	4088(5.32%)	4215(5.389%)	4379(5.081%)	4112(4.811%)	4029(4.551%)
115 & 116	0(0%)	0(0%)	0(0%)	0(0%)	0(0%)	46(0.09%)	50(0.094%)	70(0.123%)	168(0.279%)	173(0.287%)	214(0.31%)	221(0.281%)	230(0.299%)	244(0.312%)	231(0.268%)	226(0.264%)	214(0.242%)
117 & 118	645(1.834%)	677(1.807%)	743(1.817%)	780(1.779%)	831(1.786%)	918(1.804%)	905(1.701%)	912(1.6%)	896(1.488%)	877(1.456%)	901(1.304%)	952(1.212%)	951(1.238%)	1019(1.303%)	1077(1.25%)	1064(1.245%)	1120(1.265%)
119 & 120	0(0%)	0(0%)	0(0%)	0(0%)	0(0%)	0(0%)	0(0%)	0(0%)	0(0%)	0(0%)	0(0%)	0(0%)	0(0%)	0(0%)	0(0%)	0(0%)	0(0%)
121 & 122	559(1.589%)	560(1.495%)	536(1.311%)	539(1.229%)	522(1.122%)	483(0.949%)	477(0.897%)	421(0.739%)	437(0.726%)	508(0.843%)	596(0.863%)	602(0.766%)	593(0.772%)	493(0.63%)	511(0.593%)	496(0.58%)	509(0.575%)

Table 6.9. Longitudinal Probabilistic Distribution of Points per ROIs using Asymmetric JHU Parcellation Map with 122 ROIs given as: Number of points per ROI (Percentage on surface %)

Week\ ROI#	28	29	30	31	32	33	34	35	36	37	38	39	40	41	42	43	44
1	363(1.041%)	432(1.17%)	466(1.15%)	583(1.334%)	544(1.171%)	594(1.159%)	431(0.801%)	365(0.616%)	333(0.519%)	333(0.514%)	652(0.89%)	945(1.149%)	1050(1.3%)	1203(1.462%)	1507(1.695%)	1403(1.582%)	1535(1.686%)
2	114(0.327%)	112(0.303%)	101(0.249%)	105(0.24%)	103(0.222%)	102(0.199%)	95(0.177%)	101(0.17%)	96(0.15%)	104(0.161%)	98(0.134%)	98(0.119%)	100(0.124%)	211(0.256%)	219(0.246%)	100(0.113%)	101(0.111%)
3	0(0%)	0(0%)	0(0%)	0(0%)	0(0%)	0(0%)	0(0%)	0(0%)	0(0%)	0(0%)	98(0.134%)	125(0.152%)	131(0.162%)	134(0.163%)	144(0.162%)	144(0.162%)	154(0.169%)
4	0(0%)	0(0%)	0(0%)	0(0%)	0(0%)	0(0%)	0(0%)	0(0%)	0(0%)	0(0%)	94(0.128%)	131(0.159%)	137(0.17%)	196(0.238%)	218(0.245%)	235(0.265%)	267(0.293%)
5	0(0%)	0(0%)	0(0%)	0(0%)	0(0%)	46(0.09%)	82(0.152%)	86(0.145%)	93(0.145%)	92(0.142%)	108(0.147%)	119(0.145%)	110(0.136%)	114(0.139%)	116(0.13%)	115(0.13%)	120(0.132%)
6	222(0.637%)	200(0.542%)	201(0.496%)	221(0.506%)	242(0.521%)	278(0.542%)	263(0.489%)	269(0.454%)	282(0.439%)	246(0.38%)	244(0.333%)	268(0.326%)	274(0.339%)	268(0.326%)	306(0.344%)	307(0.346%)	317(0.348%)
7	0(0%)	0(0%)	0(0%)	0(0%)	0(0%)	0(0%)	0(0%)	0(0%)	0(0%)	0(0%)	0(0%)	0(0%)	0(0%)	0(0%)	0(0%)	0(0%)	0(0%)
8	0(0%)	0(0%)	0(0%)	0(0%)	0(0%)	0(0%)	0(0%)	0(0%)	0(0%)	0(0%)	0(0%)	0(0%)	0(0%)	0(0%)	0(0%)	0(0%)	0(0%)
9	0(0%)	0(0%)	0(0%)	0(0%)	0(0%)	0(0%)	0(0%)	0(0%)	0(0%)	0(0%)	0(0%)	0(0%)	0(0%)	0(0%)	0(0%)	0(0%)	0(0%)
10	0(0%)	0(0%)	0(0%)	0(0%)	0(0%)	0(0%)	0(0%)	0(0%)	0(0%)	0(0%)	0(0%)	0(0%)	0(0%)	0(0%)	0(0%)	0(0%)	0(0%)
11	0(0%)	0(0%)	0(0%)	0(0%)	0(0%)	0(0%)	0(0%)	0(0%)	0(0%)	0(0%)	0(0%)	0(0%)	0(0%)	0(0%)	0(0%)	0(0%)	0(0%)
12	0(0%)	0(0%)	0(0%)	0(0%)	0(0%)	0(0%)	0(0%)	0(0%)	0(0%)	0(0%)	0(0%)	0(0%)	0(0%)	0(0%)	0(0%)	0(0%)	0(0%)
13	0(0%)	0(0%)	0(0%)	0(0%)	0(0%)	0(0%)	0(0%)	0(0%)	0(0%)	0(0%)	0(0%)	0(0%)	0(0%)	0(0%)	0(0%)	0(0%)	0(0%)
14	0(0%)	0(0%)	0(0%)	0(0%)	0(0%)	0(0%)	0(0%)	0(0%)	0(0%)	0(0%)	0(0%)	0(0%)	0(0%)	0(0%)	0(0%)	0(0%)	0(0%)
15	0(0%)	0(0%)	0(0%)	0(0%)	0(0%)	0(0%)	0(0%)	0(0%)	0(0%)	0(0%)	0(0%)	0(0%)	0(0%)	0(0%)	0(0%)	0(0%)	0(0%)
16	0(0%)	0(0%)	0(0%)	0(0%)	0(0%)	0(0%)	0(0%)	0(0%)	0(0%)	0(0%)	0(0%)	0(0%)	0(0%)	0(0%)	0(0%)	0(0%)	0(0%)
17	275(0.789%)	262(0.71%)	240(0.592%)	239(0.547%)	238(0.512%)	254(0.495%)	235(0.437%)	230(0.388%)	214(0.333%)	215(0.332%)	210(0.287%)	209(0.254%)	219(0.271%)	218(0.265%)	181(0.204%)	165(0.186%)	173(0.19%)
18	833(2.389%)	799(2.164%)	805(1.987%)	802(1.835%)	821(1.768%)	749(1.461%)	669(1.244%)	686(1.158%)	508(0.792%)	496(0.766%)	446(0.609%)	396(0.481%)	427(0.529%)	405(0.492%)	379(0.426%)	368(0.415%)	359(0.394%)
19	88(0.252%)	114(0.309%)	180(0.444%)	214(0.49%)	219(0.471%)	265(0.517%)	295(0.548%)	408(0.689%)	447(0.696%)	441(0.681%)	339(0.463%)	337(0.41%)	308(0.381%)	319(0.388%)	339(0.381%)	328(0.37%)	343(0.377%)
20	0(0%)	0(0%)	110(0.271%)	116(0.265%)	157(0.338%)	251(0.49%)	255(0.474%)	267(0.451%)	309(0.481%)	295(0.456%)	344(0.469%)	326(0.396%)	322(0.399%)	268(0.326%)	242(0.272%)	333(0.375%)	347(0.381%)
21	0(0%)	0(0%)	0(0%)	0(0%)	0(0%)	0(0%)	0(0%)	0(0%)	0(0%)	0(0%)	0(0%)	0(0%)	0(0%)	0(0%)	0(0%)	0(0%)	0(0%)
22	0(0%)	183(0.496%)	268(0.661%)	322(0.737%)	356(0.766%)	393(0.767%)	335(0.623%)	353(0.596%)	431(0.672%)	373(0.576%)	456(0.622%)	548(0.666%)	558(0.691%)	305(0.371%)	349(0.392%)	431(0.486%)	499(0.548%)
23	0(0%)	0(0%)	0(0%)	0(0%)	0(0%)	0(0%)	0(0%)	0(0%)	0(0%)	0(0%)	0(0%)	0(0%)	0(0%)	0(0%)	0(0%)	0(0%)	0(0%)
24	0(0%)	0(0%)	0(0%)	0(0%)	0(0%)	0(0%)	0(0%)	0(0%)	0(0%)	0(0%)	0(0%)	0(0%)	0(0%)	120(0.146%)	182(0.205%)	43(0.048%)	0(0%)

25	0(0%)	0(0%)	0(0%)	0(0%)	0(0%)	0(0%)	0(0%)	0(0%)	0(0%)	0(0%)	0(0%)	0(0%)	0(0%)	0(0%)	0(0%)	0(0%)	0(0%)
26	0(0%)	0(0%)	0(0%)	0(0%)	0(0%)	0(0%)	0(0%)	0(0%)	0(0%)	0(0%)	0(0%)	0(0%)	0(0%)	0(0%)	0(0%)	0(0%)	0(0%)
27	0(0%)	0(0%)	0(0%)	0(0%)	0(0%)	0(0%)	0(0%)	0(0%)	0(0%)	0(0%)	0(0%)	0(0%)	0(0%)	0(0%)	0(0%)	0(0%)	0(0%)
28	0(0%)	0(0%)	0(0%)	0(0%)	0(0%)	0(0%)	0(0%)	0(0%)	0(0%)	0(0%)	0(0%)	0(0%)	0(0%)	0(0%)	0(0%)	0(0%)	0(0%)
29	0(0%)	0(0%)	0(0%)	0(0%)	0(0%)	0(0%)	0(0%)	0(0%)	0(0%)	0(0%)	0(0%)	0(0%)	0(0%)	0(0%)	0(0%)	0(0%)	0(0%)
30	0(0%)	0(0%)	0(0%)	0(0%)	0(0%)	0(0%)	0(0%)	0(0%)	0(0%)	0(0%)	0(0%)	0(0%)	0(0%)	160(0.194%)	202(0.227%)	198(0.223%)	188(0.206%)
31	0(0%)	0(0%)	0(0%)	0(0%)	0(0%)	0(0%)	0(0%)	0(0%)	0(0%)	0(0%)	0(0%)	0(0%)	0(0%)	0(0%)	0(0%)	0(0%)	0(0%)
32	0(0%)	0(0%)	0(0%)	0(0%)	0(0%)	0(0%)	0(0%)	0(0%)	0(0%)	0(0%)	0(0%)	0(0%)	0(0%)	0(0%)	0(0%)	0(0%)	0(0%)
33	627(1.798%)	656(1.777%)	708(1.747%)	763(1.746%)	803(1.729%)	795(1.551%)	796(1.48%)	809(1.366%)	883(1.376%)	853(1.317%)	920(1.255%)	928(1.128%)	898(1.112%)	920(1.118%)	969(1.09%)	973(1.097%)	964(1.059%)
34	566(1.623%)	553(1.498%)	392(0.967%)	420(0.961%)	417(0.898%)	456(0.89%)	495(0.92%)	510(0.861%)	546(0.851%)	558(0.862%)	594(0.811%)	596(0.725%)	520(0.644%)	543(0.66%)	531(0.597%)	544(0.613%)	516(0.567%)
35	285(0.817%)	323(0.875%)	384(0.948%)	409(0.936%)	457(0.984%)	535(1.044%)	496(0.922%)	507(0.856%)	597(0.93%)	586(0.905%)	546(0.745%)	591(0.719%)	597(0.739%)	588(0.714%)	683(0.768%)	720(0.812%)	729(0.8%)
36	460(1.319%)	471(1.276%)	536(1.323%)	572(1.309%)	637(1.371%)	765(1.492%)	771(1.434%)	886(1.496%)	926(1.443%)	929(1.435%)	911(1.243%)	981(1.193%)	983(1.217%)	1003(1.219%)	1070(1.203%)	1099(1.239%)	1110(1.219%)
37	0(0%)	0(0%)	0(0%)	0(0%)	0(0%)	0(0%)	0(0%)	0(0%)	0(0%)	0(0%)	0(0%)	0(0%)	0(0%)	0(0%)	0(0%)	0(0%)	0(0%)
38	0(0%)	0(0%)	0(0%)	0(0%)	0(0%)	0(0%)	0(0%)	0(0%)	0(0%)	0(0%)	0(0%)	0(0%)	0(0%)	0(0%)	0(0%)	0(0%)	0(0%)
39	113(0.324%)	125(0.339%)	167(0.412%)	192(0.439%)	201(0.433%)	332(0.648%)	392(0.729%)	386(0.652%)	450(0.701%)	366(0.565%)	422(0.576%)	548(0.666%)	571(0.707%)	581(0.706%)	884(0.994%)	786(0.886%)	857(0.941%)
40	92(0.264%)	105(0.284%)	118(0.291%)	143(0.327%)	144(0.31%)	192(0.375%)	235(0.437%)	328(0.554%)	383(0.597%)	411(0.635%)	514(0.701%)	602(0.732%)	730(0.904%)	683(0.83%)	866(0.974%)	734(0.828%)	839(0.921%)
41	0(0%)	0(0%)	0(0%)	0(0%)	0(0%)	0(0%)	0(0%)	0(0%)	0(0%)	0(0%)	0(0%)	0(0%)	0(0%)	0(0%)	0(0%)	0(0%)	0(0%)
42	0(0%)	0(0%)	0(0%)	0(0%)	0(0%)	0(0%)	0(0%)	0(0%)	0(0%)	0(0%)	0(0%)	0(0%)	0(0%)	0(0%)	0(0%)	0(0%)	0(0%)
43	0(0%)	0(0%)	0(0%)	0(0%)	0(0%)	0(0%)	0(0%)	0(0%)	0(0%)	0(0%)	0(0%)	0(0%)	0(0%)	0(0%)	0(0%)	0(0%)	0(0%)
44	0(0%)	0(0%)	0(0%)	0(0%)	0(0%)	0(0%)	0(0%)	0(0%)	0(0%)	0(0%)	0(0%)	0(0%)	0(0%)	0(0%)	0(0%)	0(0%)	0(0%)
45	0(0%)	0(0%)	0(0%)	0(0%)	0(0%)	0(0%)	0(0%)	0(0%)	0(0%)	0(0%)	0(0%)	0(0%)	0(0%)	0(0%)	0(0%)	0(0%)	0(0%)
46	0(0%)	0(0%)	0(0%)	0(0%)	0(0%)	0(0%)	0(0%)	0(0%)	0(0%)	0(0%)	0(0%)	0(0%)	0(0%)	0(0%)	0(0%)	0(0%)	0(0%)
47	0(0%)	0(0%)	0(0%)	0(0%)	0(0%)	0(0%)	0(0%)	0(0%)	0(0%)	0(0%)	0(0%)	0(0%)	0(0%)	0(0%)	0(0%)	0(0%)	0(0%)
48	0(0%)	0(0%)	0(0%)	0(0%)	0(0%)	0(0%)	0(0%)	0(0%)	0(0%)	0(0%)	0(0%)	0(0%)	0(0%)	0(0%)	0(0%)	0(0%)	0(0%)
49	0(0%)	0(0%)	0(0%)	0(0%)	0(0%)	0(0%)	0(0%)	0(0%)	0(0%)	0(0%)	0(0%)	0(0%)	0(0%)	0(0%)	0(0%)	0(0%)	0(0%)
50	0(0%)	0(0%)	0(0%)	0(0%)	0(0%)	0(0%)	0(0%)	0(0%)	0(0%)	0(0%)	0(0%)	0(0%)	0(0%)	0(0%)	0(0%)	0(0%)	0(0%)
51	0(0%)	0(0%)	0(0%)	0(0%)	0(0%)	0(0%)	0(0%)	0(0%)	0(0%)	0(0%)	0(0%)	0(0%)	0(0%)	0(0%)	0(0%)	0(0%)	0(0%)

52	0(0%)	0(0%)	0(0%)	0(0%)	0(0%)	0(0%)	0(0%)	0(0%)	0(0%)	0(0%)	0(0%)	0(0%)	0(0%)	0(0%)	0(0%)	0(0%)	0(0%)
53	0(0%)	0(0%)	0(0%)	0(0%)	0(0%)	0(0%)	0(0%)	0(0%)	0(0%)	0(0%)	0(0%)	0(0%)	0(0%)	0(0%)	0(0%)	0(0%)	0(0%)
54	0(0%)	0(0%)	0(0%)	0(0%)	0(0%)	0(0%)	0(0%)	0(0%)	0(0%)	0(0%)	0(0%)	0(0%)	0(0%)	0(0%)	0(0%)	0(0%)	0(0%)
55	0(0%)	0(0%)	0(0%)	0(0%)	0(0%)	0(0%)	0(0%)	0(0%)	0(0%)	0(0%)	0(0%)	0(0%)	0(0%)	0(0%)	0(0%)	0(0%)	0(0%)
56	0(0%)	0(0%)	0(0%)	0(0%)	0(0%)	0(0%)	0(0%)	0(0%)	0(0%)	0(0%)	0(0%)	0(0%)	0(0%)	0(0%)	0(0%)	0(0%)	0(0%)
57	0(0%)	0(0%)	0(0%)	0(0%)	0(0%)	0(0%)	0(0%)	0(0%)	0(0%)	0(0%)	0(0%)	0(0%)	0(0%)	0(0%)	0(0%)	0(0%)	0(0%)
58	0(0%)	0(0%)	0(0%)	0(0%)	0(0%)	0(0%)	0(0%)	0(0%)	0(0%)	0(0%)	0(0%)	0(0%)	0(0%)	81(0.098%)	0(0%)	0(0%)	0(0%)
59	0(0%)	0(0%)	0(0%)	0(0%)	0(0%)	0(0%)	0(0%)	0(0%)	0(0%)	0(0%)	0(0%)	0(0%)	0(0%)	0(0%)	0(0%)	0(0%)	0(0%)
60	0(0%)	0(0%)	0(0%)	0(0%)	0(0%)	0(0%)	0(0%)	0(0%)	0(0%)	0(0%)	0(0%)	0(0%)	0(0%)	0(0%)	0(0%)	0(0%)	0(0%)
61	0(0%)	0(0%)	0(0%)	0(0%)	0(0%)	0(0%)	0(0%)	0(0%)	0(0%)	0(0%)	0(0%)	0(0%)	0(0%)	0(0%)	0(0%)	0(0%)	0(0%)
62	0(0%)	0(0%)	0(0%)	0(0%)	0(0%)	0(0%)	0(0%)	0(0%)	0(0%)	0(0%)	0(0%)	0(0%)	0(0%)	0(0%)	0(0%)	0(0%)	0(0%)
63	0(0%)	0(0%)	0(0%)	0(0%)	0(0%)	0(0%)	0(0%)	0(0%)	0(0%)	0(0%)	0(0%)	0(0%)	0(0%)	0(0%)	0(0%)	0(0%)	0(0%)
64	0(0%)	0(0%)	0(0%)	0(0%)	0(0%)	0(0%)	0(0%)	0(0%)	0(0%)	0(0%)	0(0%)	0(0%)	0(0%)	0(0%)	0(0%)	0(0%)	0(0%)
65	0(0%)	0(0%)	0(0%)	0(0%)	0(0%)	0(0%)	0(0%)	0(0%)	0(0%)	0(0%)	0(0%)	0(0%)	0(0%)	0(0%)	0(0%)	0(0%)	0(0%)
66	0(0%)	0(0%)	0(0%)	0(0%)	0(0%)	0(0%)	0(0%)	0(0%)	0(0%)	0(0%)	0(0%)	0(0%)	0(0%)	0(0%)	0(0%)	0(0%)	0(0%)
67	1689(4.843%)	1800(4.875%)	1956(4.827%)	2068(4.732%)	2288(4.926%)	2646(5.162%)	2693(5.007%)	3073(5.187%)	3258(5.076%)	3362(5.192%)	4151(5.665%)	4637(5.637%)	4551(5.635%)	4558(5.538%)	5098(5.733%)	4920(5.547%)	5064(5.561%)
68	1537(4.408%)	1589(4.303%)	1707(4.213%)	1874(4.288%)	2014(4.336%)	2254(4.397%)	2367(4.401%)	2666(4.5%)	2986(4.653%)	3172(4.899%)	3754(5.123%)	4199(5.105%)	4116(5.096%)	4310(5.236%)	4632(5.209%)	4668(5.263%)	4702(5.163%)
69	1221(3.501%)	1291(3.496%)	1451(3.581%)	1577(3.608%)	1693(3.645%)	1829(3.568%)	1959(3.642%)	2143(3.617%)	2209(3.442%)	2222(3.432%)	2362(3.223%)	2643(3.213%)	2541(3.146%)	2605(3.165%)	2805(3.154%)	2779(3.133%)	2881(3.164%)
70	1406(4.032%)	1498(4.057%)	1708(4.215%)	1878(4.297%)	1998(4.302%)	2235(4.36%)	2419(4.498%)	2702(4.561%)	2827(4.405%)	2806(4.333%)	3026(4.129%)	3352(4.075%)	3301(4.087%)	3396(4.126%)	3499(3.935%)	3601(4.06%)	3598(3.951%)
71	819(2.349%)	861(2.332%)	938(2.315%)	969(2.217%)	1027(2.211%)	1080(2.107%)	1138(2.116%)	1204(2.032%)	1291(2.012%)	1233(1.904%)	1348(1.84%)	1504(1.828%)	1580(1.956%)	1539(1.87%)	1595(1.794%)	1680(1.894%)	1684(1.849%)
72	883(2.532%)	944(2.556%)	1024(2.527%)	1048(2.398%)	1100(2.368%)	1186(2.314%)	1207(2.244%)	1288(2.174%)	1355(2.111%)	1397(2.157%)	1417(1.934%)	1683(2.046%)	1700(2.105%)	1720(2.09%)	1680(1.889%)	1773(1.999%)	1762(1.935%)
73	435(1.247%)	479(1.297%)	519(1.281%)	572(1.309%)	606(1.305%)	654(1.276%)	708(1.316%)	762(1.286%)	803(1.251%)	775(1.197%)	861(1.175%)	1018(1.238%)	945(1.17%)	1005(1.221%)	1126(1.266%)	1127(1.271%)	1183(1.299%)
74	210(0.602%)	248(0.672%)	289(0.713%)	334(0.764%)	367(0.799%)	436(0.85%)	475(0.883%)	524(0.885%)	553(0.862%)	529(0.817%)	578(0.789%)	684(0.832%)	664(0.822%)	693(0.842%)	795(0.894%)	785(0.885%)	861(0.945%)
75	702(2.013%)	721(1.953%)	751(1.853%)	775(1.773%)	782(1.684%)	765(1.492%)	771(1.434%)	827(1.396%)	826(1.287%)	795(1.228%)	796(1.086%)	907(1.103%)	894(1.107%)	931(1.131%)	937(1.054%)	939(1.059%)	946(1.039%)
76	555(1.592%)	546(1.479%)	537(1.325%)	538(1.231%)	537(1.156%)	516(1.007%)	502(0.933%)	480(0.81%)	519(0.809%)	441(0.681%)	483(0.659%)	579(0.704%)	547(0.677%)	556(0.675%)	644(0.724%)	619(0.698%)	628(0.69%)
77	590(1.692%)	644(1.744%)	696(1.718%)	758(1.734%)	780(1.679%)	755(1.473%)	742(1.38%)	715(1.207%)	716(1.116%)	713(1.101%)	692(0.944%)	741(0.901%)	741(0.917%)	634(0.77%)	657(0.739%)	660(0.744%)	683(0.75%)

78	875(2.50 9%)	936(2.53 5%)	994(2.45 3%)	1012(2.3 15%)	1046(2.2 52%)	1040(2.0 29%)	1071(1.9 91%)	1062(1.7 93%)	1045(1.6 28%)	1021(1.5 77%)	1121(1.5 3%)	1260(1.5 32%)	1247(1.5 44%)	1325(1.6 1%)	1440(1.6 19%)	1420(1.6 01%)	1415(1.5 54%)
79	1008(2.8 91%)	1054(2.8 54%)	1250(3.0 85%)	1224(2.8 01%)	1272(2.7 39%)	1521(2.9 67%)	1523(2.8 32%)	1569(2.6 49%)	1535(2.3 92%)	1598(2.4 68%)	1805(2.4 63%)	1904(2.3 15%)	1896(2.3 47%)	1927(2.3 41%)	2229(2.5 07%)	2026(2.2 84%)	1982(2.1 76%)
80	752(2.15 6%)	770(2.08 5%)	785(1.93 7%)	881(2.01 6%)	1002(2.1 57%)	1161(2.2 65%)	1357(2.5 23%)	1323(2.2 33%)	1335(2.0 8%)	1381(2.1 33%)	1524(2.0 8%)	1690(2.0 55%)	1679(2.0 79%)	1588(1.9 29%)	1902(2.1 39%)	1813(2.0 44%)	1913(2.1 01%)
81	607(1.74 1%)	664(1.79 8%)	734(1.81 1%)	824(1.88 5%)	894(1.92 5%)	954(1.86 1%)	1026(1.9 08%)	1142(1.9 28%)	1151(1.7 93%)	1179(1.8 21%)	1458(1.9 9%)	1426(1.7 34%)	1427(1.7 67%)	1405(1.7 07%)	1568(1.7 63%)	1549(1.7 46%)	1552(1.7 04%)
82	571(1.63 7%)	617(1.67 1%)	708(1.74 7%)	932(2.13 2%)	871(1.87 5%)	958(1.86 9%)	1046(1.9 45%)	1022(1.7 25%)	1077(1.6 78%)	1116(1.7 23%)	1182(1.6 13%)	1178(1.4 32%)	1222(1.5 13%)	1244(1.5 11%)	1198(1.3 47%)	1194(1.3 46%)	1218(1.3 37%)
83	387(1.11 %)	404(1.09 4%)	433(1.06 9%)	483(1.10 5%)	555(1.19 5%)	631(1.23 1%)	694(1.29 %)	822(1.38 8%)	907(1.41 3%)	959(1.48 1%)	1155(1.5 76%)	1340(1.6 29%)	1306(1.6 17%)	1305(1.5 85%)	1447(1.6 27%)	1419(1.6 %)	1478(1.6 23%)
84	240(0.68 8%)	251(0.68 %)	313(0.77 2%)	362(0.82 8%)	389(0.83 7%)	441(0.86 %)	495(0.92 %)	569(0.96 %)	656(1.02 2%)	713(1.10 1%)	928(1.26 6%)	1171(1.4 24%)	1087(1.3 46%)	1244(1.5 11%)	1436(1.6 15%)	1354(1.5 27%)	1435(1.5 76%)
85	0(0%)	0(0%)	0(0%)	76(0.174 %)	97(0.209 %)	119(0.23 2%)	138(0.25 7%)	187(0.31 6%)	209(0.32 6%)	231(0.35 7%)	299(0.40 8%)	373(0.45 3%)	351(0.43 5%)	409(0.49 7%)	476(0.53 5%)	451(0.50 8%)	479(0.52 6%)
86	931(2.67 %)	965(2.61 3%)	1061(2.6 18%)	956(2.18 7%)	1080(2.3 25%)	1005(1.9 6%)	951(1.76 8%)	1228(2.0 73%)	1266(1.9 73%)	1281(1.9 78%)	1556(2.1 23%)	1742(2.1 18%)	1640(2.0 3%)	1627(1.9 77%)	1587(1.7 85%)	1543(1.7 4%)	1593(1.7 49%)
87	0(0%)	0(0%)	0(0%)	0(0%)	0(0%)	158(0.30 8%)	300(0.55 8%)	531(0.89 6%)	1071(1.6 69%)	1281(1.9 78%)	1449(1.9 77%)	1623(1.9 73%)	1430(1.7 7%)	1397(1.6 97%)	1441(1.6 2%)	1537(1.7 33%)	1765(1.9 38%)
88	44(0.126 %)	192(0.52 %)	335(0.82 7%)	464(1.06 2%)	422(0.90 9%)	480(0.93 6%)	550(1.02 3%)	849(1.43 3%)	1852(2.8 86%)	2095(3.2 35%)	2545(3.4 73%)	2700(3.2 83%)	2727(3.3 76%)	2629(3.1 94%)	2688(3.0 23%)	2847(3.2 1%)	2875(3.1 57%)
89	299(0.85 7%)	316(0.85 6%)	369(0.91 1%)	413(0.94 5%)	483(1.04 %)	512(0.99 9%)	573(1.06 5%)	671(1.13 3%)	756(1.17 8%)	777(1.2 %)	890(1.21 5%)	1013(1.2 32%)	1070(1.3 25%)	1095(1.3 3%)	1291(1.4 52%)	1384(1.5 6%)	1413(1.5 52%)
90	235(0.67 4%)	258(0.69 9%)	283(0.69 8%)	307(0.70 2%)	347(0.74 7%)	409(0.79 8%)	456(0.84 8%)	547(0.92 3%)	600(0.93 5%)	589(0.91 %)	696(0.95 %)	860(1.04 6%)	931(1.15 3%)	933(1.13 4%)	1133(1.2 74%)	1147(1.2 93%)	1134(1.2 45%)
91	674(1.93 3%)	687(1.86 %)	729(1.79 9%)	778(1.78 %)	802(1.72 7%)	848(1.65 4%)	881(1.63 8%)	936(1.58 %)	943(1.46 9%)	954(1.47 3%)	995(1.35 8%)	1082(1.3 15%)	1017(1.2 59%)	1114(1.3 53%)	1206(1.3 56%)	1126(1.2 7%)	1170(1.2 85%)
92	970(2.78 2%)	963(2.60 8%)	1016(2.5 07%)	1095(2.5 05%)	1157(2.4 91%)	1256(2.4 5%)	1340(2.4 91%)	1453(2.4 53%)	1544(2.4 06%)	1566(2.4 18%)	1684(2.2 98%)	1855(2.2 55%)	1879(2.3 26%)	1864(2.2 65%)	2059(2.3 15%)	2051(2.3 12%)	2125(2.3 33%)
93	545(1.56 3%)	557(1.50 8%)	637(1.57 2%)	664(1.51 9%)	711(1.53 1%)	779(1.52 %)	804(1.49 5%)	930(1.57 %)	986(1.53 6%)	964(1.48 9%)	1346(1.8 37%)	1943(2.3 62%)	1897(2.3 49%)	1470(1.7 86%)	2051(2.3 06%)	2281(2.5 72%)	2408(2.6 44%)
94	769(2.20 5%)	813(2.20 2%)	884(2.18 2%)	918(2.1 %)	996(2.14 4%)	1105(2.1 56%)	1117(2.0 77%)	1214(2.0 49%)	1299(2.0 24%)	1374(2.1 22%)	1999(2.7 28%)	2494(3.0 32%)	2427(3.0 05%)	2559(3.1 09%)	2990(3.3 62%)	3091(3.4 85%)	3245(3.5 63%)
95	881(2.52 6%)	905(2.45 1%)	983(2.42 6%)	1041(2.3 82%)	1105(2.3 79%)	1197(2.3 35%)	1272(2.3 65%)	1368(2.3 09%)	1492(2.3 25%)	1491(2.3 03%)	1608(2.1 94%)	1756(2.1 35%)	1789(2.2 15%)	1850(2.2 48%)	1814(2.0 4%)	1862(2.0 99%)	1896(2.0 82%)
96	587(1.68 3%)	612(1.65 7%)	680(1.67 8%)	753(1.72 3%)	821(1.76 8%)	921(1.79 7%)	932(1.73 3%)	1080(1.8 23%)	1198(1.8 67%)	1297(2.0 03%)	1467(2.0 02%)	1702(2.0 69%)	1746(2.1 62%)	1873(2.2 76%)	1976(2.2 22%)	1994(2.2 48%)	1994(2.1 9%)
97	468(1.34 2%)	527(1.42 7%)	620(1.53 %)	643(1.47 1%)	742(1.59 7%)	805(1.57 %)	912(1.69 6%)	994(1.67 8%)	1050(1.6 36%)	1048(1.6 18%)	1077(1.4 7%)	1212(1.4 73%)	1194(1.4 78%)	1272(1.5 45%)	1424(1.6 01%)	1420(1.6 01%)	1365(1.4 99%)
98	1329(3.8 11%)	1418(3.8 4%)	1595(3.9 36%)	1722(3.9 4%)	1827(3.9 33%)	1920(3.7 45%)	2014(3.7 45%)	2211(3.7 32%)	2305(3.5 91%)	2130(3.2 89%)	2128(2.9 04%)	2304(2.8 01%)	2174(2.6 92%)	2264(2.7 51%)	2523(2.8 37%)	2721(3.0 68%)	2794(3.0 68%)
99	1537(4.4 08%)	1495(4.0 49%)	1529(3.7 73%)	1652(3.7 8%)	1603(3.4 51%)	1783(3.4 78%)	1700(3.1 61%)	1852(3.1 26%)	1851(2.8 84%)	1842(2.8 45%)	1898(2.5 9%)	2113(2.5 69%)	2067(2.5 59%)	2172(2.6 39%)	2212(2.4 88%)	2247(2.5 33%)	2470(2.7 12%)
100	1169(3.3 52%)	1226(3.3 2%)	1316(3.2 48%)	1263(2.8 9%)	1282(2.7 6%)	1403(2.7 37%)	1467(2.7 28%)	1603(2.7 06%)	1532(2.3 87%)	1579(2.4 39%)	1619(2.2 09%)	1763(2.1 43%)	1801(2.2 3%)	1791(2.1 76%)	1799(2.0 23%)	1756(1.9 8%)	1715(1.8 83%)
101	72(0.206 %)	95(0.257 %)	117(0.28 9%)	126(0.28 8%)	137(0.29 5%)	151(0.29 5%)	171(0.31 8%)	184(0.31 1%)	188(0.29 3%)	182(0.28 1%)	189(0.25 8%)	190(0.23 1%)	185(0.22 9%)	193(0.23 4%)	190(0.21 4%)	196(0.22 1%)	177(0.19 4%)
102	0(0%)	0(0%)	0(0%)	0(0%)	0(0%)	0(0%)	0(0%)	0(0%)	0(0%)	0(0%)	0(0%)	0(0%)	0(0%)	0(0%)	0(0%)	0(0%)	0(0%)
103	393(1.12 7%)	435(1.17 8%)	465(1.14 8%)	475(1.08 7%)	517(1.11 3%)	503(0.98 1%)	527(0.98 %)	536(0.90 5%)	543(0.84 6%)	566(0.87 4%)	570(0.77 8%)	542(0.65 9%)	504(0.62 4%)	421(0.51 1%)	374(0.42 1%)	351(0.39 6%)	311(0.34 1%)

104	236(0.677%)	237(0.642%)	212(0.523%)	242(0.554%)	270(0.581%)	289(0.564%)	285(0.53%)	264(0.446%)	311(0.485%)	310(0.479%)	266(0.363%)	236(0.287%)	252(0.312%)	201(0.244%)	215(0.242%)	237(0.267%)	250(0.275%)
105	94(0.27%)	101(0.274%)	125(0.308%)	152(0.348%)	192(0.413%)	252(0.492%)	304(0.565%)	374(0.631%)	409(0.637%)	392(0.605%)	519(0.708%)	663(0.806%)	562(0.696%)	591(0.718%)	628(0.706%)	610(0.688%)	656(0.72%)
106	0(0%)	49(0.133%)	68(0.168%)	86(0.197%)	99(0.213%)	129(0.252%)	168(0.312%)	221(0.373%)	264(0.411%)	258(0.398%)	357(0.487%)	487(0.592%)	405(0.501%)	430(0.522%)	478(0.538%)	484(0.546%)	503(0.552%)
107	613(1.758%)	652(1.766%)	739(1.824%)	823(1.883%)	884(1.903%)	1054(2.056%)	1141(2.121%)	1260(2.127%)	1333(2.077%)	1326(2.048%)	1513(2.065%)	1785(2.17%)	1632(2.021%)	1800(2.187%)	1958(2.202%)	1843(2.078%)	1980(2.174%)
108	758(2.174%)	768(2.08%)	868(2.142%)	947(2.167%)	1005(2.164%)	1174(2.29%)	1297(2.411%)	1456(2.458%)	1534(2.39%)	1494(2.307%)	1672(2.282%)	1992(2.422%)	1791(2.217%)	1864(2.265%)	1971(2.216%)	1971(2.222%)	2043(2.243%)
109	260(0.746%)	312(0.845%)	385(0.95%)	442(1.011%)	506(1.089%)	557(1.087%)	621(1.155%)	657(1.109%)	678(1.056%)	691(1.067%)	744(1.015%)	862(1.048%)	772(0.956%)	859(1.044%)	866(0.974%)	817(0.921%)	854(0.938%)
110	331(0.949%)	367(0.994%)	439(1.083%)	518(1.185%)	575(1.238%)	655(1.278%)	730(1.357%)	820(1.384%)	841(1.31%)	841(1.299%)	928(1.266%)	1063(1.292%)	1043(1.291%)	1108(1.346%)	1127(1.267%)	1085(1.223%)	1093(1.2%)
111	341(0.978%)	328(0.888%)	382(0.943%)	405(0.927%)	533(1.148%)	586(1.143%)	609(1.132%)	716(1.209%)	792(1.234%)	792(1.223%)	1079(1.472%)	1250(1.52%)	1323(1.638%)	1299(1.578%)	1443(1.623%)	1366(1.54%)	1363(1.497%)
112	381(1.093%)	411(1.113%)	428(1.056%)	437(1%)	554(1.193%)	614(1.198%)	578(1.075%)	646(1.09%)	857(1.335%)	840(1.297%)	1099(1.5%)	1236(1.503%)	1218(1.508%)	1260(1.531%)	1102(1.239%)	1136(1.281%)	1160(1.274%)
113	839(2.406%)	927(2.51%)	959(2.367%)	1091(2.496%)	1101(2.37%)	1290(2.516%)	1352(2.514%)	1605(2.709%)	1711(2.666%)	1682(2.598%)	1822(2.486%)	1945(2.365%)	1824(2.258%)	1814(2.204%)	1932(2.173%)	1810(2.041%)	1760(1.933%)
114	948(2.719%)	961(2.603%)	1101(2.717%)	1200(2.746%)	1211(2.607%)	1342(2.618%)	1522(2.83%)	1694(2.86%)	1876(2.923%)	1813(2.8%)	1899(2.591%)	1990(2.419%)	1905(2.359%)	1950(2.369%)	1861(2.093%)	1872(2.111%)	1878(2.062%)
115	0(0%)	0(0%)	0(0%)	0(0%)	0(0%)	0(0%)	0(0%)	0(0%)	0(0%)	0(0%)	110(0.15%)	110(0.134%)	107(0.132%)	72(0.087%)	114(0.128%)	119(0.134%)	127(0.139%)
116	0(0%)	0(0%)	0(0%)	0(0%)	0(0%)	0(0%)	0(0%)	0(0%)	105(0.164%)	103(0.159%)	129(0.176%)	149(0.181%)	124(0.154%)	70(0.085%)	66(0.074%)	69(0.078%)	66(0.072%)
117	141(0.404%)	161(0.436%)	182(0.449%)	196(0.448%)	198(0.426%)	222(0.433%)	232(0.431%)	225(0.38%)	226(0.352%)	232(0.358%)	198(0.27%)	209(0.254%)	227(0.281%)	285(0.346%)	255(0.287%)	255(0.288%)	269(0.295%)
118	0(0%)	0(0%)	0(0%)	0(0%)	0(0%)	0(0%)	115(0.214%)	142(0.24%)	291(0.453%)	248(0.383%)	362(0.494%)	429(0.522%)	421(0.521%)	568(0.69%)	516(0.58%)	547(0.617%)	558(0.613%)
119	0(0%)	0(0%)	0(0%)	0(0%)	0(0%)	0(0%)	0(0%)	0(0%)	0(0%)	0(0%)	0(0%)	0(0%)	0(0%)	0(0%)	0(0%)	0(0%)	0(0%)
120	0(0%)	0(0%)	0(0%)	0(0%)	0(0%)	0(0%)	0(0%)	0(0%)	0(0%)	0(0%)	0(0%)	0(0%)	0(0%)	0(0%)	0(0%)	0(0%)	0(0%)
121	342(0.981%)	348(0.942%)	351(0.866%)	404(0.924%)	412(0.887%)	446(0.87%)	456(0.848%)	465(0.785%)	475(0.74%)	519(0.802%)	666(0.909%)	664(0.807%)	679(0.841%)	692(0.841%)	814(0.915%)	854(0.963%)	928(1.019%)
122	160(0.459%)	188(0.509%)	195(0.481%)	207(0.474%)	219(0.471%)	231(0.451%)	231(0.429%)	237(0.4%)	245(0.382%)	254(0.392%)	265(0.362%)	253(0.308%)	277(0.343%)	209(0.254%)	269(0.303%)	262(0.295%)	250(0.275%)

7. Appendix 2

7.1. Ray Triangle Intersection

In 1997, a benchmark fast linear solution to find the intersection between any ray and triangle was proposed by [189] where the plane equation is not needed to compute the intersection. Denoting the three vertices of the triangle by $V_0, V_1, and\ V_2$, the barycentric coordinate (u, v) equation of any point inside the triangle is given in equation (7.1):

$$P(u, v) = (1 - u - v)V_0 + uV_1 + vV_2 \tag{7.1}$$

A ray originated at O with direction D intersects the triangle by a displacement t that aligns the ray origin with a point inside the triangle as given in equation (7.2) (see Figure 7.1):

$$O + tD = (1 - u - v)V_0 + uV_1 + vV_2 \tag{7.2}$$

Rearranging the terms will provide the following linear system of equations in (7.3), a solution through which the intersection can be found:

$$[-D, \quad V_1 - V_0, \quad V_2 - V_0]\begin{bmatrix} t \\ u \\ v \end{bmatrix} = O - V_0 \tag{7.3}$$

Where both u and $v \geq 0$ for the intersection to be within the triangle, and $u + v \leq 1$. If one of u or $v = 1$, then the ray is parallel with one of the triangle's edges. And if $t < 0$, the triangle is not visible to the ray (e.g. the ray intersects the triangle in the opposite direction of D).

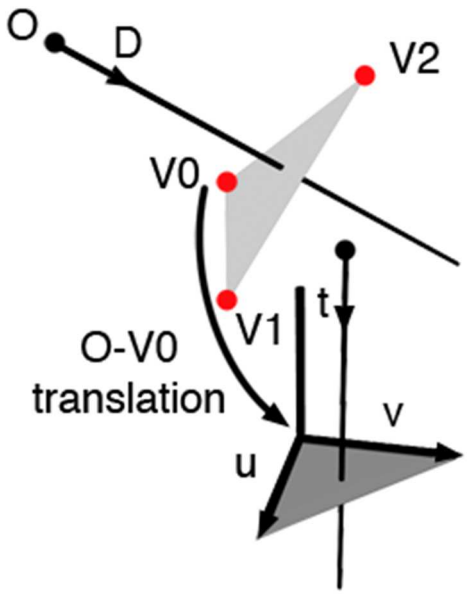

Figure 7.1. Translation t maps the ray to the barycentric coordinate (u, v) (Source: www.scratchapixel.com)

7.2. Surface Points Normal Calculations

For any surface approximated as a polygonal or triangular mesh, the surface vertices normal vectors are usually computed by averaging the normal vectors of the facets surrounding these vertices. For example, with reference to Figure 7.2, the normal vector at vertex V_0 will be given by the normalized average of the facets sharing vertex V_0 as shown in equation (7.4):

$$\overrightarrow{N_0} = \frac{\sum_{i=1}^{n} \overrightarrow{N_i}}{\left|\sum_{i=1}^{n} \overrightarrow{N_i}\right|} \tag{7.4}$$

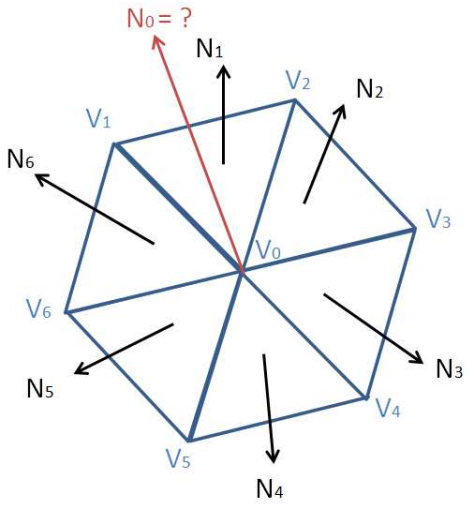

Figure 7.2. Illustration of surface vertex normal vector calculation using surrounding facets normal vectors.

where each facet normal is computed by the cross product of two of its edges. i.e. $\overrightarrow{N_1} = (V_1 - V_0) \times (V_2 - V_0)$. Equal weights for the contribution of the facets in the average is initially suggested by Gouraud [196]. While Thürrner and Wüthrich adjusted the weights to accounts for the angle of each facet such that facets with the same normal vectors contribute only once [197], Max suggested taking the area of the facet into account by assigning larger weights for small facets [198]. Gouraud's normal calculation using equal weights is efficient and convenient for shading and rendering, but Max's method seems superior, especially with spherical like surfaces.

Bibliography

[1] NS Green, K Damus, JL Simpson, J Iams, EA Reece, CJ Hobel, et al. Research agenda for preterm birth: recommendations from the March of Dimes, Obstet.Gynecol. 193 (2005) 626-635.

[2] WM Callaghan, MF MacDorman, SA Rasmussen, C Qin, EM Lackritz. The contribution of preterm birth to infant mortality rates in the United States, Pediatrics. 118 (2006) 1566-1573.

[3] N Marlow, D Wolke, MA Bracewell, M Samara. Neurologic and developmental disability at six years of age after extremely preterm birth, N.Engl.J.Med. 352 (2005) 9-19.

[4] BR Vohr, LL Wright, AM Dusick, L Mele, J Verter, JJ Steichen, et al. Neurodevelopmental and functional outcomes of extremely low birth weight infants in the National Institute of Child Health and Human Development Neonatal Research Network, 1993-1994, Pediatrics. 105 (2000) 1216-1226.

[5] R Pienaar, B Fischl, V Caviness, N Makris, PE Grant. A methodology for analyzing curvature in the developing brain from preterm to adult, Int J Imaging Syst Technol. 18 (2008) 42-68.

[6] S Budday, P Steinmann, E Kuhl. The role of mechanics during brain development, J.Mech.Phys.Solids. 72 (2014) 75-92.

[7] N Richard, M Dojat, C Garbay. Automated segmentation of human brain MR images using a multi-agent approach, Artif.Intell.Med. 30 (2004) 153-176.

[8] H Gray, Anatomy of the human body, Lea & Febiger 1918.

[9] S Budday, C Raybaud, E Kuhl. A mechanical model predicts morphological abnormalities in the developing human brain, Scientific reports. 4 (2014).

[10] W Li. Automated parcellation on the surface of human cerebral cortex generated from MR images. Doctoral dissertation, University of Iowa. (2012).

[11] TL Angtuaco. Ultrasound imaging of fetal brain abnormalities: three essential anatomical levels, Ultrasound Q. 21 (2005) 287-294.

[12] T Paus, D Collins, A Evans, G Leonard, B Pike, A Zijdenbos. Maturation of white matter in the human brain: a review of magnetic resonance studies, Brain Res.Bull. 54 (2001) 255-266.

[13] SJ Counsell, NL Kennea, AH Herlihy, JM Allsop, MC Harrison, FM Cowan, et al. T2 relaxation values in the developing preterm brain, AJNR Am.J.Neuroradiol. 24 (2003) 1654-1660.

[14] JP Boardman, LE Dyet. Recent advances in imaging preterm brain injury, Minerva Pediatr. 59 (2007) 349-368.

[15] J Kolasinski, CJ Stagg, SA Chance, GC Deluca, MM Esiri, EH Chang, et al. A combined post-mortem magnetic resonance imaging and quantitative histological study of multiple sclerosis pathology, Brain. 135 (2012) 2938-2951.

[16] C Beaulieu. The basis of anisotropic water diffusion in the nervous system–a technical review, NMR Biomed. 15 (2002) 435-455.

[17] KL Miller, CJ Stagg, G Douaud, S Jbabdi, SM Smith, TE Behrens, et al. Diffusion imaging of whole, post-mortem human brains on a clinical MRI scanner, Neuroimage. 57 (2011) 167-181.

[18] D Prayer, PC Brugger, U Nemec, RI Milos, C Mitter, G Kasprian, Cerebral malformations, Fetal MRI, Springer, 2011, pp. 287-308.

[19] F Rousseau, OA Glenn, B Iordanova, C Rodriguez-Carranza, DB Vigneron, JA Barkovich, et al. Registration-based approach for reconstruction of high-resolution in utero fetal MR brain images, Acad.Radiol. 13 (2006) 1072-1081.

[20] S Jiang, H Xue, A Glover, M Rutherford, D Rueckert, JV Hajnal. MRI of moving subjects using multislice snapshot images with volume reconstruction (SVR): application to fetal, neonatal, and adult brain studies, Medical Imaging, IEEE Transactions on. 26 (2007) 967-980.

[21] JG Sled, AP Zijdenbos, AC Evans. A nonparametric method for automatic correction of intensity nonuniformity in MRI data, Medical Imaging, IEEE Transactions on. 17 (1998) 87-97.

[22] NJ Tustison, BB Avants, PA Cook, Y Zheng, A Egan, PA Yushkevich, et al. N4ITK: improved N3 bias correction, Medical Imaging, IEEE Transactions on. 29 (2010) 1310-1320.

[23] WJ Hamilton, JD Boyd, HW Mossman. Human embryology (prenatal development of form and function). Human embryology (prenatal development of form and function). (1945).

[24] MA Rutherford, MRI of the Neonatal Brain, WB Saunders Co 2002.

[25] C Limperopoulos, JS Soul, K Gauvreau, PS Huppi, SK Warfield, H Bassan, et al. Late gestation cerebellar growth is rapid and impeded by premature birth, Pediatrics. 115 (2005) 688-695.

[26] PS Hüppi, S Warfield, R Kikinis, PD Barnes, GP Zientara, FA Jolesz, et al. Quantitative magnetic resonance imaging of brain development in premature and mature newborns, Ann.Neurol. 43 (1998) 224-235.

[27] J Ferrie, L Barantin, E Saliba, S Akoka, F Tranquart, D Sirinelli, et al. MR assessment of the brain maturation during the perinatal period: quantitative T2 MR study in premature newborns, Magn.Reson.Imaging. 17 (1999) 1275-1288.

[28] SJ Counsell, EF Maalouf, AM Fletcher, P Duggan, M Battin, HJ Lewis, et al. MR imaging assessment of myelination in the very preterm brain, AJNR Am.J.Neuroradiol. 23 (2002) 872-881.

[29] C Laule, IM Vavasour, SH Kolind, DK Li, TL Traboulsee, G Moore, et al. Magnetic resonance imaging of myelin, Neurotherapeutics. 4 (2007) 460-484.

[30] M Kuklisova-Murgasova, P Aljabar, L Srinivasan, SJ Counsell, V Doria, A Serag, et al. A dynamic 4D probabilistic atlas of the developing brain, Neuroimage. 54 (2011) 2750-2763.

[31] M Knaap, J Valk, C Bakker, M Schooneveld, J Faber, J Willemse, et al. Myelination as an expression of the functional maturity of the brain, Developmental Medicine & Child Neurology. 33 (1991) 849-857.

[32] SJ Counsell, MA Rutherford, FM Cowan, AD Edwards. Magnetic resonance imaging of preterm brain injury, Arch.Dis.Child.Fetal Neonatal Ed. 88 (2003) F269-74.

[33] AJ Barkovich. Concepts of myelin and myelination in neuroradiology, AJNR Am.J.Neuroradiol. 21 (2000) 1099-1109.

[34] Van der Knaap, Marjo S, J Valk, Magnetic resonance of myelination and myelin disorders, Springer 2005.

[35] PI Yakovlev, A Lecours. The myelogenetic cycles of regional maturation of the brain, Regional development of the brain in early life. (1967) 3-70.

[36] M Nishida, N Makris, DN Kennedy, M Vangel, B Fischl, KS Krishnamoorthy, et al. Detailed semiautomated MRI based morphometry of the neonatal brain: preliminary results, Neuroimage. 32 (2006) 1041-1049.

[37] J Dobbing, J Sands. Quantitative growth and development of human brain, Arch.Dis.Child. 48 (1973) 757-767.

[38] M Wilke, V Schmithorst, S Holland. Normative pediatric brain data for spatial normalization and segmentation differs from standard adult data, Magnetic Resonance in Medicine. 50 (2003) 749-757.

[39] M Häggström. Medical gallery of Mikael Häggström 2014, Wikiversity Journal of Medicine. 1 (2014).

[40] A Serag. Spatio-temporal modeling and analysis of brain development, Doctoral dissertation, Imperial College London. (2013).

[41] P Rakic. Evolution of the neocortex: a perspective from developmental biology, Nature Reviews Neuroscience. 10 (2009) 724-735.

[42] N Ulfig, F Neudorfer, J Bohl. Transient structures of the human fetal brain: subplate, thalamic reticular complex, ganglionic eminence, Histol.Histopathol. 15 (2000) 771-790.

[43] JG Parnavelas, P Alifragis, B Nadarajah. The origin and migration of cortical neurons, Prog.Brain Res. 136 (2002) 73-80.

[44] Z Petanjek, I Kostovic, M Esclapez. Primate-specific origins and migration of cortical GABAergic neurons, Front.Neuroanat. 3 (2009) 26.

[45] AE Ayoub, S Oh, Y Xie, J Leng, J Cotney, MH Dominguez, et al. Transcriptional programs in transient embryonic zones of the cerebral cortex defined by high-resolution mRNA sequencing, Proc.Natl.Acad.Sci.U.S.A. 108 (2011) 14950-14955.

[46] I Bystron, C Blakemore, P Rakic. Development of the human cerebral cortex: Boulder Committee revisited, Nature Reviews Neuroscience. 9 (2008) 110-122.

[47] O Marín, JL Rubenstein. A long, remarkable journey: tangential migration in the telencephalon, Nature Reviews Neuroscience. 2 (2001) 780-790.

[48] O Marín, JL Rubenstein. Cell migration in the forebrain, Annu.Rev.Neurosci. 26 (2003) 441-483.

[49] M Sild, ES Ruthazer. Radial glia: progenitor, pathway, and partner, Neuroscientist. 17 (2011) 288-302.

[50] P Rakic. Mode of cell migration to the superficial layers of fetal monkey neocortex, J.Comp.Neurol. 145 (1972) 61-83.

[51] P Rakic. Specification of cerebral cortical areas, Science. 241 (1988) 170-176.

[52] J Kolasinski, E Takahashi, AA Stevens, T Benner, B Fischl, L Zöllei, et al. Radial and tangential neuronal migration pathways in the human fetal brain: Anatomically distinct patterns of diffusion MRI coherence, Neuroimage. 79 (2013) 412-422.

[53] PA Habas, JA Scott, A Roosta, V Rajagopalan, K Kim, F Rousseau, et al. Early folding patterns and asymmetries of the normal human brain detected from in utero MRI, Cereb.Cortex. 22 (2012) 13-25.

[54] P Rakic, AE Ayoub, JJ Breunig, MH Dominguez. Decision by division: making cortical maps, Trends Neurosci. 32 (2009) 291-301.

[55] R Toro, Y Burnod. A morphogenetic model for the development of cortical convolutions, Cereb.Cortex. 15 (2005) 1900-1913.

[56] DC Van Essen. A tension-based theory of morphogenesis and compact wiring in the central nervous system, NATURE-LONDON-. (1997) 313-318.

[57] J Lefèvre, J Mangin. A reaction-diffusion model of human brain development, PLoS computational biology. 6 (2010) e1000749.

[58] DC Van Essen, DL Dierker. Surface-based and probabilistic atlases of primate cerebral cortex, Neuron. 56 (2007) 209-225.

[59] J Hill, D Dierker, J Neil, T Inder, A Knutsen, J Harwell, et al. A surface-based analysis of hemispheric asymmetries and folding of cerebral cortex in term-born human infants, J.Neurosci. 30 (2010) 2268-2276.

[60] G Li, L Wang, F Shi, W Lin, D Shen, Constructing 4D Infant Cortical Surface Atlases Based on Dynamic Developmental Trajectories of the Cortex, Medical Image Computing and Computer-Assisted Intervention–MICCAI 2014, Springer, 2014, pp. 89-96.

[61] A Serag, IS Gousias, A Makropoulos, P Aljabar, JV Hajnal, JP Boardman, et al., Unsupervised learning of shape complexity: application to brain development, Spatio-temporal Image Analysis for Longitudinal and Time-Series Image Data, Springer, 2012, pp. 88-99.

[62] J Dubois, M Benders, C Borradori-Tolsa, A Cachia, F Lazeyras, R Ha-Vinh Leuchter, et al. Primary cortical folding in the human newborn: an early marker of later functional development, Brain. 131 (2008) 2028-2041.

[63] J Dubois, M Benders, A Cachia, F Lazeyras, R Ha-Vinh Leuchter, SV Sizonenko, et al. Mapping the early cortical folding process in the preterm newborn brain, Cereb.Cortex. 18 (2008) 1444-1454.

[64] S Horsch, B Hallberg, K Leifsdottir, B Skiöld, Z Nagy, M Mosskin, et al. Brain abnormalities in extremely low gestational age infants: a Swedish population based MRI study, Acta Paediatrica. 96 (2007) 979-984.

[65] A Serag, P Aljabar, S Counsell, J Boardman, JV Hajnal, D Rueckert, Tracking developmental changes in subcortical structures of the preterm brain using multi-modal MRI, (2011) 349-352.

[66] A Vardhan, M Prastawa, C Vachet, J Piven, G Gerig, Characterizing growth patterns in longitudinal MRI using image contrast, (2014) 90340D-90340D-8.

[67] VB Mountcastle. Modality and topographic properties of single neurons of cat's somatic sensory cortex, J.Neurophysiol. 20 (1957) 408-434.

[68] F Sanides. Structure and function of the human frontal lobe, Neuropsychologia. 2 (1964) 209-219.

[69] SG Waxman, Clinical neuroanatomy, McGraw-Hill Medical New York 2010.

[70] JH Gilmore, W Lin, MW Prastawa, CB Looney, YS Vetsa, RC Knickmeyer, et al. Regional gray matter growth, sexual dimorphism, and cerebral asymmetry in the neonatal brain, J.Neurosci. 27 (2007) 1255-1260.

[71] K Oishi, S Mori, PK Donohue, T Ernst, L Anderson, S Buchthal, et al. Multi-contrast human neonatal brain atlas: application to normal neonate development analysis, Neuroimage. 56 (2011) 8-20.

[72] IS Gousias, AD Edwards, MA Rutherford, SJ Counsell, JV Hajnal, D Rueckert, et al. Magnetic resonance imaging of the newborn brain: manual segmentation of labelled atlases in term-born and preterm infants, Neuroimage. 62 (2012) 1499-1509.

[73] IS Gousias, A Hammers, SJ Counsell, L Srinivasan, MA Rutherford, RA Heckemann, et al. Magnetic resonance imaging of the newborn brain: automatic segmentation of brain images into 50 anatomical regions, PloS one. 8 (2013) e59990.

[74] F Shi, P Yap, G Wu, H Jia, JH Gilmore, W Lin, et al. Infant brain atlases from neonates to 1-and 2-year-olds, PLoS One. 6 (2011) e18746.

[75] Alhazen, AI Al-Haytham, A Sabra, Kitab al-Manazir, National Council for Culture, Arts and Letters 1983.

[76] AW Toga, JC Mazziotta, Brain mapping: The methods, Academic press 2002.

[77] W Sudhoff. Die Lehre von den Hirnventrikeln in textlicher und graphischer Tradition des Altertums und Mittelalters, Archiv für Geschichte der Medizin. (1913) 149-205.

[78] A Vesalius, De humani corporis fabrica, Norman Publishing 1998.

[79] K Brodmann, Vergleichende Lokalisationslehre der Grosshirnrinde in ihren Prinzipien dargestellt auf Grund des Zellenbaues, Barth 1909.

[80] MA Rocca, A Ceccarelli, A Falini, B Colombo, P Tortorella, L Bernasconi, et al. Brain gray matter changes in migraine patients with T2-visible lesions: a 3-T MRI study, Stroke. 37 (2006) 1765-1770.

[81] K Kleist. Schizophrenic symptoms and cerebral pathology. Journal of Mental Science. (1960).

[82] NC Andreasen. Negative symptoms in schizophrenia: definition and reliability, Arch.Gen.Psychiatry. 39 (1982) 784-788.

[83] TE Goldberg, JR Kelsoe, DR Weinberger, NH Pliskin, PD Kirwin, KF Berman. Performance of schizophrenic patients on putative neuropsychological tests of frontal lobe function, Int.J.Neurosci. 42 (1988) 51-58.

[84] JP Kesslak, O Nalcioglu, CW Cotman. Quantification of magnetic resonance scans for hippocampal and parahippocampal atrophy in Alzheimer's disease, Neurology. 41 (1991) 51-54.

[85] CR Jack Jr, RC Petersen, PC O'Brien, EG Tangalos. MR-based hippocampal volumetry in the diagnosis of Alzheimer's disease, Neurology. 42 (1992) 183-188.

[86] S Lehericy, M Baulac, J Chiras, L Pierot, N Martin, B Pillon, et al. Amygdalohippocampal MR volume measurements in the early stages of Alzheimer disease, AJNR Am.J.Neuroradiol. 15 (1994) 929-937.

[87] M Laakso, H Soininen, K Partanen, E Helkala, P Hartikainen, P Vainio, et al. Volumes of hippocampus, amygdala and frontal lobes in the MRI-based diagnosis of early Alzheimer's disease: correlation with memory functions, Journal of Neural Transmission-Parkinson's Disease and Dementia Section. 9 (1995) 73-86.

[88] S Sandor, R Leahy. Surface-based labeling of cortical anatomy using a deformable atlas, Medical Imaging, IEEE Transactions on. 16 (1997) 41-54.

[89] DC Van Essen, K Ugurbil, E Auerbach, D Barch, T Behrens, R Bucholz, et al. The Human Connectome Project: a data acquisition perspective, Neuroimage. 62 (2012) 2222-2231.

[90] DC Van Essen, K Ugurbil. The future of the human connectome, Neuroimage. 62 (2012) 1299-1310.

[91] J Talairach, P Tournoux, Co-planar stereotaxic atlas of the human brain : 3-dimensional proportional system : an approach to cerebral imaging, G. Thieme ; New York : Thieme Medical Publishers, Stuttgart ; New York, 1988.

[92] B Fischl, A van der Kouwe, C Destrieux, E Halgren, F Segonne, DH Salat, et al. Automatically parcellating the human cerebral cortex, Cereb.Cortex. 14 (2004) 11-22.

[93] PE Roland, K Zilles. Structural divisions and functional fields in the human cerebral cortex, Brain Res.Rev. 26 (1998) 87-105.

[94] C Destrieux, B Fischl, A Dale, E Halgren. Automatic parcellation of human cortical gyri and sulci using standard anatomical nomenclature, Neuroimage. 53 (2010) 1-15.

[95] R Wright, V Kyriakopoulou, C Ledig, M Rutherford, J Hajnal, D Rueckert, et al. Automatic quantification of normal cortical folding patterns from fetal brain MRI, Neuroimage. 91 (2014) 21-32.

[96] B Crespo-Facorro, J Kim, NC Andreasen, R Spinks, DS O'Leary, HJ Bockholt, et al. Cerebral cortex: a topographic segmentation method using magnetic resonance imaging, Psychiatry Research: Neuroimaging. 100 (2000) 97-126.

[97] A Evans, C Beil, S Marrett, C Thompson, A Hakim. Anatomical-functional correlation using an adjustable MRI-based region of interest atlas with positron emission tomography, Journal of Cerebral Blood Flow & Metabolism. 8 (1988) 513-530.

[98] JL Lancaster, MG Woldorff, LM Parsons, M Liotti, CS Freitas, L Rainey, et al. Automated Talairach atlas labels for functional brain mapping, Hum.Brain Mapp. 10 (2000) 120-131.

[99] T Greitz, C Bohm, S Holte, L Eriksson. A computerized brain atlas: construction, anatomical content, and some applications. J.Comput.Assist.Tomogr. 15 (1991) 26-38.

[100] FL Bookstein, Thin-plate splines and the atlas problem for biomedical images, (1991) 326-342.

[101] DL Collins, CJ Holmes, TM Peters, AC Evans. Automatic 3-D model-based neuroanatomical segmentation, Hum.Brain Mapp. 3 (1995) 190-208.

[102] DL Collins, TM Peters, AC Evans, Automated 3D nonlinear deformation procedure for determination of gross morphometric variability in human brain, (1994) 180-190.

[103] DL Collins, P Neelin, TM Peters, AC Evans. Automatic 3D intersubject registration of MR volumetric data in standardized Talairach space, J.Comput.Assist.Tomogr. 18 (1994) 192-205.

[104] B Fischl, MI Sereno, RB Tootell, AM Dale. High-resolution intersubject averaging and a coordinate system for the cortical surface, Hum.Brain Mapp. 8 (1999) 272-284.

[105] BT Yeo, M Sabuncu, T Vercauteren, N Ayache, B Fischl, P Golland, Spherical demons: Fast surface registration, Medical Image Computing and Computer-Assisted Intervention–MICCAI 2008, Springer, 2008, pp. 745-753.

[106] BT Yeo, MR Sabuncu, T Vercauteren, N Ayache, B Fischl, P Golland. Spherical demons: fast diffeomorphic landmark-free surface registration, Medical Imaging, IEEE Transactions on. 29 (2010) 650-668.

[107] B Fischl, MI Sereno, AM Dale. Cortical surface-based analysis: II: Inflation, flattening, and a surface-based coordinate system, Neuroimage. 9 (1999) 195-207.

[108] G Le Goualher, E Procyk, DL Collins, R Venugopal, C Barillot, AC Evans. Automated extraction and variability analysis of sulcal neuroanatomy, Medical Imaging, IEEE Transactions on. 18 (1999) 206-217.

[109] F Shi, L Wang, G Wu, G Li, JH Gilmore, W Lin, et al. Neonatal atlas construction using sparse representation, Hum.Brain Mapp. (2014).

[110] N Tzourio-Mazoyer, B Landeau, D Papathanassiou, F Crivello, O Etard, N Delcroix, et al. Automated anatomical labeling of activations in SPM using a macroscopic anatomical parcellation of the MNI MRI single-subject brain, Neuroimage. 15 (2002) 273-289.

[111] F Shi, Y Fan, S Tang, JH Gilmore, W Lin, D Shen. Neonatal brain image segmentation in longitudinal MRI studies, Neuroimage. 49 (2010) 391-400.

[112] A Serag, V Kyriakopoulou, M Rutherford, A Edwards, J Hajnal, P Aljabar, et al. A multi-channel 4D probabilistic atlas of the developing brain: application to fetuses and neonates, Annals of the British Machine Vision Association. (2012) 1-14.

[113] SM Smith. Fast robust automated brain extraction, Hum.Brain Mapp. 17 (2002) 143-155.

[114] DW Shattuck, RM Leahy. Automated graph-based analysis and correction of cortical volume topology, Medical Imaging, IEEE Transactions on. 20 (2001) 1167-1177.

[115] R Goebel, F Esposito, E Formisano. Analysis of FIAC data with BrainVoyager QX: from single-subject to cortically aligned group GLM analysis and self-organizing group ICA, Hum.Brain Mapp. 27 (2006) 392-401.

[116] D Seghers, E D'Agostino, F Maes, D Vandermeulen, P Suetens, Construction of a brain template from MR images using state-of-the-art registration and segmentation

techniques, Medical Image Computing and Computer-Assisted Intervention–MICCAI 2004, Springer, 2004, pp. 696-703.

[117] Y Zhang, M Brady, S Smith. Segmentation of brain MR images through a hidden Markov random field model and the expectation-maximization algorithm, Medical Imaging, IEEE Transactions on. 20 (2001) 45-57.

[118] WD Penny, KJ Friston, JT Ashburner, SJ Kiebel, TE Nichols, Statistical parametric mapping: the analysis of functional brain images: the analysis of functional brain images, Academic press 2011.

[119] AM Dale, B Fischl, MI Sereno. Cortical surface-based analysis: I. Segmentation and surface reconstruction, Neuroimage. 9 (1999) 179-194.

[120] AC Evans, DL Collins, S Mills, E Brown, R Kelly, TM Peters, 3D statistical neuroanatomical models from 305 MRI volumes, (1993) 1813-1817.

[121] H Park, PH Bland, AO Hero III, CR Meyer, Least biased target selection in probabilistic atlas construction, Medical Image Computing and Computer-Assisted Intervention–MICCAI 2005, Springer, 2005, pp. 419-426.

[122] TF Cox, MA Cox, Multidimensional scaling, CRC Press 2000.

[123] B Avants, JC Gee. Geodesic estimation for large deformation anatomical shape averaging and interpolation, Neuroimage. 23 (2004) S139-S150.

[124] S Joshi, B Davis, M Jomier, G Gerig. Unbiased diffeomorphic atlas construction for computational anatomy, Neuroimage. 23 (2004) S151-S160.

[125] KK Bhatia, JV Hajnal, BK Puri, AD Edwards, D Rueckert, Consistent groupwise non-rigid registration for atlas construction, (2004) 908-911.

[126] BB Avants, P Yushkevich, J Pluta, D Minkoff, M Korczykowski, J Detre, et al. The optimal template effect in hippocampus studies of diseased populations, Neuroimage. 49 (2010) 2457-2466.

[127] EG Miller, NE Matsakis, PA Viola, Learning from one example through shared densities on transforms, 1 (2000) 464-471.

[128] T Rohlfing, NM Zahr, EV Sullivan, A Pfefferbaum, The SRI24 multichannel brain atlas: construction and applications, (2008) 691409-691409-12.

[129] SK Balci, P Golland, M Shenton, WM Wells. Free-Form B-spline Deformation Model for Groupwise Registration, Med.Image Comput.Comput.Assist.Interv. 10 (2007) 23-30.

[130] P Lorenzen, BC Davis, S Joshi, Unbiased atlas formation via large deformations metric mapping, Medical Image Computing and Computer-Assisted Intervention–MICCAI 2005, Springer, 2005, pp. 411-418.

[131] H Jia, G Wu, Q Wang, D Shen. ABSORB: Atlas building by self-organized registration and bundling, Neuroimage. 51 (2010) 1057-1070.

[132] V Fonov, AC Evans, K Botteron, CR Almli, RC McKinstry, DL Collins. Unbiased average age-appropriate atlases for pediatric studies, Neuroimage. 54 (2011) 313-327.

[133] X Artaechevarria, A Munoz-Barrutia, C Ortiz-de-Solórzano. Combination strategies in multi-atlas image segmentation: Application to brain MR data, Medical Imaging, IEEE Transactions on. 28 (2009) 1266-1277.

[134] T Rohlfing, R Brandt, R Menzel, CR Maurer. Evaluation of atlas selection strategies for atlas-based image segmentation with application to confocal microscopy images of bee brains, Neuroimage. 21 (2004) 1428-1442.

[135] EA Nadaraya. On estimating regression, Theory of Probability & Its Applications. 9 (1964) 141-142.

[136] BC Davis, PT Fletcher, E Bullitt, S Joshi. Population shape regression from random design data, International journal of computer vision. 90 (2010) 255-266.

[137] A Ericsson, P Aljabar, D Rueckert, Construction of a patient-specific atlas of the brain: Application to normal aging, (2008) 480-483.

[138] A Gholipour, C Limperopoulos, S Clancy, C Clouchoux, A Akhondi-Asl, JA Estroff, et al., Construction of a Deformable Spatiotemporal MRI Atlas of the Fetal Brain: Evaluation of Similarity Metrics and Deformation Models, Medical Image Computing and Computer-Assisted Intervention–MICCAI 2014, Springer, 2014, pp. 292-299.

[139] A Schuh, M Murgasova, A Makropoulos, C Ledig, SJ Counsell, JV Hajnal, et al., Construction of a 4D Brain Atlas and Growth Model Using Diffeomorphic Registration, Spatio-temporal Image Analysis for Longitudinal and Time-Series Image Data, Springer, 2015, pp. 27-37.

[140] A Serag, P Aljabar, G Ball, SJ Counsell, JP Boardman, MA Rutherford, et al. Construction of a consistent high-definition spatio-temporal atlas of the developing brain using adaptive kernel regression, Neuroimage. 59 (2012) 2255-2265.

[141] P Bazin, DL Pham. Topology-preserving tissue classification of magnetic resonance brain images, Medical Imaging, IEEE Transactions on. 26 (2007) 487-496.

[142] DL Pham, JL Prince. An adaptive fuzzy C-means algorithm for image segmentation in the presence of intensity inhomogeneities, Pattern Recog.Lett. 20 (1999) 57-68.

[143] M Prastawa, JH Gilmore, W Lin, G Gerig. Automatic segmentation of MR images of the developing newborn brain, Med.Image Anal. 9 (2005) 457-466.

[144] SK Warfield, M Kaus, FA Jolesz, R Kikinis. Adaptive, template moderated, spatially varying statistical classification, Med.Image Anal. 4 (2000) 43-55.

[145] NI Weisenfeld, SK Warfield. Automatic segmentation of newborn brain MRI, Neuroimage. 47 (2009) 564-572.

[146] CA Cocosco, AP Zijdenbos, AC Evans. A fully automatic and robust brain MRI tissue classification method, Med.Image Anal. 7 (2003) 513-527.

[147] B Fischl, DH Salat, E Busa, M Albert, M Dieterich, C Haselgrove, et al. Whole brain segmentation: automated labeling of neuroanatomical structures in the human brain, Neuron. 33 (2002) 341-355.

[148] K Van Leemput, F Maes, D Vandermeulen, P Suetens. Automated model-based bias field correction of MR images of the brain, Medical Imaging, IEEE Transactions on. 18 (1999) 885-896.

[149] J Ashburner, KJ Friston. Unified segmentation, Neuroimage. 26 (2005) 839-851.

[150] KM Pohl, J Fisher, WEL Grimson, R Kikinis, WM Wells. A Bayesian model for joint segmentation and registration, Neuroimage. 31 (2006) 228-239.

[151] F Wang, BC Vemuri, SJ Eisenschenk. Joint registration and segmentation of neuroanatomic structures from brain MRI, Acad.Radiol. 13 (2006) 1104-1111.

[152] A Yezzi, L Zöllei, T Kapur. A variational framework for integrating segmentation and registration through active contours, Med.Image Anal. 7 (2003) 171-185.

[153] P Anbeek, KL Vincken, F Groenendaal, A Koeman, MJ Van Osch, J Van der Grond. Probabilistic brain tissue segmentation in neonatal magnetic resonance imaging, Pediatr.Res. 63 (2008) 158-163.

[154] PA Habas, K Kim, F Rousseau, OA Glenn, AJ Barkovich, C Studholme, A spatio-temporal atlas of the human fetal brain with application to tissue segmentation, Medical Image Computing and Computer-Assisted Intervention–MICCAI 2009, Springer, 2009, pp. 289-296.

[155] AP Dempster, NM Laird, DB Rubin. Maximum likelihood from incomplete data via the EM algorithm, Journal of the royal statistical society.Series B (methodological). (1977) 1-38.

[156] Z Song, SP Awate, DJ Licht, JC Gee, Clinical neonatal brain MRI segmentation using adaptive nonparametric data models and intensity-based Markov priors, Medical Image Computing and Computer-Assisted Intervention–MICCAI 2007, Springer, 2007, pp. 883-890.

[157] CJ Burges. A tutorial on support vector machines for pattern recognition, Data mining and knowledge discovery. 2 (1998) 121-167.

[158] Y Boykov, O Veksler, R Zabih. Fast approximate energy minimization via graph cuts, Pattern Analysis and Machine Intelligence, IEEE Transactions on. 23 (2001) 1222-1239.

[159] H Xue, L Srinivasan, S Jiang, M Rutherford, AD Edwards, D Rueckert, et al. Automatic segmentation and reconstruction of the cortex from neonatal MRI, Neuroimage. 38 (2007) 461-477.

[160] K Kazemi, HA Moghaddam, R Grebe, C Gondry-Jouet, F Wallois. A neonatal atlas template for spatial normalization of whole-brain magnetic resonance images of newborns: preliminary results, Neuroimage. 37 (2007) 463-473.

[161] F Shi, P Yap, Y Fan, JH Gilmore, W Lin, D Shen. Construction of multi-region-multi-reference atlases for neonatal brain MRI segmentation, Neuroimage. 51 (2010) 684-693.

[162] D Shen, C Davatzikos. HAMMER: hierarchical attribute matching mechanism for elastic registration, Medical Imaging, IEEE Transactions on. 21 (2002) 1421-1439.

[163] MH Alassaf, JK Hahn, Automatic Parcellation of Longitudinal Cortical Surfaces, SPIE medical imaging. International Society for Optics and Photonics (2015).

[164] L Vincent, P Soille. Watersheds in digital spaces: an efficient algorithm based on immersion simulations, IEEE Trans.Pattern Anal.Mach.Intell. 13 (1991) 583-598.

[165] BJ Frey, D Dueck. Clustering by passing messages between data points, Science. 315 (2007) 972-976.

[166] PA Habas, K Kim, JM Corbett-Detig, F Rousseau, OA Glenn, AJ Barkovich, et al. A spatiotemporal atlas of MR intensity, tissue probability and shape of the fetal brain with application to segmentation, Neuroimage. 53 (2010) 460-470.

[167] WE Lorensen, HE Cline, Marching cubes: A high resolution 3D surface construction algorithm, 21 (1987) 163-169.

[168] W Crum, C Tanner, D Hawkes. Anisotropic multi-scale fluid registration: evaluation in magnetic resonance breast imaging, Phys.Med.Biol. 50 (2005) 5153.

[169] R Bajcsy, S Kovačič. Multiresolution elastic matching, Computer vision, graphics, and image processing. 46 (1989) 1-21.

[170] D Rueckert, LI Sonoda, C Hayes, DL Hill, MO Leach, DJ Hawkes. Nonrigid registration using free-form deformations: application to breast MR images, Medical Imaging, IEEE Transactions on. 18 (1999) 712-721.

[171] J Thirion. Fast non-rigid matching of 3D medical images, (1995).

[172] MF Beg, MI Miller, A Trouvé, L Younes. Computing large deformation metric mappings via geodesic flows of diffeomorphisms, International journal of computer vision. 61 (2005) 139-157.

[173] PJ Besl, ND McKay, Method for registration of 3-D shapes, (1992) 586-606.

[174] Z Zhang. Iterative point matching for registration of free-form curves and surfaces, International journal of computer vision. 13 (1994) 119-152.

[175] S Rusinkiewicz, M Levoy, Efficient variants of the ICP algorithm, (2001) 145-152.

[176] S Rusinkiewicz, O Hall-Holt, M Levoy, Real-time 3D model acquisition, 21 (2002) 438-446.

[177] MH Alassaf, Y Yim, JK Hahn. Non-rigid Surface Registration using Cover Tree based Clustering and Nearest Neighbor Search, Proceedings of the 9th International Conference on Computer Vision Theory and Applications. (2014) 579-587.

[178] JP Pluim, JA Maintz, MA Viergever. Mutual-information-based registration of medical images: a survey, Medical Imaging, IEEE Transactions on. 22 (2003) 986-1004.

[179] J Maintz, MA Viergever. A survey of medical image registration, Med.Image Anal. 2 (1998) 1-36.

[180] TS Yoo, Insight into images: principles and practice for segmentation, registration, and image analysis, AK Peters Ltd 2004.

[181] MA Audette, FP Ferrie, TM Peters. An algorithmic overview of surface registration techniques for medical imaging, Med.Image Anal. 4 (2000) 201-217.

[182] GK Tam, Z Cheng, Y Lai, FC Langbein, Y Liu, D Marshall, et al. Registration of 3D point clouds and meshes: A survey from rigid to nonrigid, Visualization and Computer Graphics, IEEE Transactions on. 19 (2013) 1199-1217.

[183] KK Bhatia, J Hajnal, A Hammers, D Rueckert, Similarity metrics for groupwise non-rigid registration, Medical Image Computing and Computer-Assisted Intervention–MICCAI 2007, Springer, 2007, pp. 544-552.

[184] G Hirota, R Maheshwari, MC Lin. Fast volume-preserving free-form deformation using multi-level optimization, Comput.-Aided Des. 32 (2000) 499-512.

[185] BK Horn. Closed-form solution of absolute orientation using unit quaternions, JOSA A. 4 (1987) 629-642.

[186] A Beygelzimer, S Kakade, J Langford, Cover trees for nearest neighbor, (2006) 97-104.

[187] DW Marquardt. An algorithm for least-squares estimation of nonlinear parameters, Journal of the Society for Industrial & Applied Mathematics. 11 (1963) 431-441.

[188] A Appel, Some techniques for shading machine renderings of solids, (1968) 37-45.

[189] T Möller, B Trumbore. Fast, minimum storage ray-triangle intersection, Journal of graphics tools. 2 (1997) 21-28.

[190] A Papoulis. Probability, random variables, and stochastic processes, 1991, Joseph Tabrikian (S'89-M'97-SM'98) received the B.Sc., M.Sc., and Ph.D.degrees in Electrical Engineering from the Tel-Aviv University, Tel-Aviv, Israel, in. 1992 (1986) 1996-1998.

[191] Y Bengio, O Delalleau, N Le Roux. Label propagation and quadratic criterion, Semi-supervised learning. (2006) 193-216.

[192] S Toub, PC Platform. Patterns of parallel programming, Microsoft Corporation. (2010).

[193] G Li, D Shen. Consistent sulcal parcellation of longitudinal cortical surfaces, Neuroimage. 57 (2011) 76-88.

[194] LR Dice. Measures of the amount of ecologic association between species, Ecology. 26 (1945) 297-302.

[195] G Li, J Nie, L Wang, F Shi, W Lin, JH Gilmore, et al. Mapping region-specific longitudinal cortical surface expansion from birth to 2 years of age, Cereb.Cortex. 23 (2013) 2724-2733.

[196] H Gouraud. Continuous shading of curved surfaces, Computers, IEEE Transactions on. 100 (1971) 623-629.

[197] G Thürrner, CA Wüthrich. Computing vertex normals from polygonal facets, Journal of Graphics Tools. 3 (1998) 43-46.

[198] N Max. Weights for computing vertex normals from facet normals, Journal of Graphics Tools. 4 (1999) 1-6.